



THE HONG KONG  
POLYTECHNIC UNIVERSITY

香港理工大學

Pao Yue-kong Library

包玉剛圖書館

---

## Copyright Undertaking

This thesis is protected by copyright, with all rights reserved.

**By reading and using the thesis, the reader understands and agrees to the following terms:**

1. The reader will abide by the rules and legal ordinances governing copyright regarding the use of the thesis.
2. The reader will use the thesis for the purpose of research or private study only and not for distribution or further reproduction or any other purpose.
3. The reader agrees to indemnify and hold the University harmless from and against any loss, damage, cost, liability or expenses arising from copyright infringement or unauthorized usage.

If you have reasons to believe that any materials in this thesis are deemed not suitable to be distributed in this form, or a copyright owner having difficulty with the material being included in our database, please contact [lbsys@polyu.edu.hk](mailto:lbsys@polyu.edu.hk) providing details. The Library will look into your claim and consider taking remedial action upon receipt of the written requests.

THE HONG KONG POLYTECHNIC UNIVERSITY

DEPARTMENT OF COMPUTING

**ADAPTIVE METHODS FOR TROPICAL CYCLONE  
PREDICTION FROM TIME-SERIES SATELLITE DATA**

BY

BO FENG

A THESIS SUBMITTED IN THE PARTIAL FULFILLMENT OF  
THE REQUIREMENTS FOR THE DEGREE OF  
MASTER OF PHILOSOPHY

INITIAL SUBMISSION: MARCH, 2006

# Certificate of Originality

I hereby declare that this thesis is my own work and that, to the best of my knowledge and belief, it reproduces no material previously published or written nor material which has been accepted for the award of any other degree or diploma, except where due acknowledgement has been made in the text.

\_\_\_\_\_ (Signed)

Bo Feng (Name of Student)

# Abstract

A tropical cyclone is the generic term for a non-frontal synoptic scale low-pressure system over tropical or sub-tropical waters with organized convection and definite cyclonic surface wind circulation. Associated with the potential destructive winds and heavy rains, they primarily pose a threat to life and property to coastal zones. Their early identification would allow precautions to be put in place that would minimize the associated risks to people's lives and properties. In recent years, more and more research efforts have been involved in tropical cyclone forecasting, and lots of prediction models have been proposed to simulate the intensities of a variety of tropical cyclones, including statistical models, statistical-dynamical models and dynamic models. However, each approach has its own methodologies, assumptions and design goals, making it difficult to adapt to different application requirements.

In this thesis, we aim at discovering new approaches in designing reformative forecasting models to predict tropical cyclones using methodologies at different levels that are more reliable for the collected data types, more efficient and effective in terms of predicted accuracy and computational costs, and more scalable to future system expansion. We propose a satellite interpretation based forecasting model, a neural network regression-forecasting model and a similarity retrieval model, each of which has its own background features. In the satellite interpretation-forecasting model, we introduce an integrated approach for tropical cyclone comparison based on typical spiral shapes using time warping technology. The position and the shape of a tropical cyclone extracted from a satellite image is the major concern. The Gradient Vector Flow (GVF) snake model is used to extract the contour points of a dominant tropical cyclone from the satellite image. The similarity of two tropical cyclones is compared using the angle features found among the successive contour points. Furthermore to achieve a better reflection of the spiral shape of tropical cyclones, we adopt a time warping approach to allow fast and accurate comparison of patterns. In

the neural network regression forecasting model, we propose an integrated competitive neural network classifier to predict the maximum potential intensity of a tropical cyclone, based on a 10-year sample of western North Pacific tropical cyclones and monthly mean sea surface temperature. A large amount of feature variables are used in the network training including latitude, longitude, pressure, intensity, sea surface temperatures and so on. To deal with variety of variables, we design a variable selection procedure to choose the most important training variables to enhance the speed and accuracy of neural network training. In the similarity retrieval model, we present an approach to predict TC intensities using a feed-forward neural weight generator, which is adopted to generate a set of appropriate weights for various associated features of a tropical cyclone. We also propose the time-series similarity adjustment to measure the similarity of samples on consecutive observations of a tropical cyclone. Comparing with existing similar forecasting models, the experiments show that our proposed ones can achieve promising results.

# Publications

1. Liu J.N.K., Feng B., Wang M. and Luo W.D.; Tropical Cyclone Forecast using Angle Features and Time Warping, in Proc. Of IJCNN'06, the World Congress on Computational Intelligence (WCCI'06), Vancouver, BC, Canada, 2006
2. Shiu S.C.K., Liu J.N.K., Lam J.L.C. and Feng B.; A Data Mining Approach for Branch and ATM Site Evaluation, in Lecture Notes in Computer Science, Springer, pp.303-318, 2006
3. Feng B. and Liu J.N.K.; A Neural Network Regression Model for Tropical Cyclone Forecast, in Proc. of the 3<sup>rd</sup> Int. Conf. on Machine Learning Cybernetics, vol.7, pp.4122 – 4128, Guangzhou, China, 2005
4. Feng B. and Liu J.N.K.; Similarity Retrieval from Time-Series Tropical Cyclone Observations using a Neural Weighting Generator for Forecasting Modelling, in Proc. of the 9<sup>th</sup> Int. Conf. on Knowledge-Based Intelligent Information & Engineering Systems, pp.128-134, Melbourne, Australia, 2005
5. Liu J.N.K. and Feng B.; A Novel Comparison Approach for Tropical Cyclone Satellite Images using Angle Features, in Proc. of the 18<sup>th</sup> Intel. FLAIRS Conf., pp. 690-696, Florida, USA, 2005
6. Feng B. and Liu J.N.K.; An Adaptive Neural Network Classifier for Tropical Cyclone Prediction using a two-layer Features Selector, in Proc. of the 2<sup>nd</sup> Intel. Symposium on Neural Network, pp.399-404, Chongqing, China, 2005
7. Feng B. and Liu J.N.K.; SEMO-MAMO, A 3-Phase Module to Compare Tropical Cyclone Satellite Images using a Modified Hausdorff Distance, in Proc. of the 2<sup>nd</sup> Intel. Conf. on Machine Learning Cybernetics, vol.6, pp.3808–3813, Shanghai, China, 2004
8. Liu J.N.K., Wang M. and Feng B.; iBotGuard: An Internet-based Intelligent Robot Security System Using Invariant Face Recognition against Intruder, IEEE Transaction on SMC, Part C, vol.35, Issue 1, pp.97 – 105, 2005
9. Liu J.N.K., Kwong R.W.M. and Feng B.; Chart Patterns Recognition and Forecast Using Wavelet and Radial Basis Function Work, in Proc. of the 8<sup>th</sup> Intel. Conf. on Knowledge-Based Intelligent Information & Engineering Systems, pp.564-571, Wellington, New Zealand, 2004

# Acknowledgements

First of all, I would like to take this opportunity to express my sincere gratitude towards my supervisor, Prof. James N.K. Liu, for his invaluable support and guidance throughout the last two years. It was his constant encouragement and wonderful association that has enabled me to achieve the objectives of this work.

I would also like to thank Prof. Jane You, my co-supervisor, for her kindly supervision of providing me remarkable insights into many aspects of my research study.

Sincere thanks are also expressed to many other friends and colleagues, for their correlative research works and efforts, and helps during my study to achieve targets.

My parents have been a constant source of love and affection. I am eternally grateful to them for always being with me whenever I need them.

Bo Feng  
March 5<sup>th</sup>, 2006

## Addendum / Erratum

I hereby acknowledge the reference to (2), as listed below, for my MPhil thesis entitled “Adaptive Methods for Tropical Cyclone Prediction from Time-Series Satellite Data”. In particular, part of the contents (specified in (1) below) in section 2.2.6 “TC Eye Location” are extracted from the literature review part of the technical report listed in 2(c) below.

**(1) Specific contents:**

Paragraph 1, “Tropical Cyclone (TC) eye fix is often .....”, extracted from paragraph 1 of section 2 “Methods of TC Eye Fix” in reference 3.

Paragraph 2, “In contrast, automated TC eye fix methods often .....”, extracted from paragraph 2 of section 2 in reference 3.

Paragraph 3, “For pattern matching, the TC eye is fixed by finding .....”, extracted from paragraph 3 of section 2 in reference 3.

and

First several sentences in paragraph 4 of section 2.2.6, extracted from paragraph 4 of section 2 and paragraph 1 of section 3 “A Model of TC” in reference 3.

**(2) Specific publication reference**

- a. Reference 1 (cited as a reference [58] in my thesis)  
Chi Lap Yip and Ka Yan Wong (2004), Efficient and effective tropical cyclone eye using genetic algorithms, in M. Gh. Negoita et al. (Eds.): KES 2004, LNAI 3213, pp. 654-660
- b. Reference 2 (cited as a reference [60] in my thesis)  
Ka Yan Wong and Chi Lap Yip (2005), Tropical cyclone eye fix using genetic algorithm with temporal information, in R. Khosla et al. (Eds.): KES 2005, LNAI 3681, pp. 854-860
- c. Reference 3:  
YIP Chi Lap and Wong Ka Yan (2004), Tropical cyclone eye fix using genetic algorithm, HKU CSIS Tech Report TR-2004-06

I appreciate related authors their research work which has offered much help in my MPhil study development.

Bo Feng  
2010-06-22

# Contents

Certificate of Originality	i
Publications	ii
Acknowledgements	iii
Abstract	iv
List of Figures	vi
List of Tables	viii
Contents	ix
Chapter 1. Introduction	1
1.1 Tropical Cyclone Intensity	2
1.2 Satellite Image Interpretation	3
1.3 Tropical Cyclone Intensity Mining	4
1.4 Dvorak Templates	5
1.5 Time-series prediction and neural network forecasting	7
1.6 Contributions of the Thesis	8
1.7 Organization of the Thesis	10
Chapter 2. Related Works	11
2.1 Physical Principle Models	11
2.1.1 CLIPER	11
2.1.2 SHIFOR	12
2.1.3 SHIPS	12
2.1.4 STIPS	13
2.1.5 STD5	13
2.1.6 GFDL	14
2.1.7 AMSU	15
2.2 Imagery Interpretation and Neural Network Models	15
2.2.1 Dvorak Techniques	15
2.2.2 EDGLM	16
2.2.3 NOEGM	17
2.2.4 Two-dimension Wavelet Decomposition	18
2.2.5 Case-based Forecasting	19
2.2.6 TC Eye Location	20
Chapter 3. A Satellite Interpretation Based Tropical Cyclone Forecasting System	22
3.1 Introduction and System Framework	22
3.2 Active Contour Model	24
3.3 Matching Methodology	27
3.3.1 A Fast Sequential Neighbour Checking Algorithm	27
3.3.2 Tropical Cyclone Eye Location	28
3.3.3 A Weight Calculation Algorithm	30
3.3.4 An Angle Calculation Module	31
3.3.5 A Time Warping Matching Module	32

3.4 Performance Evaluation	36
3.4.1 Definition of Hausdorff Distance	36
3.4.2 A Modified Hausdorff Distance	37
3.4.3 Experimental Results	38
3.5. Summary	43
Chapter 4. An Integrated Neural Training Based Tropical Cyclone Forecasting System	44
4.1 Introduction	45
4.1.1. Competitive Neural Network	45
4.1.2 Estimation of Regression Coefficients	47
4.2 Data Collection and Preparation	48
4.2.1 Data Collection	48
4.2.2 Data Preparation	51
4.3 Analog Tropical Cyclones Identification	53
4.3.1 Unsupervised Classification Technique	53
4.3.2 Application of the Competitive Neural Network	54
4.4 Random Variable Selection	60
4.5 Intensity Prediction Using Feedforward Neural Network	65
4.5.1 Application of Levenberg-Marquardt Backpropagation Algorithm	65
4.6 Experimental Results and Analysis	70
4.6.1 Experiment with Strong Tropical Cyclone Intensity	70
4.6.2 Experiment with Typical Tropical Cyclone Intensity	72
4.6.3 Fast Intensity Change and Re-intensification Experiments	73
4.6.4 Experiment with Tropical Cyclone Having Double Eye Walls	77
4.6.5 Comparison With Existing Models	77
4.7 Summary	81
Chapter 5. A Similarity Retrieval Model for Time-Series Tropical Cyclone Data	82
5.1 System Overview	83
5.2. Similarity Measure Function	84
5.2.1 Positional and Numerical Measure Functions	84
5.2.2 Neural Weight Generator	86
5.2.3 Time-series Adjustment Function	88
5.3 Experimental Analysis	90
5.4 Summary	92
Chapter 6. Future Research and Conclusion	93
6.1 Limitations and Future Works	93
6.1.1 Satellite Interpretation Based Forecasting	93
6.1.2 Neural Training Based Forecasting	94
6.1.3 Similarity Retrieval Forecasting	95
6.2 Conclusions	96
References	98

# List of Figures

Figure 1.1	Model vertical profile of a mature typhoon	2
Figure 1.2	Dvorak TC templates, with number assigned from T1 to T8	6
Figure 1.3	Decision tree used to determine T-number	7
Figure 3.1	System architecture of a three-layer prototype	24
Figure 3.2	Contour mapping on a satellite image	25
Figure 3.3	Clustered result for a sample tropical cyclone	27
Figure 3.4	Procedure of sequential neighbour checking algorithm	27
Figure 3.5	A pixel distance algorithm	28
Figure 3.6	Result of Positional Eye Location	29
Figure 3.7	The pixel distance algorithm	29
Figure 3.8	Algorithm of calculating weight for each point on the contour	30
Figure 3.9	Result of Weight assigned to each contour point	30
Figure 3.10	An internal angle between adjacent points	31
Figure 3.11	Set of angles for each TC (each bold round point representing an angle formed in Figure 3.10)	32
Figure 3.12	A warping path in an m-by-n grid	33
Figure 3.13	A cumulative distance matrix for angle sequences Q and S	34
Figure 3.14	A cumulative distance matrix for angle sequences Q and S1 after a left shift	35
Figure 3.15	Matching results for three approaches	39
Figure 3.16	A Grid Scanning algorithm	39
Figure 3.17	Procedure for finding the matching accuracy	40
Figure 3.18	Visual description of the experimental results	42
Figure 4.1	The Best Track Data Format	49
Figure 4.2	Display SST Values using Panoply	50
Figure 4.3	Intensity predictions for Lupit at 12 hours (November, 2003)	71
Figure 4.4	Intensity predictions for Lupit at 24 hours (November, 2003)	71
Figure 4.5	Intensity Predictions for Podul at 12 Hours (October, 2001)	72
Figure 4.6	Intensity Predictions for Podul at 24 Hours (October, 2001)	73
Figure 4.7	Forecasting for Maemi when Rapid Intensification is Presented (September, 2003)	74
Figure 4.8	Forecasting for Dujuan when Rapid Intensity Reductions is Presented (August, 2003)	75
Figure 4.9	Re-intensification of Nari (September, 2001)	76
Figure 4.10	Re-intensification of Parma (October, 2003)	76
Figure 4.11	Intensity predictions for Dujuan at 12 hours (September, 2003)	77
Figure 4.12	NN Model Enhancements over Regression Model for Rusa at 12 Hours (August, 2002)	80
Figure 5.1	Overview of the proposed prediction model	83
Figure 5.2	Latitude-Longitude coordinate system using in similarity	86

	functions	
Figure 5.3	Structure of the neural weight generator	86
Figure 5.4	Steps to predict the intensity of current tropical cyclone sample	90
Figure 5.5	Intensity prediction results and errors	91
Figure5.6	Predicted precision of three approaches	92

# List of Tables

Table 1.1	Classification of tropical cyclones in Hong Kong	2
Table 3.1	Retrieved accuracy for the results in Figure 3.15	40
Table 3.2	Average Accuracy (%) comparison of the Angle Feature Matching (AFM) and the Modified Hausdorff Distance	41
Table 3.3	Computational costs of three algorithms	42
Table 3.4	Computational complexities of three approaches	43
Table 4.1	Data Obtained From NCEP/NCAR Reanalysis (Sourced by NCEP)	50
Table 4.2	Tropical Cyclone Database Structure	52
Table 4.3	Data Subfields	52
Table 4.4	Variables Included In the Final Set of Analog Tropical Cyclones	58
Table 4.5	Lag Value used in the model	62
Table 4.6	Variable Contribution for the Tropical Cyclone Sample at 6, 12, 18 and 24 hours	78
Table 4.7	Comparison Between the Proposed Model and JTWC's Model	79
Table 4.8	Proposed Model's Improvement over JTWC's Model	80
Table 4.9	JTWC TC Intensity Forecast Error (Sourced by JTWC)	80
Table 4.10	Proposed Model Improvements over Multiple Linear Regression Model	81
Table 5.1	Input attributes normalization and initial number of layer units for neural weight generator	91

# Chapter 1. Introduction

A Tropical Cyclone (TC) is the generic term for a non-frontal synoptic scale low-pressure system over tropical or sub-tropical waters with organized convection and definite cyclonic surface wind circulation. It is known to form over all tropical oceans with the exception of the south Atlantic and the south Pacific east of about 140° W.

The intensity of a tropical cyclone is a measure of the destructive effects over a particular place on humans and (or) structures. It is measured by the maximum 1-min sustained surface wind in the walls of the hurricane [1]. Usually, in tropical cyclone landfall areas the resultant damages are often extensive, especially in developed coastal areas. In the September of 2005, hurricane Katrina, the most destructive and costliest natural disaster in the history of the United States, passed through the Central Gulf Coast of America and flooded and damaged the coastal regions. The official death toll stands at 1,302 and the damage higher than \$200 million. Over a million people were displaced.

Building forecasting models for tropical cyclone intensity is one of the most challenging areas in tropical cyclone research in recent years. An accurate intensity prediction is extremely important in the forecast advisory and warning process, primarily because emergency management decision-making is closely tied to the movement of tropical cyclones and the intensity of land-falling tropical cyclones. Moreover, to mitigate tropical cyclone effects, it is necessary to predict the intensity changes of a tropical cyclone with high level of accuracy in order to prevent from loss caused by this destructive natural disaster. However, such information has not been exploited to its full potential for prediction of tropical cyclone intensity changes.

In this chapter, we will first provide briefing introduction about tropical cyclone intensity, satellite image interpretation, Dvorak technique, time-series prediction and neural network forecast. Then we describe the contributions and the organization of this thesis.

## 1.1 Tropical Cyclone Intensity

Tropical Cyclones (TC), including hurricanes and typhoons, with its remarkable spiral shape and central eye, are natural phenomenon and have great destructive forces. They are huge rotating column of warm and moist air. Moreover, its wind speed usually exceeds 150km/h and torrential rain is also a common observation with the tropical cyclone. The centre of tropical cyclones has very low sea-level pressure, and is often called the “eye” (like Figure 1.1 shown below). In the region of the Western North Pacific and the South China Sea, on average there are 30 tropical cyclones formed in each year. Tropical cyclones are classified in accordance with the World Meteorological Organization’s recommendation by their maximum sustain wind speeds near the centre. Taking Hong Kong as an example, the classification is defined in terms of wind speeds averaged over a period of 10 minutes as shown in Table 1.1 [80]:

**Table 1.1:** Classification of tropical cyclones in Hong Kong

Intensity	Maximum 10-minute mean wind near the centre
Tropical Depression (TD)	Up to 62 km/h
Tropical Storm (TS)	63 to 87 km/h
Severe Tropical Storm (STS)	88 to 117 km/h
Typhoon (TY)	118 km/h or more

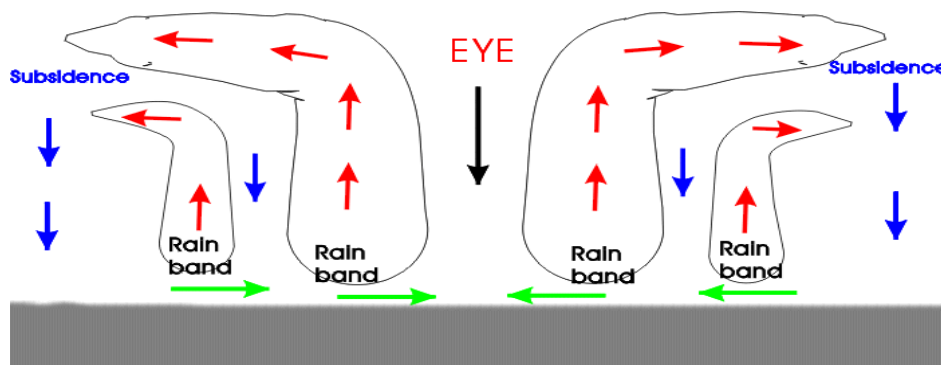


**Figure 1.1:** Model vertical profile of a mature typhoon

In recent years, lots of research efforts have been devoted to techniques recurring to physical devices, such as scatterometer technique [2], microwave radiometric [3], QuikSCAT [4] and so on. As it needs high expert information about those special settlements if the forecast is carried out using scatterometer, microwave or QuikSCAT techniques, interpretation from the satellite images directly, assisted by miscellaneous information, becomes a more and more popular research approach to achieve tropical cyclone forecasting for computer-science background researchers. One of the most widely accepted techniques is the Dvorak technique [5, 6], which assigns the wind intensity value (called TC number) based on the size, shape and vorticity of the dense cloud shield adjacent to the centre of the storm.

Owing to the high variation of cloud pattern [7] and lack of efficient scene analysis technique for the isolation and extraction of cloud systems from satellite images [8], the pattern matching jobs for tropical cyclones in Dvorak analysis are so far mostly done by subjective human justification. Very few successful alternative techniques exist to support pattern recognition automatically in Dvorak analysis [9], let alone with the automatic identification for the position of “eye” in hurricanes and typhoons [10].

## **1.2 Satellite Image Interpretation**

For more than three decades, satellite technologies have been extensively applied in various aspects, ranging from the military purpose, to the searching and discovery of natural resources. Meteorology, without saying, is one of the most typical areas, which has a high utilization of satellite technology, ranging from the observation of regional adverse weather conditions such as thunderstorms [11] and jet streams [12], to the global weather patterns such as synoptic scale cloud systems [13].

The purpose of meteorological satellite image interpretation is to relate significant features in the image to physical processes that are occurring, or have occurred in the atmosphere [14]. Much of the research in image interpretation being done today involves the development of techniques to automate the analysis of digital imagery. Over the past

few decades, the primary analysis tool has been relying on the interpretive skill of the analysts who manually view the satellite images and make a subjective assessment of the features that may be involved. Most meteorological satellites make measurements in the visible and infrared portions of the electromagnetic spectrum. Some also have additional channels that can vary from the ultraviolet to the microwave region, such as Water Vapor Imagery to indicate the relative humidity of the mid-troposphere [15] and Microwave Imagery for the observation of precipitation images [16].

Certain important atmospheric phenomena can possibly be found through the inspection of visible satellite pictures and by contrast with the difference in patterns found in other channels (such as infrared channel). These include:

- Clouds system and activities
- Storms, including tropical cyclones and severe thunderstorm
- Wind flow
- Miscellaneous phenomena such as volcanic ash, sun glint and dust storm

### **1.3 Tropical Cyclone Intensity Mining**

Over the past decades, numerical models [17] are still the most commonly used weather prediction methods adopted by meteorologists and weather forecasters. This classical approach attempts to model the fluid and thermal dynamic systems for grid-point time series prediction based on boundary meteorological data such as mean sea level pressure (MSLP), wet bulb and dry bulb temperature, and wind speed and direction. In order to improve the mining accuracy, grid point meteorological data including wind speed and direction, vorticity and divergence measurements at various atmospheric levels (e.g., 200 hPa, 300 hPa, 500 hPa, 700 hPa) are being used for simulation as well. Besides, numerical simulation often requires intensive computations involving complex differential equations and computational algorithms. The accuracy is bounded by certain inherited constraints such as the adoption of incomplete boundary conditions, model assumptions and numerical instability. The bureau numerical tropical cyclone prediction model that has run operationally and regularly in recent years is the one-way-interactive

tropical cyclone model (OTCM) used by the Joint Typhoon Warning Centre (JTWC) in Guam. The OTCM model is generally the best and most consistent performer of the entire operational objective forecast aids in the western North Pacific region [18].

The track forecast system (TFS) objective analysis utilizes the Barnes method [19] on pressure surface. The forecast component of the TFS uses fourth-order finite differencing for advection terms in flux form and a split-explicit time integration using the leapfrog scheme [20]. In order to ensure the maintenance of the vortex circulation throughout the forecast period, artificial heating options are integrated to supplement the Kuo-type cumulus parameterization [21] in the model. The TFS began operation at the Central Weather Bureau in Taiwan in 1990 and is still being used as a critical TC track-mining tool. As compared with the long-term, best performing OTCM in the western North Pacific region, TFS is out-performed by over 8% in 48-h TC track mining accuracy [22] that corresponds to 30 km of improvement.

For TC intensity and tracks mining, concurrently schema adopted by weather forecasters include: 1) subjective prediction based on combination of linear extrapolation of TC movement together with the interpretation of other weather forecasting resources such as surface and upper-air weather charts; 2) numerical weather prediction by subjective “feed in” the TC position, intensity, and central pressure extracted from Dvorak analysis into the numerical model to perform the time series grid point prediction such as OTCM model, or the integration of bogus vortices with supplementary artificial heating model into the numerical system for time series prediction such as TFS system. However, as indicated by Jeng et al. [22], due to the rapid development of TC intensity that will affect the movement in severe weather, TC intensity and track-mining process are always subject to certain degree of inaccuracy. In these situations, human justification is adopted.

## **1.4 Dvorak Techniques**

In view of the various meteorological phenomena interpreted from satellite pictures, we note that one of the most remarkable contributions of meteorological satellite is the

identification of tropical cyclones and extra-tropical cyclones. However, while shipping interests are pleased to know about the location of tropical cyclones, they also need to know the wind speed and intensity so that they can keep their ships at a safe distance.

The most important technique for estimating winds in tropical cyclones was developed by Dvorak [5, 6] in 1975. From his theory, each tropical cyclone goes through a life cycle that may be classified into one of several types by its appearance in visible images. Figure 1.2 shows the Dvorak Tropical Cyclones templates from T1 to T8, each T-number with eight sub-categories corresponding to eight different possible appearances of the TC patterns [5]. In general, the T-number of the observed storm can be determined by detailed examination of the images following a decision tree (shown in Figure 1.3 [5]) and by guidelines on the expected day-to-day change of storm patterns.

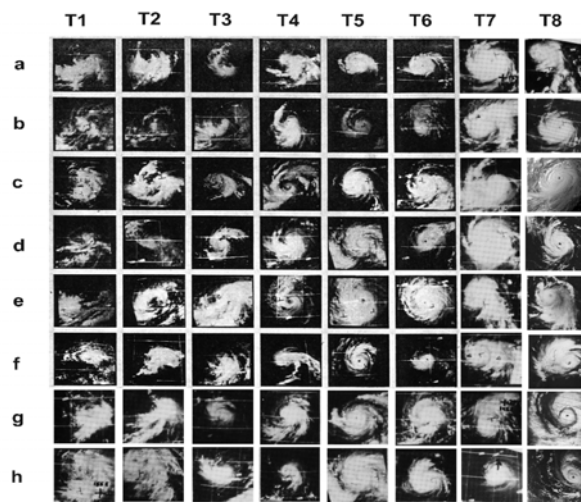


**Figure 1.2:** Dvorak TC templates, with number assigned from T1 to T8

Apart from the T-number, “Current Intensity” (CI) number can also be determined, which is related to storm’s maximum sustained surface wind speed. In 1984, Dvorak [23] introduced a variant of the above technique, called the enhanced infrared technique (EIR technique), which uses specially enhanced infrared images instead of the visible ones. This, of course, allows intensity estimates to be made at night. Nowadays, Dvorak technique is still the worldwide-agreed standard for the determination of TC intensity. But due to the highly variation of TC patterns, the visible and enhance infrared Dvorak

techniques are subjective which require professional training to be done effectively for good wind estimates. Lastly, by using the EIR Dvorak technique, and based on the contrast of the equivalent blackbody temperature of the eye of the storm against the average equivalent blackbody temperature of the surrounding cloud shield, meteorological analysts can probably estimate the T-number from these two parameters using a lookup table.

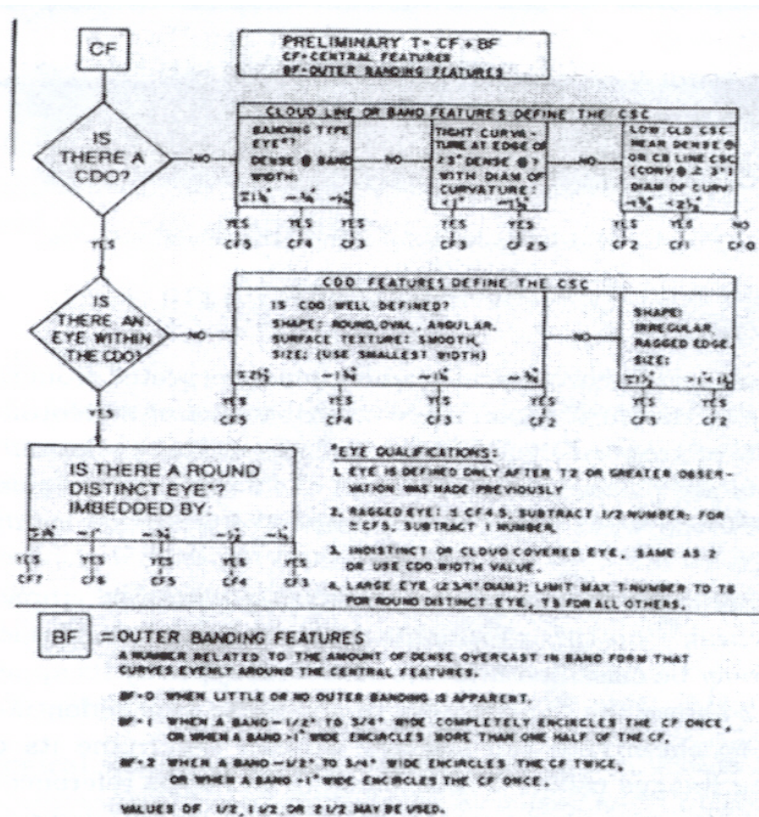


Figure 1.3: Decision tree used to determine T-number (Dvorak [5])

## 1.5 Time-series prediction and neural network forecasting

The analysis of experimental data that have been observed at different points in time leads to new and unique problems in statistical modelling and inference. The obvious correlation introduced by the sampling of adjacent points in time can severely restrict the applicability of the many conventional statistical methods traditionally dependent on the assumption that these adjacent observations are independent and identically distributed.

The systematic approach by which one goes about answering the mathematical and statistical questions posed by these time correlations is commonly referred to as time series analysis.

Many of the most intensive and sophisticated applications of time series methods have been to problems in the physical and environmental sciences. This fact accounts for the basic engineering flavor permeating the language of time series analysis. One of the earliest recorded series is the monthly sunspot numbers studied by Schuster (1906). More modern investigations may focus on whether a warming trend is present in global temperature measurements or whether levels of pollution may influence daily mortality. Geophysical time series such as those produced by yearly depositions of various kinds can provide long-range proxies for temperature and rainfall. Seismic recordings can aid in mapping fault lines or in distinguishing between earthquakes and nuclear explosions.

Time series pattern learning and prediction have been studied extensively over the past decades [20, 39]. Neural networks, as sophisticated predicting models, have proven to be promising methods for time series predictions owing to their nonlinear and distributed characteristics. Vast researches ranging from financial prediction to weather forecast have been conducted in recent years. Conventional neural network model such as feed-forward back-propagation (FFBF) network is a typical supervised learning model that is well suited to this kind of problems. However, in a temporal time series prediction problem such as approximating the TC intensity and track associated movement, for which the conventional neural network architectures and algorithms cannot incorporate with the up-coming sample sequence, therefore it fails to give accurate prediction results. In temporal time series problems, each time step of a sequence only incurs part of the final results, so the predictive outcomes can only be achieved after several time steps later. The other neural net approach that is commonly used for time series prediction is recurrent network [76]. In a fully recurrent network approach, such as the back-propagation-through-time (BPTT), learning is done through adjustment of errors regularly back propagate all the way through the initial time.

## 1.6 Contributions of the Thesis

In this research, our aim is to study the problem of Tropical Cyclone (TC) intensity mining on the principle, possible application and limits of some methods, for the construction of intensity forecasting model from a series of satellite data. The whole study can be divided into two subparts based on different methodologies adopted in the research: 1) satellite image interpretation forecasting; 2) regression neural network forecasting; each of which contains more subtasks as listed below:

- 1) **Satellite Image Interpretation Forecasting:** It includes feature extraction, pattern recognition and matching. In feature extraction part, there contains two subtasks, data collection and feature extraction. As more and more researchers have published their research works in the Web, it has been much easier to access time series satellite images of typical tropical cyclones. NOAA (National Oceanic and Atmospheric Administration) [24] is one of good Internet sources where high-resolution time series TC satellite images can be freely downloaded. For feature extraction, we focus on extracting the cyclones from satellite images in our study, and other features such as sea level pressure, wet or dry bulb temperature, wind speed and direction, and so on can be acquired separately from supplementary documents (from NOAA or Hong Kong Observatory). The Gradient Vector Flow (GVF) snake model [25] is used to extract the contour points of a dominant tropical cyclone contour from the satellite images. After the cyclones have been successfully extracted out, two another subtasks are being followed: pattern recognition and matching scheme. In this study, we propose an integrated approach for tropical cyclone comparison based on typical spiral shapes using time warping technology. We retrieve the similarity of two shapes to do matching using angle features found among the successive contour points. Furthermore to achieve a better reflection of the spiral shape of tropical cyclones, we adopt a time warping concept to result in a fast and accurate comparison.

- 2) **Regression Neural Network Forecasting:** The main contribution of this part is to

develop and implement an algorithm based on climatology, persistence and synoptic observations, incorporating neural networks algorithms with multiple linear regression model to predict the TC intensity changes at certain intervals of time (6, 12, 18, 24 hours). We have accomplished the following specific objectives.

- i. Implement a model to predict TC intensity changes at certain time intervals.
- ii. Create an interactive database with TC historical records.
- iii. Develop a random variable selection scheme to identify the variables that explain better the relationships between the inputs and output of a nonlinear dynamic system.
- iv. Test the capability of the neural networks as a tool to model highly non-linear processes such as the TC intensity process.
- v. Test the capability of the proposed method to model the fast intensification, rapid reduction and re-intensification phenomena of tropical cyclones.
- vi. Analyze the contribution of meteorological variables to the proposed neural network model and investigate the relationships between those variables and the intensity.

## **1.7 Organization of the Thesis**

The remaining parts of this thesis are organized as below. In chapter 2 we illustrate relative research works in recently years, including physical principle models, and imagery interpretation and neural network models. Then in chapter 3, 4 and 5, we describe three novel forecasting models to predict intensities of the tropical cyclones. They are a satellite interpretation based tropical cyclone forecasting system; an integrated neural training based tropical cyclone forecasting system; and a similarity retrieval model for time-series tropical cyclone data. In each chapter, detail algorithms and experimental results are given as well and shown that our proposed approaches are promising ones. At last in Chapter 6, we conclude the thesis and illustrate the limitations and the future works for each model.

# Chapter 2. Related Works

In recent years, lots of research efforts have been devoted to Tropical Cyclone (TC) forecast, such as scatterometer techniques [2], microwave radiometric [3], QuikSCAT [4], imagery interpretation [24], neural network forecasting [25] and so on. As it needs highly expert information about those special equipments if the forecast is carried out using physical principles, imagery interpretation and neural network forecasting, assisted by miscellaneous information, become a more and more popular approach to achieve TC forecasting for computer-science background researchers. In this section, we are aiming to describe the theories and arguments used in this study. A Literature review of the most important contributions for the TC intensity field is given.

## 2.1 Physical Principle Models

### 2.1.1 CLIPER

Hope et al. [26] developed the first operational model called HURRAN (HURRICANE ANalog). By identifying previous storms that had characteristics in common with a current storm, HURRAN attempted to predict the most likely track of the current storm. Nuemann [27] introduced a model to predict hurricane tracks based on climatology and persistence called CLIPER (CLImatology and PERsistence). This model was the first operational model that used these kinds of variables for prediction. The persistence variables assumed that the integrated effects of all forces, which have steered the storm during some past period, would continue to predominate during some future period. In general, persistence is taken as the smoothed motion of the tropical cyclone in the past 12- or 24- hour period. The persistence forecast is then the linear extrapolation of this motion for the next 12, 24, 36, and 72 hours. The problem with this type of forecast is that a higher order of persistence forecast requires a better knowledge of actual and past weather conditions. On the other hand, a climatological forecast makes use of the temporal and spatial repetitiveness of TC tracks produced by synoptic patterns, the

simultaneous observation of pressure, temperature, wind and other meteorological parameters [8].

### **2.1.2 SHIFOR**

Using a similar set of variables used by CLIPER, Jarvinen and Neuman [28] developed an intensity prediction model called Statistical Hurricane Intensity Forecast (SHIFOR) which is used to predict the future intensity of the storm at 12-hour periods up to 72 hours. The prediction variables included: Julian day, initial storm intensity, intensity change during the past 12 hours, initial storm latitude and longitude, and zonal and meridional components of the storm motion vector. Ten predictor terms are included in each equation; these are usually second and third order products of the seven primary predictors listed above. The most important terms are the current intensity, the 12 hour intensity change, the Julian day and the latitude. The SHIFOR equations were developed using data from all historic storms during the period 1900 – 1972 that were at least 30 nautical miles from the land. Thus, the SHIFOR intensity forecasts are not valid for storms less than 30 nautical miles from the coast.

### **2.1.3 SHIPS**

It was in the 1980's when several authors recognized the importance of synoptic data in the prediction of storm intensity. The concept of synoptic data is used to represent simultaneous observation of atmospheric variables at different spatial geographic extensions. Demaria and Kaplan presented their model called Statistical Hurricane Intensity Prediction Scheme (SHIPS) [1], a statistical-synoptic model, which was an improvement over SHIFOR because the authors were able to show that the average intensity error is 10-15% less than the error from a model that used only climatology and persistence.

In 1999, an update of SHIPS was presented by Demaria and Kaplan [29]. This version was considered as a “statistical-dynamical” model because data obtained for the first

version from global model analysis was removed and synoptic predictors from a numerical model were added. This model was developed using standard multiple regression techniques with climatological, persistence, and synoptic predictors. Estimates of future storm intensity are made for 12-hr periods up to 72 hours. The primary predictors used in the prediction are (1) Intensity potential (the difference between the current storm intensity and an estimate of the Maximum Possible Storm Intensity determined from the sea surface temperature); (2) the vertical shear of the horizontal wind in the 850 – 200 millibar (mb) layer; (3) persistence (intensity change in previous 12 hrs); (4) average 200 mb temperature; (5) average 200 mb east wind component; (6) average 850 mb vorticity; (7) day of the year; and (8) the flux convergence of eddy angular momentum evaluated at 200 mb.

#### **2.1.4 STIPS**

Knaff, DeMaria and Sampson introduced a new statistical intensity model called **Statistical Typhoon Intensity Prediction Scheme (STIPS)** that was made operational at the JTWC in 2002 [30]. Development of the STIPS model closely follows the development of the SHIPS model for Atlantic and Eastern Pacific tropical cyclone basins. STIPS is a multiple linear regression model where the dependent variables are the intensity change from the initial forecast time at 12-hour intervals. As a result, there are 10 predictive equations for the 10 time periods, 12-h through 120-h forecasts. Potential predictors (independent variables) are created using current TC conditions, current TC trends, and the Navy Operational Global Atmospheric Prediction (NOGAP) analyses. The predictors are evaluated for their combined ability to predict tropical cyclone intensity change.

#### **2.1.5 STD5**

Knaff, DeMaria, Sampson and Gross presented the newly developed TC intensity models STD5 (Statistical, 5Day Tropical Cyclone Intensity Forecasts model) that extend the official forecasts of both track and intensity to 5 days [31]. The models utilize the

CLIPER approach to make forecasts through 5 days for Atlantic, eastern North Pacific, and western North Pacific basins. Results using independent input data show that these new models possess similar error and bias characteristics when compared with their predecessors in the North Atlantic and eastern North Pacific but that the west Pacific model shows a statistically significant improvement when compared with its forerunner.

In this decade, the use of satellite data has brought a new beginning to hurricane research. DeMaria developed new improvements to the SHIPS model. Data from **Geostationary Operational Environmental Satellites (GOES)** infrared imagery (10.7  $\mu\text{m}$ ), identified more specific brightness temperatures which were previously azimuthally averaged on a 4 km, storm-centred radial grid, and Ocean heat content (OHC) data which at some depth of the ocean is important for tropical cyclone intensity changes.

### **2.1.6 GFDL**

The **Geophysical Fluid Dynamic Laboratory (GFDL)** developed a model known as GFDL model which belongs to the third category of hurricane intensity models and it was developed specifically for hurricane tracking and hurricane intensity prediction [32]. It includes 18 sigma levels and uses a horizontal finite-difference method with three nested grids. The two inner grids move to follow the storm, and the resolution of the inner domain is 1/6 degree. The GFDL model includes convective, radiated and boundary layer parameterizations and has a specialized method for initializing the storm circulation. The initial and boundary conditions are obtained from the Aviation run of the **Medium Range Forecast (MRF)** model. The representation of the storm circulation in the global analysis is replaced with the sum of an environmental flow and a vortex generating by nudging the fields in a separate run of the model to an idealized vortex. This idealized vortex is based upon a few parameters of the observed storm. The environmental flow is the global analysis modified by a filtering technique that removes the hurricane circulation. The forecasts from the interpolated GFDL forecasts are known as the **Geophysical Fluid Dynamic Intensity (GFDI)** model.

### **2.1.7 AMSU**

Kidder et. al. [33] has described the potential of the **Advance Microwave Sounding Unit** (AMSU) and how it can be used to predict hurricane intensity. A relationship between temperature anomalies and both the surface wind speed and central pressure of tropical cyclones was found. In general, the temperature anomalies closely follow both the wind speeds and the pressures. Gaps in the data are caused by the storm being located between orbital swaths or by missing AMSU data. Correlating intensity versus maximum temperature yields a correlation coefficient of 0.84 and a standard error of 19 kt. Correlating central pressure versus maximum temperature yields a correlation coefficient of 0.86 and a standard error of 12 hPa.

## **2.2 Imagery Interpretation and Neural Network Models**

In addition to the above prediction models, there are other approaches to predict the tropical cyclone intensity. Using satellite imagery and neural networks are two of the most popular and effective approaches.

### **2.2.1 Dvorak Techniques**

Dvorak [5, 6] has provided a reliable method to estimate TC intensity manually from visible and infrared (vis/IR) satellite imagery by using subjective pattern recognition and a set of applicable rules. Meteorological analysts rely on the Dvorak technique to produce initial intensity estimates, and it can also be used to produce intensity forecasts. In this pattern recognition technique, tropical cyclone intensity change is deduced from successive estimates of intensity fitted to climatological deepening and filling models. However, the use of this technique in operational intensity forecasts has occasionally resulted in substantial errors as this technique is subject to human justification. The Dvorak technique is also limited to producing intensity forecasts up to 24 h. Velden et al.

[9] introduced an objective Dvorak technique (ODT) to eliminate much of the subjectivity in the standard Dvorak method.

One of the main limitations of the Dvorak technique (and any vis/IR technique) is that low- and upper-level clouds can obscure mid-level clouds. Unknown low-level structure and circulation make estimating intensity and locating the circulation center difficult. For **Special Sensor Microwave Imager (SSM/I)** passive microwave channel images, most upper-level (non-precipitating) clouds are essentially transparent. Using SSM/I images to examine TC structure has an advantage when compared with the limitations of other types of imagery. Rain bands and a TC center (when it exists) can be seen in the 85-GHz channel images when upper-level clouds as seen in IR imagery often obscure the banding structure. Richard and Paul [34] developed an automated method to estimate tropical cyclone intensity by using extracted characteristics from SSM/I imagery.

### **2.2.2 EDGLM**

In [35], Lee and Liu proposed an Elastic Graphic Dynamic Link Model (EDGLM) to automate the satellite interpretation process and provide an objective analysis for tropical cyclones. It integrates Dynamic Link Architecture (DLA) for neural dynamics and Active Contour Model (ACM) [36] for contour extraction of tropical cyclone patterns. The idea of Dynamic Link Architecture was first proposed by C. von der Maslburg [37] in 1981 in the “Correlation Theory of Brain Function”, where he condensed the whole idea into a separate neural network framework by extending the synaptic plasticity theory of brain model. One of the powerful features of DLA is the flexibility and robustness for invariant pattern recognition. And most remarkable feature of this approach is that the pattern-matching scheme under this architecture is inherently invariant under various transformations such as translation, relation, reflection, dilation and distortion. The deficiency of the EDGLM approach is that it is highly dependent on satellite image processing, with lack of other important meteorological properties of tropical cyclones, such as mean sea level pressure, wind direction and speed at different levels for TC

movement, intensity changes and so on. This limitation determines the faultiness of EGDLM in TC tracking mining.

### **2.2.3 NOEGM**

In [25], Lee and Liu proposed an extended integrated neural network-based tropical cyclone identification and track mining system, based on their previous research work [35], which consists of two main modules: 1) TC pattern recognition system from satellite pictures known as neural oscillatory elastic graph matching (NOEGM) model, a neural network-based model that involves the automatic TC pattern segmentation and elastic pattern matching [38] from the predefined TC template, a process that simulates human TC identification technique known as Dvorak analysis [5, 6]. 2) A time series TC intensity and track mining system using a hybrid radial basis function (HRBF) network [39], a neural network time series prediction model that integrates the conventional RBF network with time difference and structural learning (TDSL) [40] techniques.

The NOEGM model itself involves three main modules: 1) Multi-frequency bands feature extraction from satellite imageries using Gabor filters [41]; 2) automatic figure-around TC pattern segmentation using composite neural oscillatory model, and 3) TC pattern matching using elastic graph dynamic link model. As an extension to traditional neural oscillator models [42, 43], a composite neural oscillator [44] is proposed to segment colour scene images into individual figure objects. Unlike the traditional models, a composite “Trinity” neuron oscillator model with common inhibitory neuron is employed to safeguard global phase locking of composite neural oscillators, which stimulate the visual cortex [45] of colour image perceptions. The proposed hybrid RBF network in [25] incorporates two main technologies into the conventional RBF network for temporal time series prediction problem: 1) structural learning technique that integrates the “forgetting” factor into the RBF BP algorithm; 2) a time difference with decay method is incorporated into the network to strengthen the temporal time series relation of the input data sequence for network training.

Although NOEGM model has enhanced the EDGLM model, by integrating various elements of tropical cyclones into a hybrid RBF neural model, it still needs to be further enhanced, especially in these two aspects. Firstly, relationships between successive satellite pictures can be generated to recognize the TC pattern and mine the time series development. Secondly, interactions of multiple TC systems within the same satellite images should be taken into account, as another one in the same region may influence the movement of one tropical cyclone.

#### **2.2.4 Two-dimension Wavelet Decomposition**

Wavelet analysis has been widely applied in the area of signal processing, image processing and pattern recognition with encouraging results [46]. Wavelet transform is chosen to be used in image frequency analysis and image decomposition because 1) by decomposing an image using wavelet transform, the resolutions of the sub-band images are reduced. In turn, the computational complexity will be reduced dramatically by working on a lower resolution image; 2) Wavelet decomposition provides local information in both space domain and frequency domain [47]. Liu et al. [48] proposed a new approach on automatic tropical cyclone detection from satellite images by using wavelet multi-resolution analysis [49]. Low and high frequencies signals are extracted from the satellite images for the segmentation and recognition processes. Genetic algorithm [50] was also applied for searching and finding the proper spiral shape. After the type of TC is identified, an enhanced RBF neural network is used in discovering the TC moving track. The Wavelet Decomposition module makes use of 2D wavelet analysis to decompose the image into higher frequency and lower frequency signals. The Image Segmentation module extracts all possible cyclone locations by using the lower frequency signal from the image. The higher frequency signal is used for analyzing the spiral feature. For the TC moving track discovery, an enhanced RBFNN is used. The disadvantage of Wavelet analysis is very obvious that it cannot solve the problem of multiple cyclones within the same satellite images. The proper number of levels of wavelet decomposition is not easy to decide, which leads to the inaccuracy for the

prediction. Lastly, the eye of the cyclone may not be located precisely as it only considers the processing on satellite image itself.

### **2.2.5 Case-based Forecasting**

In [51], Pedro and Burstein proposed a multi-stage framework for combining case-based reasoning (CBR) and fuzzy multi-criteria decision making (FMDM) with the aim of building a model for intelligent decision support and carrying an application to Tropical Cyclone forecasting, which was proved to be successful. The proposed multi-stage framework is an extension of a two-stage task-based framework for CBR that uses FMDM technique to solve the case selection problem in CBR. It consists of three stages, namely: 1) Stage 0: Case representations; 2) Stage 1: Case selection; 3) Stage 2: Case adaptation and retention. To apply the proposed framework to Tropical Cyclone forecasting, Pedro and Burstein considered a particular stage of Hurricane Alberto [52] as a current TC case. Given the past 24 hours observation of Alberto on its latitude, longitude, minimum central pressure (MCP) and maximum sustained winds (MSW), its track position for the next 3 days can be predicted by selecting the best analog from the case bases from the past tropical cyclones.

In stage 0, the cases are represented in terms of multiple attributes, multiple criteria and the order of importance. For similarity assessment, track positions are considered as first most important attributes and rack position, MCP and MSW as second most important set of attributes. The criteria for evaluating the usefulness of the past cyclones are synoptic history, meteorological statistics, and forecast critique and satellite image. In stage 1, a subset of past tropical cyclones is selected to depict similar past 24-hour track position. Fuzzy measure for “slightly similar”, “similar” and “very similar” are defined in terms of great circle distance between the track positions of past cases and track position of the current tropical cyclone. For example, a past tropical cyclone with slightly different structure as the current tropical cyclone may be regarded as either “slightly useful” or “useful” or “very useful” to the current situation. A past tropical cyclone that had been predicted with large errors may be “very useful” to the current situation, potentially

indicating the difficulty of predicting the future location and intensity of the current cyclone. In stage 2, these superior cases are then weighted accordingly and a weighted mean of attributes of the corresponding superior cases determine the position and intensity forecasts for all leads time.

The case-based approach for TC forecasting has its obvious advantage at present stage, if it can be further improved by enhancing knowledge acquisition, reuse and creation, capturing experts' knowledge, learning from past experience and imparting such knowledge for future decision making. Also, comparing with other proposed TC forecasting models should be included in the case-base forecasting approach.

### **2.2.6 TC Eye Location**

Tropical Cyclone (TC) eye fix is often done manually in practice. Forecasters estimate the center location by tracing the movement of spiral rain bands using consecutive remote sensing images, or by overlaying spiral templates on remote sensing images for the best match [53]. These techniques are intuitive to forecasters since they are trained to identify the spiral structure of TCs, but are not completely objective.

In contrast, automated TC eye fix methods often employ objective measures. Major approaches include wind field analysis and pattern matching. In wind field analysis, motion estimation techniques are applied on adjacent frames of images to construct a motion vector field. Examples include the use of the TREC (Tracking Radar Echoes by Correlation) algorithm [54] or automatic cloud features tracking technique [55]. The TC center is found by analyzing the motion field [56].

For pattern matching, the TC eye is fixed by finding the best match of a predefined TC model, whose parameters are estimated from remote sensing data. A method that is applicable to ideal TCs [57] identifies shear patterns of large axisymmetric wind circulation systems to fix the TC eye. As another example, in [58], the spiral rain band of a TC is modelled by the equation  $r = ae^{\theta \cot \alpha}$ , where  $a$  and  $\alpha$  are found by transformation

techniques. Templates generated by the estimated parameters are used to match against radar images at plausible latitude-longitude positions. An alternative method for finding spiral parameters involves the method of least squares [59].

These eye fix methods require computationally expensive operations such as wind field or motions vector field construction, parameter estimation using searching algorithms, and extensive block or object matching. With the large volume and rate of data, this problem is often solved using mainframe computers or clusters to generate timely results. Yip and Wong [60] provided more details on the eye fix method using genetic algorithm. Rather than using traditional gradient ascend algorithms to search for the location of best match, genetic algorithm is used to speed up the search and to break out the local maxima. A time-honored technique of manual TC eye fix is to overlay spiral templates on a printout of remote sensing image for the best match of the spiral rain bands. Yip and Wong automated this process by choosing a simple model of TC and doing the match using genetic algorithm. Wang et al. [59] advanced a new system to locate the tropical cyclone center based on the satellite imageries, by putting forward several center location technologies based on tropical cyclone's structure, the whirl and the whole movement. Some logarithmic helix is adapted in [61] to fit part of the cyclone feature cloud and the center of the helix can be considered as the center of the cyclone. Meanwhile, according to the cyclone's movement feature, a rotation matching method is presented, where the rotation center point is just the tropical cyclone center.

Although [59] and [60] have proposed two effective and efficient approaches for TC eye fix problem, there are still several difficult but important issues unsolved or ignored for fixing the eye. In [59], the method is only suitable for the tropical cyclone in mature status and only small distortion is covered, otherwise the objectivity and precision will be greatly degraded, which has already been examined by experiments. And in [60] the authors only considered the geographical position of a tropical cyclone, based on which the genetic algorithm was applied to deduce the eye location. If the tropical cyclone in the pre-processed satellite image is not a regular shape in which the swirl rainband and polar equation can be applied, the deduced result is highly suspected.

# **Chapter 3. A Satellite Interpretation Based Tropical Cyclone Forecasting System**

The most popular approach to compare two given Tropical Cyclones (TCs) is to measure the distances between various contour points of the tropical cyclones extracted from satellite images. However, this measure has a very high computational cost as it involves large amount of point-to-point calculations. Moreover, this measure does not reflect the most important characteristic of a tropical cyclone, spiral shape feature, during the comparison of two images. In this section, we illustrate our research efforts upon developing an effective and efficient TC forecasting system based on TC's typical spiral shapes using time warping technology. Dvorak templates are used as the references to determine the intensity of the tropical cyclone to be predicted. Experimental results have proven that our approach is better than other conventional comparison approaches such as modified Hausdorff distance measure.

In this part, at first an introduction with the system framework is given including three module layers. Then an introduction is provided to talk about the Active Contour Model, which is very popular and has been widely applied for feature extraction in this system. After that, a sequential neighbour checking algorithm is described to select the dominant cyclone from all cyclones appearing in the satellite image. Then, a point weight-assigning algorithm, including an eye location method, is introduced to determine the significance of each point on the TC contour according to its distance to the located eye. The remaining part of this chapter focuses on how we make use of the angle features to carry out prediction using dynamic time warping technique. The last section provides the evaluation of the system.

## **3.1 Introductions and System Framework**

Cloud patterns exhibit considerable variation and there currently exist very few scene analysis techniques that would allow the efficient isolation and extraction of cloud systems from satellite images. Consequently, research into tropical cyclone pattern matching using Dvorak analysis has largely relied on subjective human justification. It should also be noted that the shapes and features of atmospheric systems as observed in remotely sensed satellite imagery are inherently ambiguous and this is reflected in ambiguity or fuzziness in the image processing. Recently, there has been considerable research into the extraction and comparison of time series objects from images and, more generally, shape matching. Pang et al. [6] presented a novel method for resolving the occlusion of vehicles seen in a sequence of traffic images which was able to extract the vehicle shape, represented as a cubical model, out of the background ignoring the effect of shadows and visual artefacts. In [7], Kamberov et al. developed a new conformal method for quantitative shape extraction from unorganized 3D oriented point clouds. This method evaluates empirical performance using synthetic, ground truth data and by comparison with other quantitative extraction methods.

In this chapter then, we propose a comparison algorithm, angle feature matching, which is novel in that it makes use of the distinctive spiral features of tropical cyclones. As it is very difficult to define cyclones and to directly compare their shapes, we adopt an approximation method that compares pairs of corresponding angles formed by three adjacent contour points taken from each cyclone. We choose to measure these angles because they control the cyclone's shape internally. We extract the active contour points of the cyclones using the popular active GVF snake model [14] and determine the distance between two sets of angles using a time warping algorithm. The particular advantage of time warping is that it allows the matching of similar yet out-of-phase sequences, or even the sequences of different lengths. In recent years, a great deal of work has been done on efficient searching and indexing of time warping. In [16] authors provided a new definition of similarity by regarding a time series as a multi-dimensional position vector, thus allowing any scaling and shifting operation on the sequences to be regarded as, respectively, vector multiplication and vector addition. In [17] authors suggested a method for handling subsequence matching. The sequences are divided into

pieces and the distance between any two sequences is the sum of the time warping distance between each two pairs of pieces. Our publications related to this chapter can be referred to [Publication 3,5,7], in which major images and tables in this chapter can also be found.

To implement our proposed matching approach, we designed a three-layer prototype, which includes an Extraction Module, an Angle Calculation Module and a Time Warping Matching Module. Figure 3.1 illustrates the flow of the system architecture in detail. The Extraction Module is tasked with picking up from the satellite images the dominant points which depict the contours of a tropical cyclone. The Angle Calculation Module then assigns a weight to every contour point based on its distance from the eye of the cyclone. All contour points from each image are then used to calculate a set of angles for comparison. The Time Warping Matching Module then uses the angle sets to finally retrieve the best-matched image from the template set.

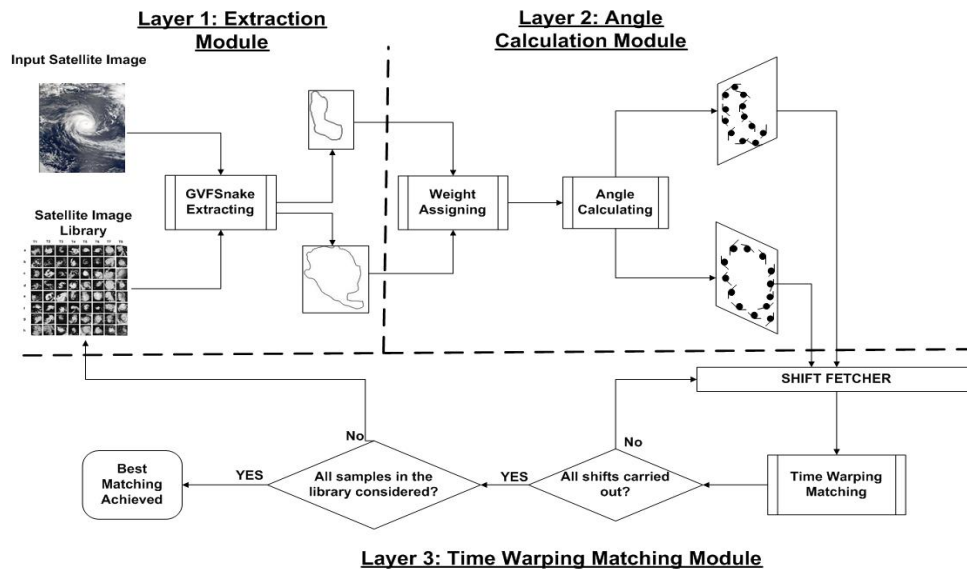


**Figure 3.1:** System architecture of a three-layer prototype

### 3.2 Active Contour Model

As a pre-processing step towards the tropical cyclone recognition, we need to extract patterns and detect contours from satellite images. In this chapter, an instance of the Active Contour Mode, GVF snake mode is used to achieve this target. The main

advantage of using such a snake model is that it allows the using of an initial contour estimation to overcome photometric abnormalities such as contour gaps, hidden contours, or edge points due to noise and texture. A scene of satellite picture with active contour extracted out is shown in Figure 3.2 for illustration. In this study our focus is to mine the shapes of two tropical cyclones and propose a prediction model. As a result, we assume that this is an acceptable tolerance in our research.

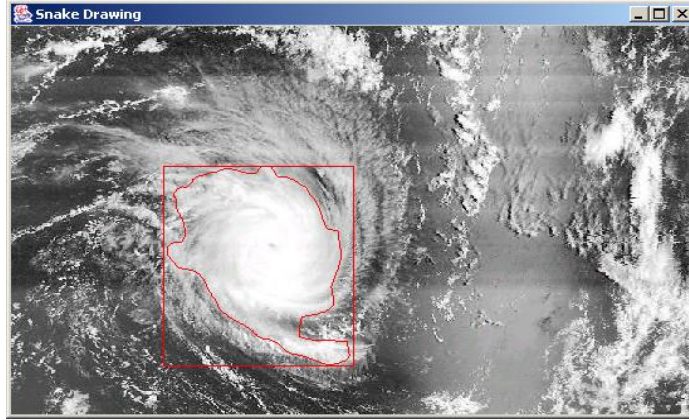


**Figure 3.2:** Contour mapping on a satellite image

Active contours are defined as energy-minimizing splines under the influence of internal and external forces [3]. The internal forces of the active contour serve as a smoothness constraint designed to hold the active contour together and to keep it from bending too much. The external forces guide the active contour towards image features such as high intensity gradients. The optimal contour position is computed such that the total energy is minimized. Let the active contour be given by a parametric representation  $v(s) = (x(s), y(s))$ , with  $s$  as the normalized arc length of the contour. The expression for the total energy can then be decomposed as follows:

$$E_{total} = \int_0^1 E(v(s))ds = \int_0^1 [E_{int}(v(s)) + E_{image}(v(s)) + E_{con}(v(s))]ds \quad (3.1)$$

where  $E_{int}$  represents the internal forces which encourage smooth curves,  $E_{image}$  represents the local correspondence with the image function, and  $E_{con}$  represents a constraint force that can be included to attract the contour to specific points in the image plane. The  $E_{int}$  is:

$$E_{int}(v(s)) = \alpha(s) \left\| \frac{dv(s)}{ds} \right\|^2 + \beta(s) \left\| \frac{d^2v(s)}{ds^2} \right\|^2 \quad (3.2)$$

where  $||$  is the Euclidean norm. The first order continuity term, weighted by  $\alpha(s)$ , makes the contour behave elastically, while the second order curvature term, weighted by  $\beta(s)$ , makes it resistant to bending. The use of internal energy allows active contours to interpolate gaps in the edge phenomena known as subjective contours. The image energy term derived from the image data over which the active contour lies is  $E_{image}$ . This is constructed to attract the active contour to desired feature points in the image, such as edges and lines.  $E_{image}$  can be associated with a potential  $P(x, y)$  which can be defined in terms of the gradient module of the image convoluted either by the Gaussian function:

$$P(x, y) = -|\nabla(G(x, y) * I(x, y))| \quad (3.3)$$

or as a distance map of the edge points:

$$P(x, y) = -e^{-d(x,y)^2} \quad (3.4)$$

where  $d(x, y)$  denotes the distance between the pixel  $(x, y)$  and its closest edge point. Potential forces move the snake and it tries to fall into a valley as if it were under the effect of gravity. In this chapter, we use the Gradient Vector Flow (GVF), one instance of the Active Contour Model, as it has the ability to both inflate and deflate the contour, to deform to concavities, and to increase the capture range of the external forces. The external force is computed as a diffusion of the gradient vectors of an image, without blurring the edges. Xu and Prince [62] defined the GVF field to the vector field  $v(i,j)=(u(i,j),v(i,j))$  which is updated with every iteration of the diffusion equations, as in the following Equations 3.5 and 3.6.

$$u_{i,j}^{n+1} = (1 - b_{i,j})u_{i,j}^n + (u_{i+1,j}^n + u_{i,j+1}^n + u_{i-1,j}^n + u_{i,j-1}^n - 4u_{i,j}^n) + c_{i,j}^1 \quad (3.5)$$

$$v_{i,j}^{n+1} = (1 - b_{i,j})v_{i,j}^n + (v_{i+1,j}^n + v_{i,j+1}^n + v_{i-1,j}^n + v_{i,j-1}^n - 4v_{i,j}^n) + c_{i,j}^2 \quad (3.6)$$

The initial values of  $u$  and  $v$  are the gradient values.

$$b_{i,j} = G_i(i, j)^2 + G_j(i, j)^2 \quad (3.7)$$

where  $G_i$  is the first element of the gradient vector and  $G_j$  is the second element. The variables  $c_{i,j}^1$  and  $c_{i,j}^2$  in Equation 3.5 and 3.6 are derived by following calculations:

$$f(i, j) = -E_{ext}(i, j)$$

$$u_t(i, j, t) = u \nabla^2 u(i, j, t) - [u(i, j, t) - f_i(x, y)] * [f_i(i, j)^2 + f_j(i, j)^2]$$

$$u_i(i, j, t) = u \nabla^2 u(i, j, t) - b(i, j)u(i, j, t) + c^1(i, j)$$

## 3.3 Matching Methodology

### 3.3.1 A Fast Sequential Neighbour Checking Algorithm

The GVF snake model is applied not only on the input satellite images, but also on the Dvorak template images. As more than one tropical cyclone may appear in the satellite image, we select only the dominant cyclone, that is, the one with the largest area. The boundary edge points of the extracted cyclone are then recorded in the library database for future reference. To achieve this, we propose a fast algorithm called Sequential Neighbour Checking, which proceeds by first checking a single pixel within the tropical cyclone, then checking its neighbours and each neighbour's eight neighbours to see whether they also belong to the designated tropical cyclone. This allows every pixel within the same cluster of the tropical cyclone to be correctly examined. We have 50 contour points for each TC, which is supposed to be enough to represent the basic boundary of a TC in our study. Figure 3.3 gives the clustered result and Figure 3.4 provides the pseudo-code of this algorithm.

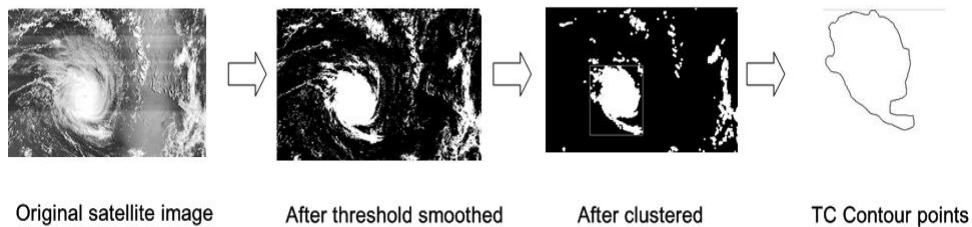


**Figure 3.3:** Clustered result for a sample tropical cyclone

```
Convert the image into Binary format: BI
Procedure CheckNeighbor (x,y)
1. For each pixel P1 (x1, y1) within BI
2.   If gradient of P1 is white
3.     Set P1 to black
4.     For each right (Up or Down) neighbor P2 (x2, y2) of P1
5.       If gradient of P2 is white
6.         CheckNeighbor (x2, y2)
7.       End If
8.     End For
9.     For each left (Up or Down) neighbor P3 (x3, y3) of P1
10.      If gradient of P3 is white
11.        CheckNeighbor (x3, y3)
12.      End If
13.    End For
14.  End If
15. End Procedure CheckNeighbor (x, y)
```

**Figure 3.4:** Procedure of sequential neighbour checking algorithm

After extracting the contour points of the dominant cyclone, the Angle Calculation Module starts and, to locate the positional centroid of the tropical cyclone, an Eye Location algorithm is proposed. Different weights are then calculated and assigned to different contour points, based on their distance to the cyclone eye. A sequence of angles is then formed between every three consecutive points on the contour. Using these sets of angles, as well as the associated weights, the Time Warping Matching Module then retrieves the best-matched image from the template set. A shift fetcher is designed to work as a rotator, comparing two cyclone contours in all possible rotations.

### 3.3.2 Tropical Cyclone Eye Location

One of the most characteristic features of a tropical cyclone is its spiral shape. This shape can be represented using the active contour points extracted from the satellite images but GVF extraction is not able to reflect the internal helix structure of a tropical cyclone. Using shapes can reduce the accuracy of the prediction. It is very difficult to detect the eye of a tropical cyclone using image processing techniques, as the location of the cyclone eye is related to many other factors, for example, intensity, speed, and acreage. In this paper, given a tropical cyclone contour, we aim to find its positional centroid. Here, to detect the positional centre point  $O$ , we first introduce the definition of a pixel distance algorithm. This concept is illustrated in Figure 3.5.

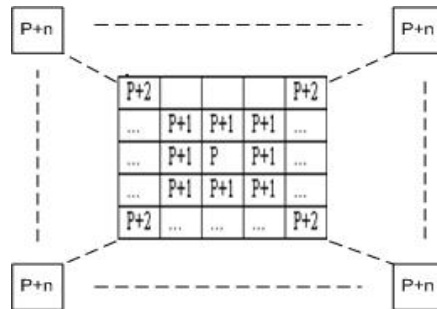


**Figure 3.5:** A pixel distance algorithm

The pixel distance algorithm is implemented using an intermediate clustered image, like the middle image in Figure 3.3. All the pixels in a clustered image are either black or white. We set the pixel distance of  $P$  to  $1$  for every pixel  $P$  within the tropical cyclone, that is, for all pixels belonging to the largest cyclone shape in the image, so long as all of its eight neighbours (pixels in positions  $P+1$  in Figure 3.5) have the same gradient values.

Accordingly, if the pixels in positions of  $P+1$  to  $P+n$  all have the same gradient values, the pixel distance of  $P$  is set to  $n$ , otherwise the distance is set to  $n-1$ . In this way, it is possible to find the location centroid  $O(x, y)$  of an extracted contour such that a centroid with a radius  $R$  contains the largest number of pixel points within the contour. Figure 3.6 shows an example of this. Figure 3.7 provides details of the pixel distance algorithm [67].

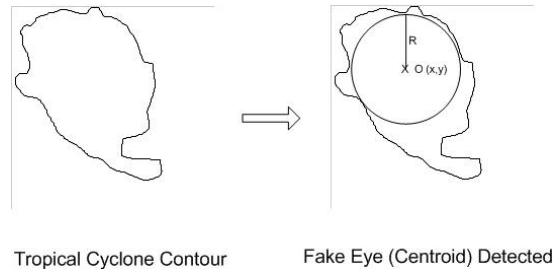


**Figure 3.6:** Result of Positional Eye Location

```

Given an extracted contour of a tropical cyclone;
m = 1;
For all pixels within the cyclone contour
  Procedure EyeLocationFind (Pixel i)
    For all pixels j whose pixel distance to i is m
      If j is within the cyclone contour
        Check pixel gradient values;
      Else
        Break;
      End If
    If m doesn't change
      Break;
    End If
    If all pixels j has the same gradient value with i
      For every j
        EyeLocationFind (j);
      End For
      m ++;
    End If
  End Procedure EyeLocationFind
End For

```

**Figure 3.7:** The pixel distance algorithm

### 3.3.3 A Weight Calculation Algorithm

Having located the eye of the tropical cyclone  $O(x, y)$ , we start the critical task of assigning weights to each point of the active contour. Conceptually, points which are nearer to the positional eye  $O(x, y)$  should have higher weights, as their influence on

controlling the spiral shape, the intensity, or other properties of the tropical cyclone will be greater. Based on this, we designed the following algorithm to determine the weight according to the distance between the positional eye and individual contour point. This is illustrated in Figures 3.8 and 3.9.

```

Procedure AssignWeight(contourset T)
1. Locate the centroid  $O(x,y)$ 
2. For contourset  $T = \{T_1, T_2, \dots, T_n\}$ 
3. Find four extreme points: Leftmost A, Rightmost B, Upmost C, Downmost D
4. Calculate distances:  $R_4 = |OA|$ ,  $R_1 = |OB|$ ,  $R_2 = |OC|$ ,  $R_3 = |OD|$ 
5.  $\text{minDis} = \min(R_1, R_2, R_3, R_4)$ 
   End For
6. For all  $t_i \in T$ 
7. Calculate  $\text{dist} = \|t_i - O\|$ 
8. If  $\text{dist} \leq \text{minDis}$ 
9.    $\text{Weight}_i = \text{minDis} - \text{dist}$ 
10.  else
11.    $\text{Weight}_i = 1$ 
   End If
   End For
End Procedure AssignWeight

```

**Figure 3.8:** Algorithm of calculating weight for each point on the contour

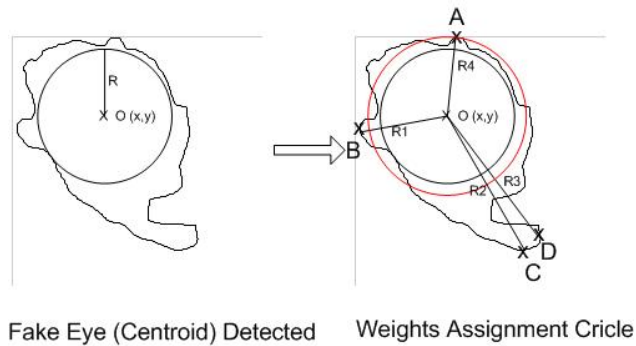


**Figure 3.9:** Result of Weight assigned to each contour point

Figure 3.9 shows two circles. In the right circle of Figure 3.9, the inner circle remarks how the cyclone eye  $O(x,y)$  is achieved: its radius is the largest pixel distance among all pixels within the contour. The outer circle is the boundary derived from the minimum of  $\{R_1, R_2, R_3, R_4\}$ , where A, B, C and D are four extreme points on the contour. Different weights are assigned to those contour points based on their Euclidean distance to the eye O. In practice, any of  $\{R_1, R_2, R_3, R_4\}$  can be used to determine the size of the outer cycle. In this subpart, for ease of illustration we choose the minimum figure. We can use a set of feature vectors to describe the contour points of a tropical cyclone:

$$T = \{n_1, n_2, \dots, n_i\}, n_i = [x, y, w] \quad (3.7)$$

where  $x$  and  $y$  are coordinates for each contour point and  $w$  is the correlated weight.

### 3.3.4 An Angle Calculation Module

There has recently been considerable research in the area of image comparison: in colour histograms [64], motion vectors [65], contour measures [66], and so on. Our algorithm uses the shape of the tropical cyclone to match two images but as it is difficult to describe these features, we approximate it using the angles of every third adjacent contour point, forming a set of sequential angles for each image. Figure 3.10 shows an example of angle and adjacent contour points, where  $A$ ,  $B$  and  $C$  are three adjacent points on the contour edge of the tropical cyclone and  $\theta$  is the internal angle.

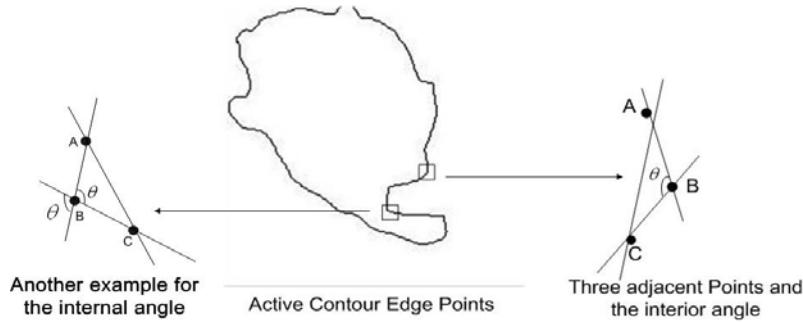


**Figure 3.10:** An internal angle between adjacent points

Here we consider only the angle  $\theta$  formed by vector  $\overline{AB}$  and  $\overline{CB}$  and, the interior angle of the triangle  $ABC$ , according to their sequential positions on the contour edge. Thus  $\theta$  is limited within the range  $0$  to  $\pi$ . The expansion of the contour points creates a concave angle and a convex one, as in the two examples in Figure 3.10. This interior angle,  $\theta$ , can be derived using the inversion of a trigonometric function as follows:

$$\theta = \arccos((|AC|^2 - |BC|^2 - |AB|^2) / 2 * |AB| * |BC|) \quad \pi \geq \theta \geq 0 \quad (3.8)$$

So, we can modify the feature vector for a tropical cyclone from Equation 3.7 into the following format:

$$T = \{n_1, n_2, \dots, n_i\}, n_i = [\theta, w] \quad (3.9)$$

where the weight of the angle  $\theta$ ,  $w$ , contains the weight value of the middle element of three adjacent points forming the angle. The weight of angle ABC for example is just the weight value of the contour point B. In this way, two input tropical cyclone satellite images provide two sets of angles, as shown in Figure 3.11. The major challenge here is to find an effective and efficient approach to derive the similarity of two sets or to determine the relationships between different distances/differences ( $d_n$ ) for every corresponding pair of nodes in Figure 3.11.

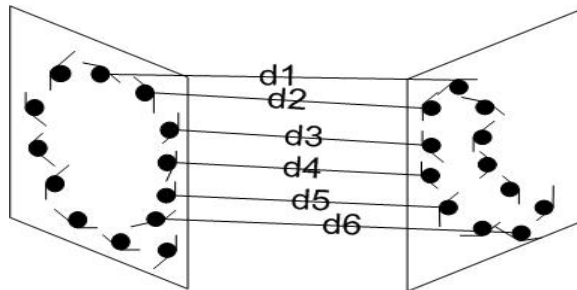


**Figure 3.11:** Set of angles for each TC (each bold round point representing an angle formed in Figure 3.10)

### 3.3.5 A Time Warping Matching Module

Once we have formed a set of angles associated with weights for a tropical cyclone in a satellite image it is necessary to address the critical issue of determining the similarity between two sets. There are two factors to consider here. First, sets do not in general have the same number of angles. The comparison of two sets thus calls for the use of an efficient algorithm. Second, in order to approximately compare the shapes of two cyclones synchronously, the angles of each set should be kept in sequence. In this part, then, instead of directly calculating the distance of every pair of two angles from one set to another, we adopt the time warping concept [69] as it provides an accurate algorithm for the comparison of two sequences of different lengths. The idea is as follows.

Given two angle sets,  $S$  and  $Q$  of lengths  $n$  and  $m$ , as well as the corresponding weights respectively,

$$S = \langle s_1w_1, s_2w_2, \dots, s_{n-1}w_{n-1}, s_nw_n \rangle \quad (0 \leq s_n \leq \pi)$$

$$Q = \langle q_1 w_1, q_2 w_2, \dots, q_{m-1} w_{m-1}, q_m w_m \rangle \quad (0 \leq q_m \leq \pi)$$

where  $s_n$  and  $q_m$  are sets of angles formed by Equation 3.8 for two input tropical cyclones and  $w_i$  is the corresponding weight for the associated angle, we can develop an  $m$ -by- $n$  grid, as illustrated in Figure 3.12.

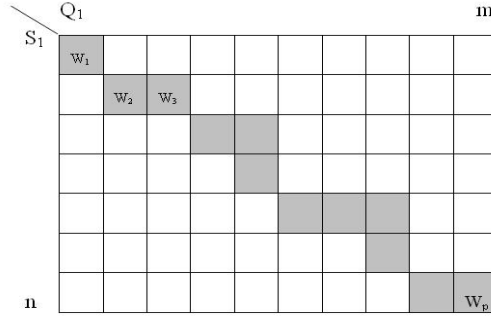


**Figure 3.12:** A warping path in an  $m$ -by- $n$  grid

Each grid element,  $(i, j)$ , represents an alignment between angle  $s_i$  and  $q_j$ . A warping path  $W$  is a sequence of grid elements that define an alignment between  $S$  and  $Q$ .

$$W = (i_1, j_1), (i_2, j_2), \dots, (i_p, j_p) \quad \max(n, m) \leq p < m + n - 1 \quad (3.10)$$

where  $(i_p, j_p)$  corresponds to the  $p^{\text{th}}$  grid element in the warping path. For example,  $(i_2, j_3)$  in Figure 3.12 represents the grid element  $(2, 3)$ , which implies that  $s_2$  is aligned with  $q_3$ . For practical reasons, several types of constraints, which concern the warping path, are introduced in prevalent research work [70].

- **End Point Constraints:** The warping path should start at  $(1, 1)$  and end at  $(n, m)$ .
- **Monotonicity and Continuity:** Given two grid elements in a warping path,  $(i_k, j_k)$  and  $(i_{k+1}, j_{k+1})$ , then  $0 \leq i_{k+1} - i_k \leq 1$  and  $0 \leq j_{k+1} - j_k \leq 1$ . This restricts the allowable transitions of a node to adjacent elements, which are located at east, south, or southeast with respect to Figure 3.12.
- **Global Path Constraint:** The global path constraint defines the region of grid elements that searched for the optimal warping path. The warping path is limited within the warping window, which is known as Sakoe-Chiba Band. The constraint can be defined as follows:

$$\forall (i_k, j_k) \in W, i_k - r \leq j_k \leq i_k + r \quad (3.11)$$

where  $r$  is the width of the warping window. In Figure 3.12,  $r = 1$ .

After aligning the sequences  $S$  and  $Q$ , their similarity can be measured by the cumulative distance of the warping path between them. Each element in the warping path is associated with a distance:

$$d(i_k, j_k) = \|s_{i_k}w_{i_k} - q_{j_k}w_{j_k}\| \quad (3.12)$$

Thus the cumulative distance of a warping path is defined as:

$$D_c(W) = \sum_{k=1}^p d(i_k, j_k) \quad (3.13)$$

It is possible to have many warping paths. We choose an optimal warping path such that its cumulative distance  $D_c$  is the minimum. The corresponding distance is defined as  $D_{tw}$ :

$$D_{tw}(S, Q) = \min_{\forall W} \{D_c(W)\} \quad (3.13)$$

It would be computationally expensive to search through every warping path, so we find the optimal warping path using a dynamic programming approach. This approach is based on a recurrence formula that defines the cumulative distance,  $\gamma(i, j)$ , between angle  $s_i$  and  $q_j$ , where,

$$\gamma(i, j) = d(i, j) + \min\{\gamma(i-1, j), \gamma(i, j-1), \gamma(i-1, j-1)\} \quad (3.14)$$

By adopting Equations 3.10 to 3.14, we can construct a cumulative matrix as shown in Figure 3.13. This matrix represents such an algorithm using typical angle sequences  $Q = \{7/8\pi, 3/4\pi, 6/7\pi, 1/2\pi\}$  and  $S = \{2/3\pi, 4/5\pi, 1/3\pi, 6/7\pi, 5/8\pi, 8/9\pi\}$ . Each value in the cell represents the cumulative distance  $\gamma(i, j)$  of that cell, and it is supposed that all weights  $w_i$  for the angles are set to 1.0 equally.

S \ Q	$7/8\pi$	$3/4\pi$	$6/7\pi$	$1/2\pi$
$2/3\pi$	0.205 $\pi$	0.285 $\pi$	0.472 $\pi$	0.302 $\pi$
$4/5\pi$	0.28 $\pi$	0.255 $\pi$	0.312 $\pi$	0.602 $\pi$
$1/3\pi$	0.825 $\pi$	0.675 $\pi$	0.782 $\pi$	0.482 $\pi$
$6/7\pi$	0.843 $\pi$	0.782 $\pi$	0.675 $\pi$	0.839 $\pi$
$5/8\pi$	1.093 $\pi$	0.907 $\pi$	0.907 $\pi$	0.8 $\pi$
$8/9\pi$	1.108 $\pi$	1.047 $\pi$	0.94 $\pi$	1.19 $\pi$

**Figure 3.13:** A cumulative distance matrix for angle sequences  $Q$  and  $S$

After filling up the table, the optimal warping path can be found by tracing backward from the lower right corner towards the upper left corner. At each cell, we choose the

previous cell whose neighbouring cell has the minimum cumulative distance. In this way,  $1.19\pi$  in the bottom right corner cell can be regarded as the distance of angle sequence  $S$  and  $Q$ , and is marked as  $minDis(S, Q)$ .

In certain cases, after self-rotating the input tropical cyclone image by a number of degrees, the contour may provide a better match with the target tropical cyclone image. This means that we should do the comparison more than once. Where there are two angle feature sets, the functional equivalent of rotating the contour is obtained if the element in the angle sequence is shifted once to the left or right. A Shift Fetcher, shown in Figure 3.1, is designed to repeatedly shift the sequence of  $S$  (or  $Q$ ) and calculates a new cumulative distance matrix like the one in Figure 3.13. For example, sequence  $S = \{2/3\pi, 4/5\pi, 1/3\pi, 6/7\pi, 5/8\pi, 8/9\pi\}$  will be  $S' = \{4/5\pi, 1/3\pi, 6/7\pi, 5/8\pi, 8/9\pi, 2/3\pi\}$  after shifting one position to the left. Then we have a new cumulative distance matrix for  $Q$  and  $S'$  and a new  $minDis_1(Q, S')$ , as in Figure 3.14.

$S' \backslash Q$	$7/8\pi$	$3/4\pi$	$6/7\pi$	$1/2\pi$
$4/5\pi$	$0.075\pi$	$0.05\pi$	$0.057\pi$	$0.3\pi$
$1/3\pi$	$0.545\pi$	$0.47\pi$	$0.362\pi$	$0.087\pi$
$6/7\pi$	$0.018\pi$	$0.125\pi$	$0.964\pi$	$0.462\pi$
$5/8\pi$	$0.25\pi$	$0.143\pi$	$0.732\pi$	$0.819\pi$
$8/9\pi$	$0.015\pi$	$0.155\pi$	$0.985\pi$	$1.077\pi$
$2/3\pi$	$0.205\pi$	$0.095\pi$	$0.747\pi$	$1.152\pi$

**Figure 3.14:** A cumulative distance matrix for angle sequences  $Q$  and  $S_1$  after a left shift. After a loop of shifting all elements of one sequence, we select the smallest one of  $minDis_n(Q, S_n)$  as the final distance of  $Q$  and  $S$ , as shown in Equation 3.15:

$$Dis(Q, S) = \min(\min dis_1(Q, S_1), \min dis_2(Q, S_2), \dots, \min dis_n(Q, S_n)) \quad (3.15)$$

As a result, given a query angle sequence,  $Q$ , for all sets of angle sequences in the database, we want to find the sequence  $Q$  with a minimum  $Dis(Q, S)$  as the sequence best matched to the queried sequence. In this way, the input tropical cyclone and its best match are considered to have a similar intensity. After we have retrieved the best-

matched sample from the database, we can assign the features of current tropical cyclones using those of the best-matched sample.

### **3.4 Performance Evaluation**

To evaluate the efficiency and the effectiveness of our proposed approach, we carried out a set of experiments in which an image is input in order to retrieve a most-like satellite image from the database. The image database contains a total of 64 Dvorak template images with a resolution of 100 x 100. The input is another set of tropical cyclone satellite images collected from an official U.S. Navy web site [71], having a resolution of 800 x 600. The main reason that we selected images with different resolutions was to test the predictive performance of our system when there were great differences in the image relations. Dvorak templates were used because they are relatively informative as to the tropical cyclone's intensity. In one of our previous research works [67], we proposed a modified Hausdorff distance measure [68] for use in the matching of significance-based points in tropical cyclone satellite images. Along with the time warping distance measure, these comparisons also made use of another model from our previous research, a modified Hausdorff distance measure. To carry out our idea, we designed the interface of an integrated system which first extracts the active contour points from each input satellite image then assigns separate weights to those points, calculates corresponding angle sequences, and finally retrieves a most-like Dvorak template image. The following section provides a brief introduction to the modified Hausdorff distance measure.

#### **3.4.1 Definition of Hausdorff Distance**

The Hausdorff distance is a shape comparison metric based on binary images. It is a distance defined between two point sets. Unlike most shape comparison methods that build a point-to-point correspondence between a model and a test image, the Hausdorff distance can be calculated without explicit point correspondence. Huttenlocher et al. [72] argued that the Hausdorff distance for binary image matching is more tolerant to

perturbations in the locations of points than binary correlations techniques, since it measures proximity rather than exact superposition. Here we modify the Hausdorff distance measure and apply it to Active Contour Matching.

Given two finite point sets  $M = \{m_1, m_2, \dots, m_p\}$  (representing a model in the database) and  $T = \{t_1, t_2, \dots, t_q\}$  (representing a test image), the Hausdorff distance is defined as:

$$H(M, T) = \max(h(M, T), h(T, M)) \quad (3.16)$$

where  $h(M, T) = \max_{m_i \in M} \min_{t_j \in T} \|m_i - t_j\|$  and  $\|m_i - t_j\|$  is the Euclidean norm of the points  $m_i$  and  $t_j$ . The function  $h(M, T)$  is called the directed Hausdorff distance from  $M$  to  $T$ . It identifies the point  $m_i \in M$  that is the farthest from any point of  $T$  and measures the distance from  $m_i$  to its nearest neighbour in  $T$ . The Hausdorff distance  $H(M, T)$  is the maximum of  $h(M, T)$  and  $h(T, M)$ . Thus it measures the degree of mismatch between two sets by measuring the distances of the points of  $M$  that is farthest from any point of  $T$ , and *vice versa*.

### 3.4.2 A Modified Hausdorff Distance

Dubuisson and Jain [68] investigated 24 forms of different Hausdorff distance measures and found that the performance of a modified Hausdorff distance (MHD) measure was the best. The directed MHD is defined as:

$$h(M, T) = \frac{1}{P} \sum_{m_i \in M} \min_{t_j \in T} \|m_i - t_j\| \quad (3.17)$$

where  $P$  is the number of points in  $M$ . The definition of the undirected MHD is the same as (3.16). The Hausdorff distance defined as (3.16) is very sensitive to the outlier points. A few outlier points, even only a single one, can perturb the distance considerably, though the two objects might be very similar. The MHD can alleviate the sensitivity of the Hausdorff distance to the outlier points. The partial Hausdorff distance (PHD) was suggested by Huttenlocher *et al* and other researchers [73, 74]. The PHD takes the  $k_{th}$  smallest nearest neighbour distance as the objective function to deal with occluded objects and arbitrary outliers. It has been proven to have great potential usage in robust

statistics [75], though the comparative study reported that the MHD performs better than the PHD.

As the eye is a central feature of tropical cyclones, the matching process should give greater attention to the points near the eye of the cyclone than to those distant from it. We have proposed a new formula for the modified directed Hausdorff distance, assigning individual weights assigned to the contour points. The weights are defined as follows:

$$h'(M, T) = \frac{\sum_{m_i \in M} W_{ij} \cdot \min_{t_j \in T} \|m_i - t_j\|}{N \cdot \text{Avg}(W_{ij})} \quad (3.18)$$

where  $W_{ij} = 1/2(W_i + W_j)$  is the average weight for points  $m_i$  and  $t_j$  in the contour sets  $M$  and  $T$  respectively. In this way, every  $\min_{t_j \in T} \|m_i - t_j\|$  is weighted by the average weight of  $m_i$  and  $t_j$  because its contribution to  $h'(M, T)$  is assumed to be proportional to the significances of the two points being compared. By averaging the sum of weighted minimum distances between points  $m_i$  and  $t_j$ ,  $h'(M, T)$  produces a more balanced and accurate matching result. The undirected Hausdorff distance is thus rewritten as:

$$H(M, T) = \max(h'(M, T), h'(T, M)) \quad (3.19)$$

### 3.4.3 Experimental Results

In this part, to illustrate the success of our proposed algorithm, we will discuss the experimental results from the points of view of accuracy and computational costs. Figure 3.15 shows the experimental results for three typical comparison approaches, Time Warping Matching, Modified Hausdorff Distance, and Human Justification, all using the same input satellite image. The original satellite images from which the contour points are extracted are shown beside the contour. It is quite difficult to tell how much a retrieved contour is similar to the input one. Mostly, this matter is judged, subjectively and imprecisely, with human eyes. Figure 3.15 provides the retrieved results of two approaches, and also provides a retrieved result gT4 acquired using human visual justification. Visually we can consider that eT8 and gT4 in Figure 3.15 have more in

common with the input contour than eT4 does, yet human visual justification is notoriously subjective and cannot be regarded as scientifically convincing.

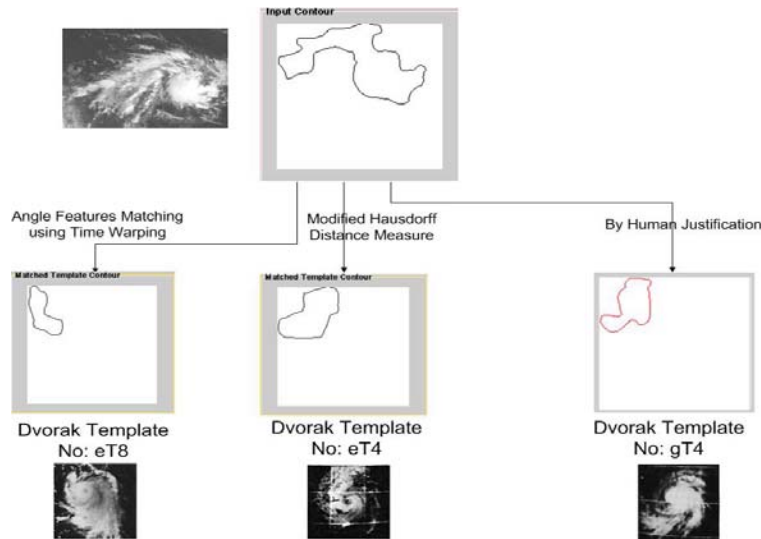


**Figure 3.15:** Matching results for three approaches

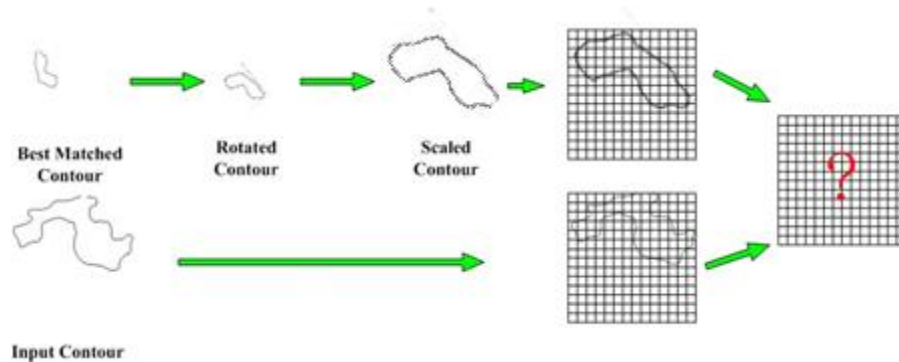


**Figure 3.16:** A Grid Scanning algorithm

Nevertheless, it is obvious that in both cases, retrieved results and input, all data to be processed are sets of contour points. To calculate the accuracy of how similar of two sets of contour points are, we consider their positional relationships. We have designed a Grid Scan method that scales and transforms two sets of contour points into a similar position and size by putting their location eyes in the centre. A system flow is given in Figure 3.16. First, from the SHIFT FETCHER we can ascertain the number of shifts it has undergone before retrieval of a result, so we rotate either the input contour or the best matched sequence to make sure their coordinates consistent with the sequences at the time the best matched contour is found. To scale the smaller contour of the two to the same size as the larger contour, we divide both into  $N \times N$  Blocks, where  $N$  is a predefined number.

To see whether the grid contains a contour point, we next superimpose two blocks and check each grid having the same position in two blocks. The following equation illustrates the basis of this type of comparison.

$$Accuracy = \frac{\sum_{i \in N \times N} (B_i \otimes A_i)}{\sum_{i \in N \times N} A_i} \quad (3.20)$$

where symbol  $\otimes$  denotes the  $i_{th}$  grid in different blocks, both having an active contour point. Details of the procedure of this comparison are listed in Figure 3.17 as follows:

**Procedure CalculateAccuracy (A, B)**  
*Count* = 0;  
 1. Rotate the contour *A* or *B*, making them matched best  
 2. Divide *A* and *B* into  $N \times N$  blocks  
 3. Scan the blocks, two sequences are achieved as:  
      $SA = \{ \langle a_1, p_1 \rangle, \langle a_2, p_2 \rangle, \dots, \langle a_n, p_n \rangle \}$   
      $SB = \{ \langle b_1, q_1 \rangle, \langle b_2, q_2 \rangle, \dots, \langle b_n, q_n \rangle \}$   
 4. For each point  $a_i$   
     If  $p_i$  and  $q_i$  both contain contour points  
         *Count* ++  
     End If  
 End For  
 5.  $Accuracy = Count / (No. \ of \ Contour \ Points \ in \ A)$

**Figure.3.17. Procedure for finding the matching accuracy**

Table 3.1 shows the experimental results. Although gT4 looks very similar with the input contour, it is 10% less accurate than eT8. We do not disaffirm human visual justification, but as it is highly subjective, we do not consider it in the remaining experiments. Table 3.1 also clearly shows that the modified Hausdorff distance measure is the least accurate one among the three. This shows that algorithms that depend solely on positional relationships such as Euclidean distance do not achieve acceptable retrieval results but require additional characteristics, such as shape.

**Table 3.1:** Retrieved accuracy for the results in Figure 3.15

Algorithm	Angle Feature Matching	Modified Hausdorff Distance Measure	Human Visual Justification
Matched Image	eT8	eT4	gT4
Accuracy	72.41%	53.12%	62.86%

We further conducted a detailed experiment using a selection of 10 satellite images from the U.S. Navy official website. We input 10 Dvorak template images and calculated the

average matching accuracy. Experimental results (shown in Table 3.2) indicate that if the input image is any one of the Dvorak templates, both algorithms are 100% accurate, as both sets of compared contour points are identical. 10 out of 64 Dvorak templates are used for input testing. About the looking up database, all 64 templates are used. So, it doesn't influence the result even if we use all templates as the input images. The results differ, however, for another set of testing satellite images (marked as SI in Table 3.2) from U.S. Navy official website with the Angle Feature Matching algorithm being a little more accurate than the modified Hausdorff distance measure. The improvement values in Table 3.2 are calculated in terms of accuracy, using Angle Feature Matching algorithm over that of the modified Hausdorff distance measure. Our weighting algorithm for selecting the dominant points that reflect the shape of the tropical cyclone also contributed to the matching results. The results can be seen in Figure 3.18.

**Table 3.2:** Average Accuracy (%) comparison of the Angle Feature Matching (AFM) and the Modified Hausdorff Distance (MHD)

	<b>Input Image</b>	<b>Angle Feature Matching using Time Warping</b>	<b>Weighted Hausdorff Distance</b>	<b>Improvement</b>
<b>Accuracy</b>	Dvorak aT1	100%	100%	0
	Dvorak aT2	100%	100%	0
	Dvorak bT1	100%	100%	0
	Dvorak bT2	100%	100%	0
	Dvorak cT1	100%	100%	0
	Dvorak cT2	100%	100%	0
	Dvorak dT1	100%	100%	0
	Dvorak dT2	100%	100%	0
	Dvorak eT1	100%	100%	0
	Dvorak eT2	100%	100%	0
	SI: 1	61.23%	55.12%	1.11
	SI: 2	68.32%	66.72%	1.02
	SI: 3	70.41%	63.47%	1.11
	SI: 4	65.88%	63.92%	1.03
	SI: 5	83.69%	80.05%	1.04
	SI: 6	66.18%	59.43%	1.11
	SI: 7	57.35%	53.49%	1.07
	SI: 8	75.91%	71.15%	1.06
	SI: 9	60.36%	57.77%	1.04
	SI: 10	77.48%	74.32%	1.04

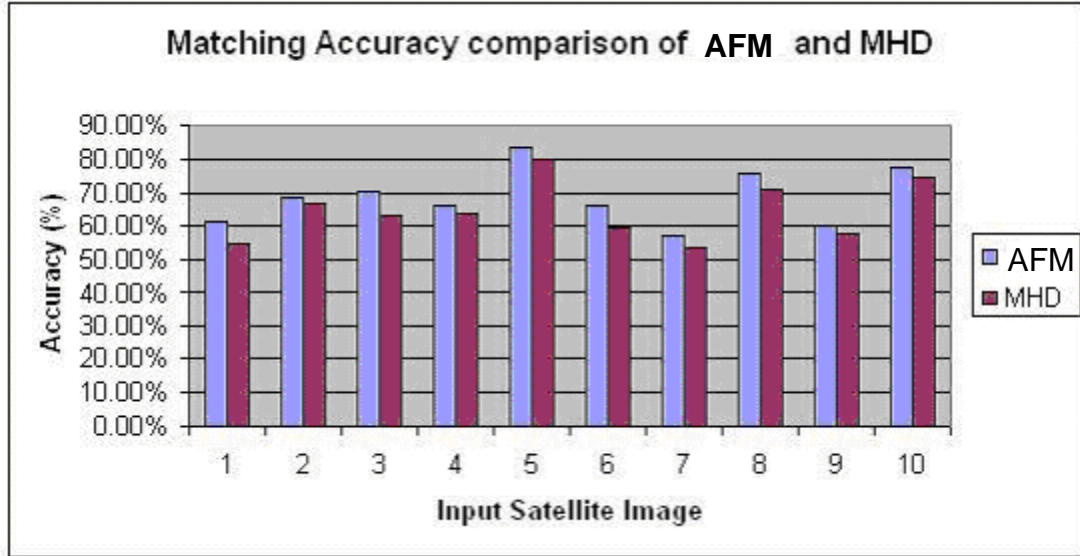


**Figure 3.18:** Visual description of the experimental results

We also assessed the computational cost of each algorithm using a computer with 2.26 GHz Intel Pentium CPU and 512M RAM. All other windows applications were shut down to ensure the most precise time-cost measurement. The total cost of processing a match is given by the following equation:

$$Total\_Cost = IO\_Cost + CPU\_Cost \quad (3.21)$$

where  $IO\_Cost$  is the cost of performing disk I/Os and  $CPU\_Cost$  is the cost of performing computation while retrieving the most similar contour from the library. The experiment took into account only the  $CPU\_COST$  and ignored the  $IO\_Cost$  as, compared to the CPU time, the time taken to read contour points from the library file was ignored. Table 3.3 shows the time cost of three algorithms using different sets of input satellite images. Time evaluation is not stable but it does indicate a trend towards the time warping distance measure being computationally faster than other two algorithms.

**Table 3.3:** Computational costs of three algorithms

	Input Image	Elastic Matching Model	Weighted Hausdorff Distance	Time Warping Distance
Average Time Cost (seconds)	Dvorak Template	49.19	43.09	37.9
	Other Satellite Images	113.797	83.375	86.28

We also can evaluate this result by analyzing the computational costs of the three algorithms. Supposing that the input contour has  $m$  points and the matched contour has  $n$  points, we can calculate the computational complexities based on different comparison algorithms. The main concern of this part covers the time cost involved in the rotation and comparison steps, excluding the contour extraction procedures. Table 3.4, which shows the computational complexities, supports our approach.

**Table 3.4:** Computational complexities of three approaches

<b>Algorithm</b>	<b>Weighted Hausdorff Distance</b>	<b>Time Warping Distance</b>
<b>Computation Complexity</b>	$O(1.5m^2n)$	$O(m^2n)$

### 3.5. Summary

In this chapter, we proposed an integrated approach to forecasting for tropical cyclone (TC) comparison that is based on a TC's typical spiral shapes using time warping technology. We first extract the contour points of a dominant tropical cyclone from the satellite image using the Gradient Vector Flow (GVF) snake model. A fast sequential neighbor-checking algorithm is designed to find the largest cyclone in the satellite image. We also proposed a pixel distance algorithm to locate the centroid of a tropical cyclone. After that a weight calculation algorithm is carried out to assign different weights to points on the active contour based on their distance related to this centroid. Given two sets of contour points, one for the input tropical cyclone image and the other for an image in the database, we use angle features between successive contour points to determine the degree of similarity of two cyclone shapes. To better reflect the spiral shape of tropical cyclones and to produce a fast, accurate comparison, we adopt a time warping approach. The proposed approach was tested against and found to be superior to an approach that uses a modified Hausdorff distance measure. We added human visual justification as a reference because in the past years, even for a scientific meteorology prediction, expert's visual justification is still worked as an important consideration, especially for TC movement's prediction. In our research, we collected about thirty persons' opinions about the prediction and made the result.

# **Chapter 4. An Integrated Neural Training Based Tropical Cyclone Forecasting System**

As forecasting based on satellite interpretation mainly concerns the features extracted out from satellite images, it doesn't reflect the influences of climatology, persistence and synoptic factors against the intensity change of tropical cyclones. Recently much effort has been made to statistically relate the tropical cyclone intensity change by using multiple linear regression techniques. Neural network can better handle unknown non-linear behavior existing in meteorological variables and they can be an effective alternative to traditional statistical techniques. In this section, neural network and upper air information are used to develop a model for predicting tropical cyclone intensity in the Western North Pacific at 6, 12, 18, 24h. Once the analog tropical cyclones are identified, the persistence, climatological and synoptic observations of analog tropical cyclones and the current storm are combined to create a training set and a multiple-regression scheme is used to identify the variables that are best correlated with storm intensity. We also design a variable selection procedure to choose the most important training variables to enhance the speed and accuracy of neural network training. Our publications related to this chapter can be referred to [Publications 1,2,4], in which major images and tables in this chapter can also be found.

The rest of this chapter is organized as follows. In section 4.1, an introduction is given to describe basic concepts about the competitive neural network and the estimation of regression coefficients. Section 4.2 tells about data collection and data preparation. In section 4.3, algorithms to identify analog tropical cyclones are described, including unsupervised classification techniques and application of the competitive neural network. In section 4.4, a variable selection procedure is implemented to choose those variables that best explain the tropical cyclone intensity behavior. At last in section 4.5, experimental results analysis is given to evaluate the performance of the proposed predicting model.

## 4.1 Introduction

### 4.1.1. Competitive Neural Network

A competitive neural network is composed generally of two layers. The first layer computes the direction and other properties of the input patterns and the second layer determines which of the prototype vector is closest to the input vectors. Hagan describes the competitive neural network as follows [76]:

The first layer is based on a single instar, which is a type of neural network that is capable of performing pattern recognition and is able to recognize only one pattern. To recognize more than one pattern, a set of instars is used. The input/output expression for the instar net is:

$$a = \text{hardlim}(Wp + b) = \text{hardlim}({}_1w^T p + b) \quad (4.1)$$

where  $W$  represents a matrix of vectors which wants to be recognized,  $b$  is set equal to the number of elements in input  $vector(p)$ , and  $\text{hardlim}$  is a transfer function that assign the number one if its net input reaches a given threshold, otherwise its outputs will be zero. This rule allows a neuron to perform a classification of the input patterns.

The instar will be activated whenever the inner product between the weight vector and the input is greater than or equal to  $-b$ :

$${}_1w^T p \geq -b \quad (4.2)$$

For two vectors of constant length, the inner product will achieve the largest value when they point in the same direction. If the following relation is set:

$$b = -\|{}_1w^T\| \|p\| \quad (4.3)$$

Then the instar will only be active when  $p$  focuses in exactly the same direction as  ${}_1w$ , ( $\theta = 0$ , where  $\theta$  is the angle between the vector  ${}_1w^T$  and  $p$ ). Thus, the neuron will recognize only the pattern  ${}_1w$ . To recognize more than one pattern, a variation of the procedure mentioned above has been implemented as follows. Given the following input vectors:

$$\{p_1, p_2, \dots, p_Q\}$$

where:  $p_1 = [p_{11} \ p_{12} \ \dots \ p_{1R}]$ ;  $p_2 = [p_{21} \ p_{22} \ \dots \ p_{2R}]$ ;  $p_Q = [p_{Q1} \ p_{Q2} \ \dots \ p_{QR}]$

The weight matrix,  $W^1$ , and the bias vector,  $b^1$ , for Layer 1 will be:

$$W_{R \times S}^1 = \begin{bmatrix} {}_1W^T \\ {}_2W^T \\ {}_3W^T \\ \vdots \\ {}_sW^T \end{bmatrix} = \begin{bmatrix} p_1^T \\ p_2^T \\ p_3^T \\ \vdots \\ p_Q^T \end{bmatrix}, \quad b_{R \times 1}^1 = \begin{bmatrix} R \\ R \\ R \\ \vdots \\ R \end{bmatrix}$$

where each row of  $W^1$  represents a prototype vector that is needed to be recognized and each element of  $b^1$  is set equal to the number of elements in each input vector ( $R$ ). The upper subscript in  $W$  and  $b$  represents the first layer. The number of neurons,  $S$  is equal to the number of prototype vectors that will be identified as  $Q$ . The upper subscript  $T$  represents the transpose operation. Each row of  $W^1$  can be expressed as follows:

$${}_1W = \begin{bmatrix} {}_1W_{11} \\ {}_1W_{12} \\ {}_1W_{13} \\ \vdots \\ {}_1W_{1Q} \end{bmatrix}, \quad {}_2W = \begin{bmatrix} {}_2W_{21} \\ {}_2W_{22} \\ {}_2W_{23} \\ \vdots \\ {}_2W_{2Q} \end{bmatrix}, \quad \dots, \quad {}_sW = \begin{bmatrix} {}_sW_{s1} \\ {}_sW_{s2} \\ {}_sW_{s3} \\ \vdots \\ {}_sW_{sQ} \end{bmatrix}$$

Thus, the output of the first layer is:

$$a^1 = W^1 p + b^1 = \begin{bmatrix} p_1^T p_1 + R \\ p_2^T p_2 + R \\ p_3^T p_3 + R \\ \vdots \\ p_Q^T p_Q + R \end{bmatrix} = \begin{bmatrix} {}_1W^T p_1 + R \\ {}_2W^T p_2 + R \\ {}_3W^T p_3 + R \\ \vdots \\ {}_sW^T p_Q + R \end{bmatrix} \quad (4.4)$$

It should be noted that the output of the first layer,  $a^1$ , is equal to the inner products of the prototype vectors with the input in addition of the constant  $R$ . These inner products indicate how close each of the prototype patterns is to the input vector.

The second layer is called ‘‘competitive layer’’ and it is initialized using the outputs of the first layer. In this layer, the neurons compete with each other to determine a winner. The winning neuron indicates which category of input was presented to the network (each prototype vector represents a category).

The first layer output,  $a^1$ , is used to initialize the second layer.

$$a^2(0) = a^1 \quad (4.5)$$

Then the second-layer output is updated according to the following recurrence relation:

$$a^2(t + 1) = \text{poslin}(W^2 a^2(t)) \quad (4.6)$$

where the transfer function *poslin* is defined as follows:

$$a = \text{poslin}(n) = \begin{cases} 0, & \text{if } n < 0 \\ n, & \text{otherwise} \end{cases}$$

The second-layer weights  $W^2$  are set so that the diagonal elements are 1, and the off-diagonal elements have a small value as follows:

$$w_{ij}^2 = \begin{cases} 1, & \text{if } i = j \\ -\varepsilon, & \text{otherwise} \end{cases} \quad \text{where } 0 < \varepsilon < \frac{1}{S-1} \quad (4.7)$$

This matrix produces an effect called lateral inhibition, in which the output of each neuron has an inhibitory effect on all of the neurons.

At this point the network has reached a steady state. The index of the second-layer neuron with a stable positive output is the index of the prototype vector that best matched the input. This process is called the “winner-take-all competition” since only one neuron will have a nonzero output. The timing for each calculation is long, say around 2 minutes, but it is still within our tolerant time range. At present stage, our research target is to achieve an accurate predicting result, so, for the current timing performance, it could be acceptable.

### 4.1.2 Estimation of Regression Coefficients

A regression model that involves more than one regressor variable is called a multiple regression model. The purpose of multiple linear regressions is to establish a quantitative relationship between a group of predictor variables (the columns of X) and a response, y. In general, given a single variable (y) depends on  $k$  independent variables (regressor or predictor variables), for example,  $x_1, x_2, \dots, x_k$ , the relationship between these variables is characterized by a mathematical model called “regression model” which can be expressed as follows:

$$y = \beta_0 + \beta_1 x_1 + \beta_2 x_2 + \dots + \beta_k x_k + \varepsilon \quad (4.8)$$

The parameters  $\beta_j, j=0, 1, 2, \dots, k$  are called the “regression coefficients”.

The method of least squares chooses the  $\beta$ 's in the above equation so that the sum of the squares of the error,  $\sum \varepsilon^2$ , is minimized. The least squares estimators can be derived as follows:

$$S(\beta_0, \beta_1, \dots, \beta_k) = \sum_{i=1}^n \varepsilon_i^2 = \sum_{i=1}^n (y_i - \beta_0 - \sum_{j=1}^k \beta_j x_{ij})^2 \quad (4.9)$$

The function  $S$  must be minimized with respect to  $\beta_0, \beta_1, \dots, \beta_k$ . The least-squares estimators of  $\beta_0, \beta_1, \dots, \beta_k$  must satisfy:

$$\left. \frac{\partial S}{\partial \beta_0} \right|_{\hat{\beta}_0, \hat{\beta}_1, \dots, \hat{\beta}_k} = -2 \sum_{i=1}^n (y_i - \hat{\beta}_0 - \sum_{j=1}^k \hat{\beta}_j x_{ij}) = 0 \quad \text{and} \quad (4.10)$$

$$\left. \frac{\partial S}{\partial \beta_j} \right|_{\hat{\beta}_0, \hat{\beta}_1, \dots, \hat{\beta}_k} = -2 \sum_{i=1}^n (y_i - \hat{\beta}_0 - \sum_{j=1}^k \hat{\beta}_j x_{ij}) x_{ij} = 0, \quad j = 1, 2, \dots, k \quad (4.11)$$

The function  $S$  in a matrix form can be given as follows:

$$\begin{aligned} S(\beta) &= \sum_{i=1}^n \varepsilon_i^2 = \varepsilon' \varepsilon = (y - X\beta)'(y - X\beta) \\ &= y'y - 2\beta'X'y + \beta'X'X\beta \end{aligned} \quad (4.12)$$

The least-squares estimators must satisfy:

$$\left. \frac{\partial S}{\partial \beta} \right|_{\hat{\beta}} = -2X'y + 2X'X\hat{\beta} = 0 \quad (4.13)$$

Then, the least-squares estimators of  $\beta$  are:

$$\hat{\beta} = (X'X)^{-1} X'y \quad (4.14)$$

## 4.2 Data Collection and Preparation

### 4.2.1 Data Collection

Data collection and analysis are the major tasks in the early stage of system development. Upper air information obtained from National Center for Environment Prediction (NCEP)

and Hong Kong Observatory [80] is used to develop a database for storing historical data of past Western North Pacific tropical cyclones, from January 1994 to December 2004.

Hong Kong Observatory provides a reliable historical data set that is usually known as the best track. The best track is a comprehensive tropical cyclone track analysis after considering all available observations and expert interpretation. Typically the observations are obtained from ships, radars, satellites, airplane reconnaissance, buoys data and other sources. The best track contains observations obtained every 6 hours and includes the following variables: tropical cyclone location, central pressure, tropical cyclone intensity, and storm dates. The tropical cyclone intensity is defined as the average 1-minute maximum sustained winds at sea level (**J**oint **T**yphoon **W**arning **C**enter) or defined in terms of wind speeds averaged over a period of 10 minutes (**W**orld **M**eteorological **O**rganization). The wind speed is measured in m/sec or in knots. In this study, the knot is adopted as a measure for tropical cyclone intensity. The best tracks are obtained from the HKO for events occurred during 1994 to 2003.

NAME	DAY	IN	LAT	LON	MSLP	SPD
TD0104	1994010400	TD	88	1326	1004	25
TD0104	1994010406	TD	92	1308	1002	30
TD0104	1994010412	TD	95	1290	1002	30
TD0104	1994010418	TD	97	1275	1002	30
TD0104	1994010500	TD	101	1267	1000	30
TD0104	1994010506	TD	105	1260	1000	30
OWEN	1994033112	TD	109	1345	1005	25
OWEN	1994033118	TD	112	1336	1000	30
OWEN	1994040100	TS	114	1329	998	35
OWEN	1994040106	TS	115	1322	998	35
OWEN	1994040112	TS	116	1315	998	35
OWEN	1994040118	TS	117	1307	998	35
OWEN	1994040200	TS	117	1302	996	40
OWEN	1994040206	TS	116	1297	996	40
OWEN	1994040212	TS	114	1292	996	40
OWEN	1994040218	TS	111	1286	990	45
OWEN	1994040300	TS	108	1280	990	45
OWEN	1994040306	ST	106	1275	985	50
OWEN	1994040312	ST	104	1270	985	50

**Figure 4.1:** The Best Track Data Format

The sea surface temperature (SST) values used in this work is obtained from the Comprehensive Ocean-Atmosphere Data Set (COADS), which is an extensive collection

of surface marine data available in the world for the past two centuries and can be downloaded from the Internet (<http://www.cdc.noaa.gov/cdc/data.coads.1deg.html>). After December 2002, the SST data is collected from Joint Institute for the Study of the Atmosphere and Ocean (JISAO) [http://www.jisao.washington.edu/data\\_sets/sst\\_oi/#data](http://www.jisao.washington.edu/data_sets/sst_oi/#data), which is an online database dedicated to provide meteorological data. Monthly mean values of SST are available on a  $1^{\circ} \times 1^{\circ}$  of resolution on the horizontal. These values are linearly interpolated in space and time and are used for estimating the SST at specific tropical cyclone location and a particular time.

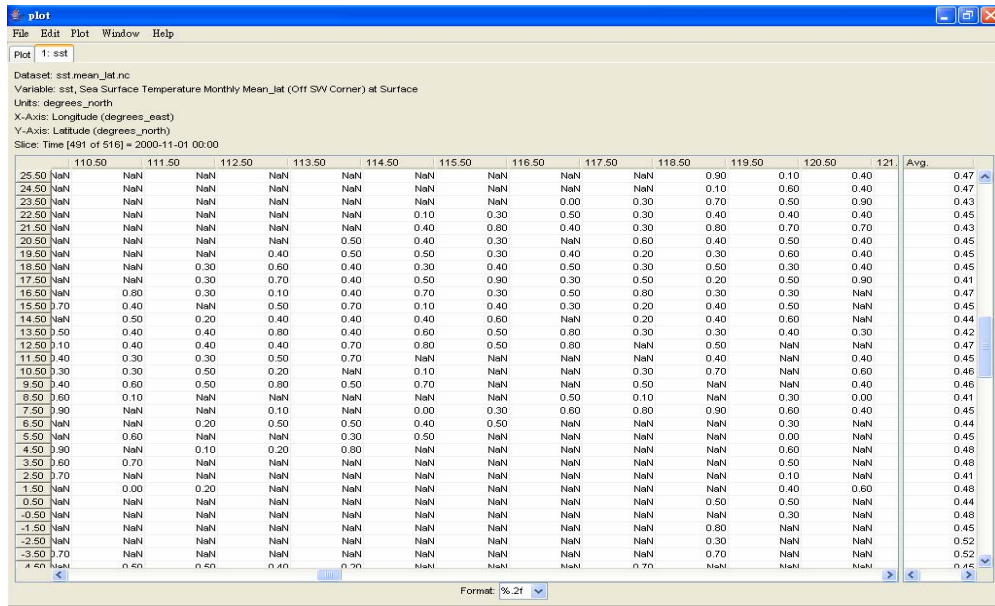


Figure 4.2: Display SST Values using Panoply

The National Center for Environmental Prediction and The National Center for Atmospheric Research (NCEP/NCAR) Reanalysis data is used to obtain the upper air observations at different pressure levels with a  $2.5^{\circ} \times 2.5^{\circ}$  horizontal resolution. This data is obtained at every six hours along the storm track. The NCEP/NCAR reanalysis project is a state-of-the-art reanalysis/forecast system to perform data assimilation using observations from 1948 to the present. A large subset of this data is available from Climate Diagnostic Center (CDC) in its original format as well as its daily averages. The obtained variables from this source are summarized in Table 4.1. More information about this data is found in its web page (<http://www.cdc.noaa.gov/cdc/data.ncep.reanalysis.html>).

**Table 4.1:** Data Obtained From NCEP/NCAR Reanalysis (Sourced by NCEP)

<b>Variables at 17 pressure levels:</b>	<b>Units</b>	<b>Least Sig. Digit</b>
U-wind speed	m/s	0.1
V-wind speed	m/s	0.1

### 4.2.2 Data Preparation

The wind speed components data obtained from NCEP/NCAR and the sea surface temperature data provided by COADS are presented in the format of **network common data form** (NetCDF) [77]. These data sources contain worldwide data and consume nearly 11 GB of disk space. In order to handle this huge amount of raw binary data and extract the relevant meteorological data along the storm track, a Matlab GUI for converting NetCDF file to ASCII file is developed using Matlab NetCDF toolbox. The data is linearly interpolated in space and time and are used for estimating the v-wind component, u-wind component and SST values at specific hurricane location and a particular time. The irrelevant data is discarded and the relevant data is inserted to SQL Server database. The goal of this operation is to prepare structured data for predicting tropical cyclone intensity. For the SST data recorded from January 1994 to December 2003, there are some missing values. This missing data may lead to the production of inaccurate prediction result and thus data-smoothing operation is needed. In order to handle the data-missing problem, the averaged SST value of each tropical cyclone is used to replace the missing SST value of each observation in the same TC. If the averaged SST value of a TC cannot be calculated, that TC data will be discarded since SST value is an important factor for predicting TC intensity. This step is important since it can improve the quality of the raw data.

A historical database is built to store the climatology, persistence and synoptic observations of the North West Pacific (NW Pacific or Western North Pacific) Tropical Cyclone since 1994. This database is an organized structure divided into fields, where each field contains a specific type of information. The system provides **Graphical User Interface** (GUI) to the users for inputting and retrieving historical TC record.

The main advantages of having a database is that the information about any TC that developed in the NW Pacific can be accessed at any time and used according to the needs. The structure of the database is shown in Table 4.2 and Table 4.3.

**Table 4.2:** Tropical Cyclone Database Structure

<b>Field</b>	<b>Value</b>	<b>Description</b>
Id Number	Number	Unique ID for TC
Name	Text	Name of TC
Initial Latitude	Float	Initial Storm Location Latitude
Initial Longitude	Float	Initial Storm Location Longitude
Initial Intensity	Number	Initial Storm Intensity
Julian Date	Number	Julian Date of storm
Initial Pressure	Number	Initial Storm Pressure
Initial Date	Date	Time of Analysis

The *Id Number* is a unique identifier for each TC. The *Name* field is used to store the name of the tropical cyclone. The *Initial Latitude* and *Initial Longitude* fields are necessary to identify the initial location of the storm. The *Initial Intensity*, *Julian Date*, *Initial Pressure* and *Initial Date* fields are utilized to save information about the initial state of the tropical cyclone. Each Tropical Cyclone contains several observations that include the following information:

**Table 4.3:** Data Subfields

<b>Subfield</b>	<b>Source</b>	<b>Description</b>
1	Best Track	Id Number
2	Best Track	Name
3	Best Track	Observation Number
4	Best Track	Year of the storm
5	Best Track	Month of the storm
6	Best Track	Day of the storm
7	Best Track	Time
8	Best Track	Storm Location Latitude
9	Best Track	Storm Location Longitude
10	Best Track	Storm Pressure
11	Best Track	Storm Intensity
12	Calculated	Storm Intensity Change
13	Calculated	Eastward component of storm motion (SMU)
14	Calculated	Northward component of storm motion (SMV)
15	Calculated	Magnitude of the storm motion (SMT)

16	Interpolated from COADS	Sea Surface Temperature (SST)
17	Calculated	Maximum Potential Intensity (MPI)
18	Interpolated from NCEP	Eastward component of wind speed at 850 mb (U850)
19	Interpolated from NCEP	Northward component of wind speed at 850 mb (V850)
20	Interpolated from NCEP	Eastward component of wind speed at 200 mb (U200)
21	Interpolated from NCEP	Northward component of wind speed at 200 mb (V200)
22	Calculated	Vertical Wind Shear (VWS)
23	Calculated	Average angular momentum at 850mb (MOM850)
24	Calculated	Average angular momentum at 200mb (MOM200)
25	Calculated	Potential Intensification (POT)
26	Calculated	Translation Speed
27	Calculated	Direction

### 4.3 Analog Tropical Cyclones Identification

A competitive neural network is used to identify analog tropical cyclones, where an analog is defined as a storm that best resembles the meteorological behavior of the current storm. It is an algorithm that learns associations from observations by identifying similarities among their properties. Once learned, associations allow networks to classify input vectors into clusters or families. This is considered as an unsupervised classification technique because no target variable or response variable is needed.

#### 4.3.1 Unsupervised Classification Technique

Unsupervised classification technique is used to identify the analog tropical cyclones since the major goal of unsupervised learning is to build representation from the inputs that can be used for reasoning, decision-making and prediction. By using such technique, it can classify the inputs into different clusters, reduce the data required in later stage and make other learning tasks easier. With unsupervised learning it is possible to learn larger

and more complex models than with supervised learning. The difficulty of the learning task increases exponentially in the number of steps between the two sets and that is why supervised learning cannot, in practice, learn models with deep hierarchies.

In unsupervised learning, the learning can precede hierarchically from the observations into every more abstraction levels of representation. Each additional hierarchy needs to learn only one step and therefore the learning time increases linearly in the number of levels in the model hierarchy. Supervised learning technique such as back-propagation learning algorithm will be described briefly in the later part and it is used to implement the tropical cyclone intensity prediction module. Supervised learning learns based on the target value or the desired outputs. During the network training it tries to match the outputs with the desired target values.

### **4.3.2 Application of the Competitive Neural Network**

In the following implementation procedure, it is important to notice that only six observations are used to explain the idea of how the competitive neural network is applied to identify analog tropical cyclones (TCs), the number of observations will increase as soon as the storm life increases. The implemented procedure includes three major steps given as follows:

1. Once a tropical cyclone is detected HKO will collect a set of parameters ( $D_A$ ) at every 6 hours since the TC detection time until the current time ( $t$ ), defined by the actual time of the TC in process. These parameters include: the Julian date, TC location (latitude and longitude), intensity, minimum central pressure, translation speed and direction. The parameter sets ( $DI_{Pi}$ ) are associated to the historical storms stored in the database that are extracted for the same storm life interval of the current storm. We assume that if the current storm has 6 observations, the analog tropical cyclones should have at least 6 observations. Based on this, tropical cyclones that have at least 6 observations are selected from database for processing. The parameter set,  $D_A$ , is a matrix whose columns are the  $D_i$  vectors ( $i=1, 2, \dots, 6$ ) and a single column can be expressed as follows:

$$D_i = \begin{bmatrix} La_i \\ Lo_i \\ I_i \\ \alpha_i \\ Ju_i \\ P_i \\ TS_i \end{bmatrix}, D_A = [D_1 D_2 \dots D_6], \quad D_A = \begin{bmatrix} La_1 & La_2 & \dots & La_6 \\ Lo_1 & Lo_2 & \dots & Lo_6 \\ I_1 & I_2 & \dots & I_6 \\ \alpha_1 & \alpha_2 & \dots & \alpha_6 \\ Ju_1 & Ju_2 & \dots & Ju_6 \\ P_1 & P_2 & \dots & P_6 \\ TS_1 & TS_2 & \dots & TS_6 \end{bmatrix}$$

where

- $D_i$  = Vector with storm's information at time 0 hr, 6 hr, 12 hr, 18 hr, 24 hr
- $La_i$  = Storm location latitude at every time
- $Lo_i$  = Storm location longitude at every time
- $I_i$  = Storm intensity at every time
- $\alpha_i$  = Storm direction at every time
- $Ju_i$  = Julian Date at every time
- $P_i$  = Minimum Central Pressure at every time
- $TS_i$  = Translation Speed at every time
- $D_A$  = Matrix of information for the current storm

$MD_P$  is the set that contains information for each of the past storm ( $DI_{Pi}$ ) selected from the database and can be expressed as follows:

$$D_{Pi,1} = \begin{bmatrix} La_{Pi,1} \\ Lo_{Pi,1} \\ I_{Pi,1} \\ \alpha_{Pi,1} \\ Ju_{Pi,1} \\ P_{Pi,1} \\ TS_{Pi,1} \end{bmatrix}, \quad DI_{Pi} = \begin{bmatrix} La_{Pi,1} & La_{Pi,2} & \dots & La_{Pi,6} \\ Lo_{Pi,1} & Lo_{Pi,2} & \dots & Lo_{Pi,6} \\ I_{Pi,1} & I_{Pi,2} & \dots & I_{Pi,6} \\ \alpha_{Pi,1} & \alpha_{Pi,2} & \dots & \alpha_{Pi,6} \\ Ju_{Pi,1} & Ju_{Pi,2} & \dots & Ju_{Pi,6} \\ P_{Pi,1} & P_{Pi,2} & \dots & P_{Pi,6} \\ TS_{Pi,1} & TS_{Pi,2} & \dots & TS_{Pi,6} \end{bmatrix}$$

$$DI_{Pi} = [D_{Pi,1} D_{Pi,2} \dots D_{Pi,6}] \text{ for } i = 1, 2, \dots, n \quad MD_P = [DI_{P1} DI_{P2} \dots DI_{Pi} \dots DI_{Pn}]$$

where

- $i$  = Storm index in the database
- $n$  = Number of tropical cyclones selected from the database
- $D_{Pi,j}$  = Vector that contains historical information for storm  $i$  ( $i = 1, 2, \dots, m$ , where  $m$  is the number of tropical cyclones in the database) in the time  $j$  ( $j = 1,$

2, ..., 6)

- $DI_{P_i}$  = Matrix that collects information for storm  $i$

$$D_T = [D_A MD_P]$$

$$D_T = \begin{bmatrix} La_1 & La_2 & \cdots & La_6 & La_{P_{1,1}} & \cdots & La_{P_{1,6}} & \cdots & La_{P_{i,1}} & \cdots & La_{P_{i,6}} & \cdots & La_{P_{n,1}} & \cdots & La_{P_{n,6}} \\ Lo_1 & Lo_2 & \cdots & Lo_6 & Lo_{P_{1,1}} & \cdots & Lo_{P_{1,6}} & \cdots & Lo_{P_{i,1}} & \cdots & Lo_{P_{i,6}} & \cdots & Lo_{P_{n,1}} & \cdots & Lo_{P_{n,6}} \\ I_1 & I_2 & \cdots & I_6 & I_{P_{1,1}} & \cdots & I_{P_{1,6}} & \cdots & I_{P_{i,1}} & \cdots & I_{P_{i,6}} & \cdots & I_{P_{n,1}} & \cdots & I_{P_{n,6}} \\ \alpha_1 & \alpha_2 & \cdots & \alpha_6 & \alpha_{P_{1,1}} & \cdots & \alpha_{P_{1,6}} & \cdots & \alpha_{P_{i,1}} & \cdots & \alpha_{P_{i,6}} & \cdots & \alpha_{P_{n,1}} & \cdots & \alpha_{P_{n,6}} \\ Ju_1 & Ju_2 & \cdots & Ju_6 & Ju_{P_{1,1}} & \cdots & Ju_{P_{1,6}} & \cdots & Ju_{P_{i,1}} & \cdots & Ju_{P_{i,6}} & \cdots & Ju_{P_{n,1}} & \cdots & Ju_{P_{n,6}} \\ P_1 & P_2 & \cdots & P_6 & P_{P_{1,1}} & \cdots & P_{P_{1,6}} & \cdots & P_{P_{i,1}} & \cdots & P_{P_{i,6}} & \cdots & P_{P_{n,1}} & \cdots & P_{P_{n,6}} \\ TS_1 & TS_2 & \cdots & TS_6 & TS_{P_{1,1}} & \cdots & TS_{P_{1,6}} & \cdots & TS_{P_{i,1}} & \cdots & TS_{P_{i,6}} & \cdots & TS_{P_{n,1}} & \cdots & TS_{P_{n,6}} \end{bmatrix}$$

Current data set
Data set for first
Data set for
Data set for last  
 $D_A$ 
storm
storm  $i$ 
storm

$D_T$  is the matrix formed by the union of the past data set ( $MD_P$ ) and current data set ( $D_A$ ). This set is used in step 2 and can be expressed as above.

2. A competitive neural network (CNN) is implemented to classify the input set ( $D_T$ ) into a preliminary set ( $D_S$ ). To accomplish this task a number ( $S$ ) of prototype vectors ( $W$ ), which are selected in a random way, are defined so that the CNN can learn to detect similarities among the provided data set  $D_T$ . This step can be represented mathematically as follows:

$$D_S = CNN(W_{S \times 7} D_{T \times Q}) \quad (4.15)$$

where

- $W$  = Prototype vectors
- $s$  = Class type ( $s = 1, \dots, S$ )
- $q$  =  $q^{\text{th}}$  observation ( $q = 1, \dots, Q$ )
- $D_T$  = is the union of historical observations ( $n$ ) and current observations

$D_S$  is a row vector with the same number of columns as  $D_T$  and its values are between 1 and  $S$ , which means that each single observation of every one of the TCs that composed  $D_T$  is classified as follows:

$$D_S = [P_{1,1} P_{1,2} P_{1,3} P_{1,4} P_{1,5} P_{1,6}; \dots; P_{i,1} P_{i,2} P_{i,3} P_{i,4} P_{i,5} P_{i,6}; \dots; P_{Q,1} P_{Q,2} P_{Q,3} P_{Q,4} P_{Q,5} P_{Q,6}] \quad (4.16)$$

where  $P_{ij}$  is the observation  $j$  ( $j = 1, \dots, 6$ ) of the storm  $i$  ( $i = 1, \dots, Q$ ), and takes value between 1 and  $S$ . For instance, if  $S$  is equal to 5,  $D_S$  may have the following distribution:

$$D_S = [5, 1, 3, 3, 4, 3; 2, 3, 4, 5, 5, 5; 1, 2, 3, 2, 2, 2; \dots; 2, 1, 1, 3, 4, 1] \quad (4.17)$$

The  $D_S$  vector means that the set composed of historical data and the actual data ( $D_T$ ) has been classified according to each one of the observations. In this way, the first observation of the first tropical cyclone that composed  $D_T$  is classified as class 5; the second observation of the first tropical cyclone is classified as the class 1, and so on.

3. A majority voting procedure is implemented to get the outcome from the generated information ( $D_S$ ) by the competitive neural network. After six observations that correspond to each one of the tropical cyclones of the dataset ( $D_T$ ) are classified in  $S$  classes, a voting procedure is used to count the decision of each observation. If a majority decision is found, then the decision procedure will determine that the storm under analysis belongs to that majority class. If a majority decision cannot be found, the voting procedure will determine that the storm belongs to several classes that have the same number of decision counts. For example

$$D_S = [1, 2, 3, 3, 4, 3; 4, 4, 5, 5, 6, 6; \dots; 1, 4, 5, 5, 5, 4]$$

Using the above rule, the vector  $V$  may be expressed as follows:

$$V = [3; 4, 5, 6; \dots; 5]$$

The first element of vector  $V$  indicates that the first tropical cyclone, the current tropical cyclone, in  $D_T$  belongs to class 3, because of the majority voting rule; the second element of vector  $V$  means that the second tropical cyclone in  $D_S$  belongs to classes 4, 5 and 6, because the decision counts of the classes 4, 5 and 6 are the same. This process is repeated over and over until the last value is found. In this case, the last element belongs to class 5. Therefore, the tropical cyclones that have the same class to the current storm are selected to be the set of analogous storms ( $D_N$ ).

$$D_N = [D_A, D_{P8}, \dots, D_{P67}, \dots]$$

$$D_N = \begin{bmatrix} La_1 & \cdots & La_6 & La_{P8,1} & \cdots & La_{P8,6} & \cdots & La_{P67,1} & \cdots & La_{P67,6} & \cdots \\ Lo_1 & \cdots & Lo_6 & Lo_{P8,1} & \cdots & Lo_{P8,6} & \cdots & Lo_{P67,1} & \cdots & Lo_{P67,6} & \cdots \\ I_1 & \cdots & I_6 & I_{P8,1} & \cdots & I_{P8,6} & \cdots & I_{P67,1} & \cdots & I_{P67,6} & \cdots \\ \alpha_1 & \cdots & \alpha_6 & \alpha_{P8,1} & \cdots & \alpha_{P8,6} & \cdots & \alpha_{P67,1} & \cdots & \alpha_{P67,6} & \cdots \\ Ju_1 & \cdots & Ju_6 & Ju_{P8,1} & \cdots & Ju_{P8,6} & \cdots & Ju_{P67,1} & \cdots & Ju_{P67,6} & \cdots \\ P_1 & \cdots & P_6 & P_{P8,1} & \cdots & P_{P8,6} & \cdots & P_{P67,1} & \cdots & P_{P67,6} & \cdots \\ TS_1 & \cdots & TS_6 & TS_{P8,1} & \cdots & TS_{P8,6} & \cdots & TS_{P67,1} & \cdots & TS_{P67,6} & \cdots \end{bmatrix}$$



$D_A$



$D_{P8}$



$D_{P67}$

$D_A$  represents the actual tropical cyclone. The  $D_N$  matrix shows that the tropical cyclone ( $D_{P8}$ ) in the database identified by ID-number 8 is analogous to the current storm and also to the storm identified by ID-number 67. It is important to notice that only two storms are used to explain the idea of how the procedure works, but this won't happen in practice because of the great amount of past analogous storms.

**Table 4.4:** Variables Included In the Final Set of Analog Tropical Cyclones

$S_{1,1,k}$	Description
1	Storm Intensity Change (INTCHANGE)
2	Eastward Component of Storm Motion (SMV)
3	Northward Component of Storm Motion (SMU)
4	Magnitude of Storm Motion (SMT)
5	Sea Surface Temperature (SST)
6	Maximum Potential Intensity (MPI)
7	Eastward Component of Wind Speed at 850 mb (U850)
8	Northward Component of Wind Speed at 850 mb (V850)
9	Eastward Component of Wind Speed at 200 mb (U200)
10	Northward Component of Wind Speed at 200 mb (V200)
11	Vertical Wind Shear (VWS)
12	Average Angular Momentum at 850 mb (MOM850)
13	Average Angular Momentum at 200 mb (MOM200)
14	Potential Intensification (POT)

The final set of analogous tropical cyclones ( $D_F$ ) is composed of the seven variables of each one of the past tropical cyclones and the current storm. In addition to these variables, another set of variables ( $D_X$ ), shown in Table 4.4 is added for each one of the past tropical cyclones and is calculated for the current storm. The set  $D_F$  is augmented with the inclusion of  $D_X$ , which is composed of synoptic and persistence variables that are not

considered in the classification process. So the variables set ( $D_X$ ) and the final set of analogous TCs ( $D_F$ ) can be expressed as follows:

$$D_X = \begin{bmatrix} SI_{1,1} & \cdots & SI_{1,14} \\ \vdots & & \vdots \\ SI_{6,1} & \cdots & SI_{6,14} \\ S_{1,1,1} & \cdots & S_{1,1,14} \\ \vdots & & \vdots \\ S_{1,6,1} & \cdots & S_{1,6,14} \\ \vdots & & \vdots \\ S_{n,1,1} & \cdots & S_{n,1,14} \\ \vdots & & \vdots \\ S_{n,6,1} & \cdots & S_{n,6,14} \end{bmatrix}, \quad D_F = (D_F)^T, \quad D_F = [D_F \ D_X]$$
  

$$D_F = \begin{bmatrix} La_1 & Lo_1 & I_1 & \alpha_1 & Ju_1 & P_1 & TS_1 & SI_{1,1} & \cdots & SI_{1,14} \\ \vdots & & \vdots \\ La_6 & Lo_6 & I_6 & \alpha_6 & Ju_6 & P_6 & TS_6 & SI_{6,1} & \cdots & SI_{6,14} \\ La_{1,1} & Lo_{1,1} & I_{1,1} & \alpha_{1,1} & Ju_{1,1} & P_{1,1} & TS_{1,1} & S_{1,1,1} & \cdots & S_{1,1,14} \\ \vdots & & \vdots \\ La_{1,6} & Lo_{1,6} & I_{1,6} & \alpha_{1,6} & Ju_{1,6} & P_{1,6} & TS_{1,6} & S_{1,6,1} & \cdots & S_{1,6,14} \\ \vdots & & \vdots \\ La_{n,1} & Lo_{n,1} & I_{n,1} & \alpha_{n,1} & Ju_{n,1} & P_{n,1} & TS_{n,1} & S_{n,1,1} & \cdots & S_{n,1,14} \\ \vdots & & \vdots \\ La_{n,6} & Lo_{n,6} & I_{n,6} & \alpha_{n,6} & Ju_{n,6} & P_{n,6} & TS_{n,6} & S_{n,6,1} & \cdots & S_{n,6,14} \end{bmatrix}$$

} Data set for current storm  
} Data set for first analog storm  
} Data set for last analog storm

↑

Latitude

↑

Longitude

↑

Intensity

↑

Direction

↑

Julian Date

↑

Pressure

↑

Transformed Speed

↑

First variable in Table 4.4  
i.e. INTCHANGE

↑

Last variable in Table 4.4  
i.e. POT

where

- $n$  is the number of analogous storms
- $SI_{1,1}$  is the first synoptic or persistence variable for the current storm and for the first observation while  $S_{6,14}$  is the 14<sup>th</sup> variable for the current storm and for the 6<sup>th</sup> observation ( $SI_{p,q}$  is the  $q^{\text{th}}$  synoptic or persistence variable for the current storm and for the  $p^{\text{th}}$  observation)

- $S_{1,6,14}$  is the last ( $14^{th}$ ) synoptic or persistence variable in Table 4.4 for the first storm and for the  $6^{th}$  observation ( $S_{i,j,k}$  is  $k^{th}$  synoptic or persistence variable in Table 4.4 for the  $i^{th}$  storm and for the  $j^{th}$  observation where  $i = 1, 2, \dots, n; j = 1, 2, \dots, 6; k = 1, 2, \dots, 14$ )

#### 4.4 Random Variable Selection

A variable selection procedure is implemented to choose among the variables generated in the previous process, those that best explained the tropical cyclone intensity behavior. The variable selection technique has been widely used throughout the years to find an appropriate number of regressors that can help to reduce the efforts of data collection and model maintenance.

The regression technique is used to correlate the intensity of a current storm with climatological, persistence and synoptic variables of analogous saved on the set ( $D_F$ ) obtained in the previous section. The process includes the following steps:

1. Divide the data into two sets: The analogous set ( $D_F$ ) is divided in two subsets: one is called the response variable ( $Y$ ), composed of the tropical cyclone intensity known up to time  $t$ , and the other is called the predictors variables represented by the matrix ( $X$ ) and its elements are the variables of the analogous tropical cyclones. The matrix representation can be expressed as follows:

$$Y = \begin{bmatrix} IO_1 \\ \vdots \\ IO_6 \\ I_{1,1} \\ \vdots \\ I_{1,6} \\ \vdots \\ I_{n,1} \\ \vdots \\ I_{n,6} \end{bmatrix} \quad X = \begin{bmatrix} La_1 & \cdots & TS_1 & SI_{1,1} & \cdots & SI_{1,14} \\ \vdots & & \vdots & \vdots & & \\ La_6 & \cdots & TS_6 & SI_{6,1} & \cdots & SI_{6,14} \\ La_{1,1} & \cdots & TS_{1,1} & S_{1,1,1} & \cdots & S_{1,1,14} \\ \vdots & & \vdots & \vdots & & \vdots \\ La_{1,6} & \cdots & TS_{1,6} & S_{1,6,1} & \cdots & S_{1,6,14} \\ \vdots & & \vdots & \vdots & & \vdots \\ La_{n,1} & \cdots & TS_{n,1} & S_{n,1,1} & \cdots & S_{n,1,14} \\ \vdots & & \vdots & \vdots & & \vdots \\ La_{n,6} & \cdots & TS_{n,6} & S_{n,6,1} & \cdots & S_{n,6,14} \end{bmatrix}$$

} Data set for current storm

} Data set for first analog storm

} Data set for last analog storm

Where  $IO_I$  is the first intensity observation for the current tropical cyclone,  $I_{1,1}$  is the first intensity observation for the first analog storm that composed of the set  $Y$ ,  $I_{n,1}$  is the first intensity observation for the last analog storm that composed of the set  $Y$  and  $n$  is the number of analogs storms.  $La_1$  is the first latitude observation for the current storm,  $La_{1,1}$  is the first latitude observation for the first analog storm and  $La_{n,1}$  is the first latitude observation for the last analog storm.  $SI_{1,1}$  and  $S_{1,14}$  are the first and last variables listed in Table 4.4 for the first observation of the current storm while  $S_{6,14}$  is the last variable (in Table 4.4) for the 6<sup>th</sup> observation of current storm.  $S_{1,1,14}$  is the last variable for the first observation of the first analog storm and  $S_{n,6,1}$  is the first variable for the 6<sup>th</sup> observation of the last analog storm.

2. Re-organize the data according to lead time: A lead time ( $t_g$ ) is defined so that the correlations between the dependent variable ( $Y$ ) and the independent variable ( $X$ ) could be lagged by  $t_g$  periods of time. The value  $t_g$  varied between 1 and 4, where  $t_g = 1$  indicates that the lag period is 6 hours, and  $t_g = 4$  indicates that the lag period is 24 hours. Considering the following information:

$$Y = \begin{bmatrix} I_1 \\ I_2 \\ I_3 \\ I_4 \\ I_5 \\ I_6 \end{bmatrix} \text{ and } X = \begin{bmatrix} La_1 & \cdots & TS_1 & S_{1,1} & \cdots & S_{1,14} \\ La_2 & \cdots & TS_2 & S_{2,1} & \cdots & S_{2,14} \\ La_3 & \cdots & TS_3 & S_{3,1} & \cdots & S_{3,14} \\ La_4 & \cdots & TS_4 & S_{4,1} & \cdots & S_{4,14} \\ La_5 & \cdots & TS_5 & S_{5,1} & \cdots & S_{5,14} \\ La_6 & \cdots & TS_6 & S_{6,1} & \cdots & S_{6,14} \end{bmatrix}$$

When the lead time ( $t_g$ ) is set at 4, this lead time indicates that the dependant variable ( $Y$ ) at time  $t$  is expanded using information ( $X$ ) at the time  $t-4$ . Thus, it follows:

$$Y = \begin{bmatrix} I_5 \\ I_6 \end{bmatrix} \text{ and } X = \begin{bmatrix} La_1 & \cdots & TS_1 & S_{1,1} & \cdots & S_{1,14} \\ La_1 & \cdots & TS_1 & S_{1,1} & \cdots & S_{1,14} \end{bmatrix}$$

The first four observations in the dependent variables ( $Y$ ) are eliminated because of the effect of the lag. The last four observations in the independent variables ( $X$ ) are removed from the matrix to be used at the prediction stage. Then, the application of a given lead time ( $t_g$ ) can be described mathematically as follows:

$$Y = \begin{bmatrix} I_{t_g+1} \\ I_{t_g+2} \\ \vdots \\ I_{t-1} \\ I_t \end{bmatrix} \text{ and } X = \begin{bmatrix} La_1 & \cdots & TS_1 & S_{1,1} & \cdots & S_{1,14} \\ La_2 & \cdots & TS_2 & S_{1,2} & \cdots & S_{2,14} \\ \vdots & & \vdots & \vdots & & \vdots \\ La_{(t-1)-t_g} & & TS_{(t-1)-t_g} & S_{(t-1)-t_g,1} & & S_{(t-1)-t_g,14} \\ La_{t-t_g} & & TS_{t-t_g} & S_{t-t_g,1} & & S_{t-t_g,14} \end{bmatrix}$$

$$\forall t - t_g \geq 1$$

**Table 4.5:** Lag Value used in the model

Lag Value ( $t_g$ )	Time (hours)
1	6
2	12
3	18
4	24

3. Implement a random variable selection scheme: A random variable selection scheme is developed. This process has the ability to select the regressors that best fit the dependent variable, in this case the tropical cyclone intensity. The number of variables in a group should be 20% or less than the number of observations contained in the response variable. This rule is implemented to avoid bias on regression estimators, which occurs when the number of variables exceeds the number of observations. The members of each group will be randomly selected. This random selection will produce a robust variable identification. The procedure can be described as follows:

A. Divide regressor set  $X$  into  $n$  subset(s) of  $m$  variable(s): Given the regressor set ( $X$ ) with  $a$  observations (rows) and  $b$  variables (columns), then the number of new variables ( $m$ ) for each  $n$  subset is calculated as follows:

(1). Number of variables per subset: If the number of variables ( $b$ ) is less than the 20% of the number of observations ( $a$ ), then the number of new variables ( $m$ ) per subset is set equal to  $b$ ; otherwise, the number of new variables ( $m$ ) is rounded to nearest integer of the twenty percent of the number of observations ( $a$ ). The following code illustrates the above rule:

$$\text{if } b \leq (a * 0.2)$$

```

    m = b;
else
    m = (round(a*0.2));
end

```

where *round* is the function to round the given number to the nearest integer

(2). Number of subsets: If the modulus of the division between the number of variables (*b*) and the new variable (*m*) is equal to zero, then the number of subsets is equal to this division; otherwise, the number of subset is equal to this division plus one, as shown in the following code:

```

if mod(b,m) == 0
    n = b/m;
else
    n = b/m;
    n = floor(n)+1;
end

```

where *mod* is the function to calculate the modulus after division; and *floor* is the function to round the given number to the nearest integer less than or equal to that number.

Then, the set *X* is divided in *n* subsets if the condition is true as follows:

$$X_{a,b} = [X_{a,m}^1 \quad X_{a,m}^2 \quad \dots \quad X_{a,m}^i \quad \dots \quad X_{a,m}^{n-1} \quad X_{a,m}^n]$$

- B. Use stepwise regression to model the response variable *Y*: Each one of these *n* or *n+1* regressor subsets and its corresponding response (*Y*) is adjusted using a Matlab function called “Stepwisefit”, which is specially designed to fit regression models using stepwise regression. Stepwise regression is the combination of two procedures called forward and backward regression and is used to find a satisfactory number of regressors that best fit to a given response variable.

To fit a regressor set ( $X_{a,m}^i$ ), the stepwisefit function is executed as many times as the set requires. The function can be expressed as follows:

```
[b, se, pval, inmodel, stats, nextstep, history] =  
    stepwisefit(X, Y, 'penter', .08, 'remove', .10, 'maxiter', 1000);
```

where

- *b* is a result vector of estimated coefficient values for all columns of *X*.
- *se* is a vector of standard errors for *b*.
- *pval* is a vector of p-values for testing whether *b* is 0.
- *inmodel* is a logical vector, whose length equals the number of columns in *X*, specifying which predictors are in the final model. A “1” in position *j* indicates that the *j*<sup>th</sup> predictor is in the final model; a “0” indicates that the corresponding predictor is not in the final model.
- *stats* is a structure containing additional statistics.
- *nextstep* is the recommended next step -- either the index of the next predictor to move in or out, or 0 if no further steps are recommended.
- *history* is a structure containing information about the history of steps taken.
- *X* is columns of matrix.
- *Y* is the response variable.
- *penter* is maximum p-value for a predictor to be added. The default is 0.05.
- *remove* is minimum p-value for a predictor to be removed. The default is 0.10.
- *maxiter* is maximum number of steps to take (default is no maximum)

Only the best regressors for each one of the  $n$  or  $n+1$  sets will be selected and collected to create a new set of regressors called the best subset ( $X_{BS}$ ). The maximum number of variables per best subset is seven. If the new set contains more than seven variables, the system will select seven of them randomly.

## 4.5 Intensity Prediction Using Feedforward Neural Network

A feedforward neural network model is characterized by receiving input information to accomplish a modeling identification task without processing feedback information. The training patterns are presented to the network model several times until eventually the algorithm determines the optimal weights and biases that minimize the deviation between the network outputs and the established targets. The feedforward neural network model uses a variation of the standard backpropagation algorithm as the learning rule, which is based on the steepest descent algorithm. The errors are used to modify the searching direction and the gradient is computed at each layer starting from the last layer and finishing with the first layer. This is the reason for the backpropagation name.

This section describes the procedure to apply the Levenberg-Marquardt backpropagation algorithm to predict the tropical cyclone intensity using the best subset obtained in the previous section.

### 4.5.1 Application of Levenberg-Marquardt Backpropagation Algorithm

The best subsets (XBS) obtained in the variable selection procedure are used as input data for this algorithm which is used to estimate the tropical cyclone intensity in a determined interval of time ( $tg$ ). The procedure used to train the neural network can be divided in seven major tasks:

#### 1. Assemble the Training Data

The current inputs ( $XBS$ ) and their target vectors (TC intensity) are arranged in the following way:

$$XBS = \begin{bmatrix} X_{1,1} & X_{1,2} & \cdots & X_{1,n-1} & X_{1,n} \\ X_{2,1} & X_{2,2} & \cdots & X_{2,n-1} & X_{2,n} \\ \vdots & \vdots & & \vdots & \vdots \\ X_{(t-1)-tg,1} & X_{(t-1)-tg,2} & \cdots & X_{(t-1)-tg,n-1} & X_{(t-1)-tg,n} \\ X_{t-tg,1} & X_{t-tg,2} & \cdots & X_{t-tg,n-1} & X_{t-tg,n} \end{bmatrix} \text{ and } Y = \begin{bmatrix} I_{tg+1} \\ I_{tg+2} \\ \vdots \\ I_{t-1} \\ I_t \end{bmatrix}$$

where  $X_{t-tg}$ ,  $n$  is the  $n$  best regressors at  $t-tg$  time and it is the intensity at the time  $t$ ,  $XBS$  is the best subset of regressors.

## 2. Create the Network Object

A Matlab routine is used to create the network object. The function “*Newff*” creates a feedforward neural network and also initializes the weights and biases of the network; therefore the network is ready for training. The function can be expressed as follows:

$$net = newff(PR, [S1 S2...SN], \{TF1 TF2...TFN\}, BTF, BLF, PF)$$

where:

-*PR* is  $R \times 2$  matrix of min and max values for  $R$  input elements.

-*Si* is Size of  $i^{th}$  layer, for  $Nl$  layers.

-*TFi* is Transfer function of  $i^{th}$  layer, default = '*tansig*'.

-*BTF* is Backpropagation network training function, in this case Levenberg-Marquardt algorithm.

-*BLF* is Backpropagation weight/bias learning function, default = '*learnqdm*'.

-*PF* is Performance function, default = '*mse*'.

## 3. Normalize Inputs and Targets

Neural network training can be made more efficient if certain preprocessing steps are performed on the network inputs and targets. Matlab routine “*prepca*” is used to increase the training efficiency.

In some situations, the dimension of the input vector is large, but the components of the vectors are highly correlated (redundant). It is useful in this situation to reduce the dimension of the input vectors. An effective procedure for performing this operation is principal component analysis. This technique has three effects: it orthogonalizes the components of the input vectors (so that they are uncorrelated with each other); it orders the resulting orthogonal components (principal components) so that those with the largest variation come first; and it eliminates those components that contribute the least to the variation in the data set. The following code illustrates the use of *prepca*, which performs a principal component analysis:

$$[pn, meanp, stdp] = prestd(p);$$
$$[ptrans, transMat] = prepca(pn, 0.02);$$

First of all, normalize the input vectors, using *prestd* which normalizes the inputs and targets so that they will have zero mean and unity standard deviation. The *pn* is the normalized inputs and the vectors *meanp* and *stdp* contain the means and standard deviations of the original targets. This is a standard procedure when using principal components. In this study, the second argument passed to *prepca* is 0.02. This means that *prepca* eliminates those principal components that contribute less than 2% to the total variation in the data set. The matrix *ptrans* contains the transformed input vectors. The matrix *transMat* contains the principal component transformation matrix. After the network has been trained, this matrix should be used to transform any future inputs that are applied to the network. It effectively becomes a part of the network, just like the network weights and biases. If multiply the normalized input vectors *pn* by the transformation matrix *transMat*, this can obtain the transformed input vectors *ptrans*.

#### 4. Apply Early Stopping to improve generalization

One of the problems that would occur during neural network training is called “*overfitting*”. The error on the training set is driven to a very small value, but when new data is presented to the network the error is large. The network has memorized the training examples, but it has not learned to generalize to new situations. Early stopping technique can be used to improving network generalization. In this technique the available data is divided into three subsets:

The first subset is the training set, which is used for training a neural network and computing the gradient and updating the network weights and biases. The second subset is the validation set, which is utilized to determine the performance of the neural network on patterns that are not trained during the learning. The error on the validation set is monitored during the training process. The validation error will normally decrease during the initial phase of training, as does the training set error. However, when the network begins to overfit the data, the error on the validation set starts to go up. When the validation error increases for a specified number of iterations, the training is stopped, and

the weights and biases at the minimum of the validation error are returned. The final set is the test set which is used to finally check the overall performance of the neural network and estimate the generalization error. Test set is not used at all during the training process. It is useful to plot the test set error during the training process. If the error in the test set reaches a minimum at a significantly different iteration number than the validation set error, this may indicate a poor division of the data set.

In this study, a quarter of the data is taken for the validation set, the other quarter for the test set and the remaining half for the training set. The sets are picked as equally spaced points throughout the original data.

## 5. Train the Network

Once the network weights and biases had been initialized, the network is ready to be trained. The training process requires a training set (network inputs and target outputs). During training, the weights and biases of the network are adjusted to minimize the sum of square errors ( $F(x)$ ). The training process is implemented using a Matlab function called “*train*” that has the following parameters:

$$[net, tr] = train (NET, p, t)$$

where:

- $NET$ =original network
- $p$  = network inputs
- $t$  = network targets
- $net$ = new network
- $tr$  = training record

In this study, a two-layer network, with tan-sigmoid transfer function, *Tansig*, in the hidden layer and a linear transfer function, *Purelin*, in the output layer is employed. The network has four neurons in the hidden layer and 1 output neuron since there is one target. The number of neurons ( $H$ ) in the hidden layer is calculated by following formula:

$$H = P / (10(m + n))$$

where

- $P$  = number of training examples
- $m$  = number of outputs
- $n$  = number of inputs

## 6. Evaluate the Network Response to New Inputs

Up to this point, the NN has been trained using the inputs (*XBS*) and compared with the known tropical cyclone intensity (*Y*) to minimize the performance function. The next step is to present current storm parameters to the trained NN for obtaining a tropical cyclone intensity prediction at the desired lead time ( $t+tg$ ) as follows:

$$XNEW = [X_{t,1} \ X_{t,2} \ \dots \ X_{t,n-1} \ X_{t,n}]$$

$$I_{t+tg} = \text{sim}(\text{net}, (XNEW)T)$$

Where *XNEW* represents the tropical cyclone parameters at the present time ( $t$ ),  $I_{t+tg}$  is the predicted intensity in the lead time ( $tg$ ) and *sim* is a Matlab function used to evaluate the neural network (*net*) when new input values are provided.

Finally, it is important to notice that each best subset (*XBS*) is used to train an NN three times and a tropical cyclone intensity prediction is obtained. Since the NN is a nonlinear optimization algorithm and highly depends on the initial point, the NN will provide different results after every training process. Thus, an individual best subset is used to perform three predictions and its median is selected as the prediction for the best subset.

## 7. Perform Post-Training Analysis

The performance of a trained network can be measured to some extent by the errors on the training, validation and test sets, but it is often useful to investigate the network response in more detail. One option is to perform a regression analysis between the network response and the corresponding targets. The routine “*postreg*” provided by Matlab is designed to perform this analysis. The following commands illustrate how a regression analysis can be performed on the network”:

$$[m,b,r] = \text{postreg}(a,t)$$

The network output *a* and the corresponding targets *t* are pass to *postreg*. It returns three parameters. The first two, *m* and *b*, correspond to the slope and the y-intercept of the best linear regression relating targets to network outputs. The third variable returned by *postreg* is the correlation coefficient (*R-value*) between the outputs and targets.

## **4.6 Experimental Results Analysis**

In this section we present the results obtained by the application of the proposed intensity prediction model to a set of tropical cyclones from the Western North Pacific. Altogether we selected 19 tropical cyclones out of 199 as the representative sample of the tropical cyclone population used in this work, and was determined using the concepts of minimizing the sampling errors. These samples are time-series distributed and recorded every 6 hours during their lives. Besides, we also collected monthly data for the Mean Sea surface Level Pressure (MSLP) and NCEP/NCAR data all over the world from RAOB of NOAA from 1994 to 2003, in which we used two years' data (2002 and 2003) for the experiments. A computer with 2.26 GHz Intel Pentium CPU and 512M RAM memory was used for the simulations. As the tropical cyclone observation sample is relatively large, we only considered those samples with equal or more observations than the input sample as the training set, which not only decreases the volume of the training set, but also improve the training accuracy of the network.

Several experiments are carried out to evaluate the ability of the model to deal with different kind of tropical cyclones. Strong and typical tropical cyclone cases are first presented, followed by a tropical cyclone with high rate of intensification. Then the rapid intensity reduction rate is presented and a tropical cyclone with re-intensification behavior is presented. Finally tropical cyclone with double eye walls is discussed.

### **4.6.1 Experiment with Strong Tropical Cyclone Intensity**

An important aspect for any intensity prediction model is the capability of modelling tropical cyclones that reaches the strongest category. The proposed model is tested using a strong tropical cyclone, Lupit, which was the most intense TC in 2003 in Western North Pacific. It formed as a tropical depression over the Pacific about 1200 km south-southwest of Wake Island on 19 November and moved generally westwards. It intensified into a tropical storm on 21 November and strengthened into a severe tropical storm the next day. Lupit further strengthened into a typhoon on 23 November and

tracked northwestwards on 24 November. It attained a maximum sustained wind speed of 125 kt (230 km/h) on the night of 26 November. Lupit turned northeastwards on 29 November and started to accelerate the next day. It weakened into a severe tropical storm on 1 December. Lupit further weakened into a tropical storm on 2 December and became an extratropical cyclone the same day. Figure 4.3 shows the official intensity (dotted line) for Lupit given by the **Hong Kong Observatory (HKO)** and the forecast intensity at 12 hours (continuous line) obtained by the proposed model. The average absolute prediction error at 12 hours interval is 7.95 knots and it is computed along of the storm.

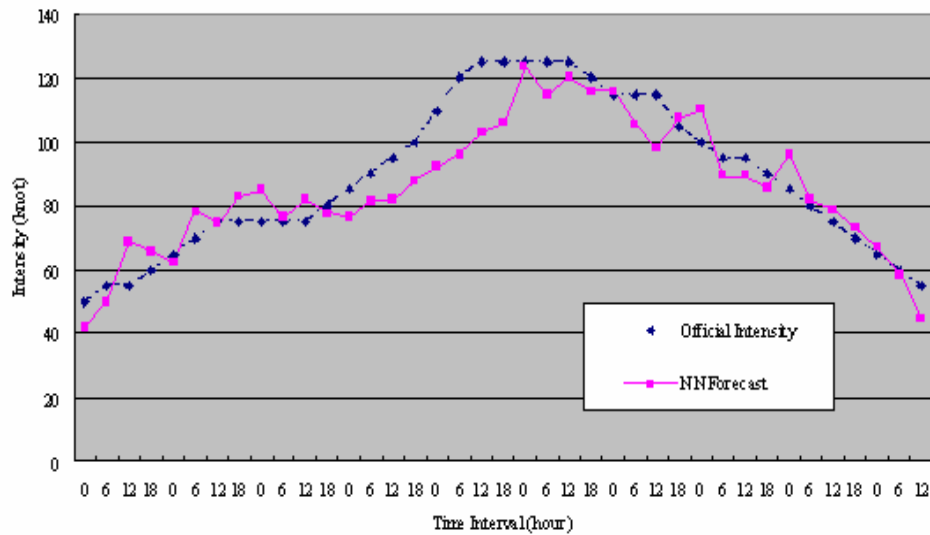


**Figure 4.3:** Intensity predictions for Lupit at 12 hours (November, 2003)

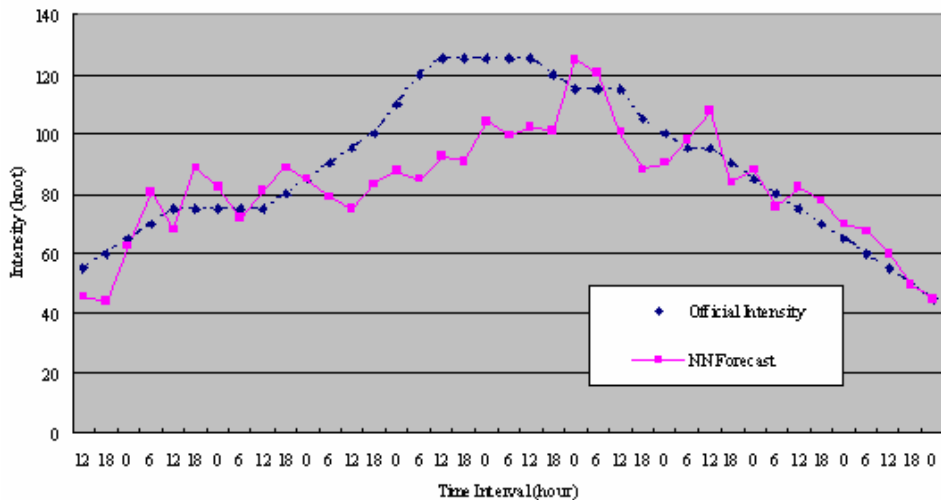


**Figure 4.4:** Intensity predictions for Lupit at 24 hours (November, 2003)



Figure 4.5 shows the outputs for Podul (2001) at 12 hours. It is a storm that reached its peak at 105 knots and is categorized as hurricane of category three. The average absolute intensity error at 12 hours interval prediction for this tropical cyclone using the proposed intensity model is 5.19 knots along of the storm.

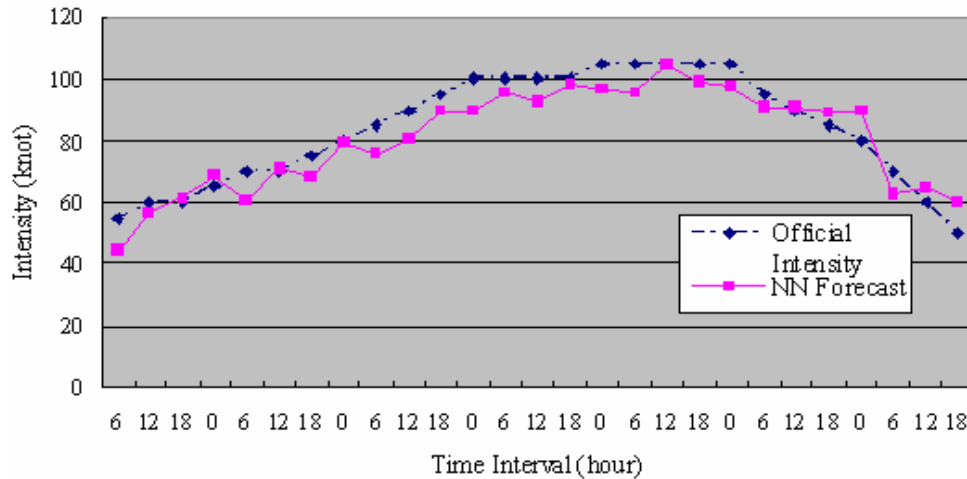


**Figure 4.6:** Intensity Predictions for Podul at 24 Hours (October, 2001)

The proposed model is also evaluated with a typical tropical cyclone at 24 hours. Figure 4.6 shows the results. The average absolute intensity error for Podul at 24 hours interval prediction using the proposed intensity model is 5.56 knots along of the storm. It can be seen that the proposed algorithm has the potential to predict better the intensity of a typical tropical cyclone than the intensity of a strong storm.

### 4.6.3 Fast Intensity Change and Re-intensification Experiments

The characteristics that are most difficult to deal with in the prediction of the tropical cyclone intensity are the fast intensification, rapid reduction and re-intensification. The proposed model is tested with tropical cyclones that exhibit at least one of these conditions. Hurricane Katrina, the sixth-strongest storm ever recorded in the Atlantic basin, passed through the Central Gulf Coast of America and flooded and damaged the coastal regions of Louisiana, Mississippi and Alabama. It is the most destructive and costliest natural disaster in the history of the United States. The official death toll now stands at 1,302 and the damage higher than \$200 million. Over a million people become

homeless. In East Asia, The Maemi passed through the seas west of Okinawa and caused in at least one death and 71 injuries. After moving across the East China Sea, Maemi made landfall near Busan in South Korea. In South Korea, Maemi killed at least 113 people and caused 14 other missing. About 34000 hectares of farmland were inundated and 5000 houses were destroyed. Hundreds of roads and bridges were damaged. The economic loss was estimated to be over USD 1.3 billions. Maemi, which reached category four status with a peak intensity of 120 knots, is used to implement the model when a rapid intensification is presented. Figure 4.7 shows the results for Maemi at 12 hours. The average absolute intensity error for this tropical cyclone is 7.50 knots at 12 hours prediction interval along of the storm.

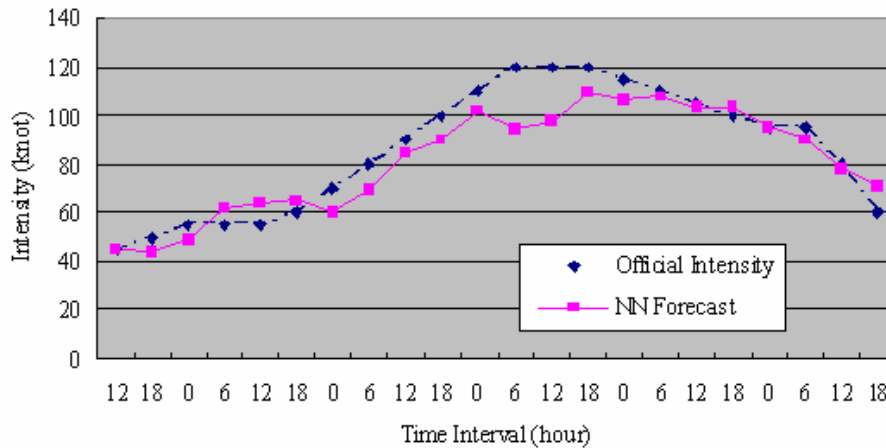


**Figure 4.7:** Forecasting for Maemi when Rapid Intensification is Presented (September, 2003)

It can be seen that the outputs from proposed model followed the official outputs up to the point where Maemi increases rapidly its intensity. However, the errors in the period of intensity peak seemed to be large (15 - 20 knots) for 12 hours, the proposed model tried to follow the observed intensity but it failed to make robust intensity estimation. After Maemi has reached its intensity peak, the proposed model gives an accurate prediction with small errors (less than 6 knots).

The rapid reduction in intensity is also another attribute that is difficult to predict for any intensity prediction model. Dujuan was originated in west-northwest of Guam and was a tropical cyclone that moved towards the seas near southern Taiwan during the peak of the

hurricane season. This tropical cyclone at 24 hours prediction interval is used to test the prediction methodology under fast intensity reduction.

The Dujuan is evaluated because after it reached its intensity peak; it underwent to a fast intensity changing from 95 knots to 35 knots in 24 hours. Figure 4.8 shows the results. The average absolute intensity error of this storm is 10.38 knots when it is evaluated along of its trajectory using 24 hours as an interval prediction.

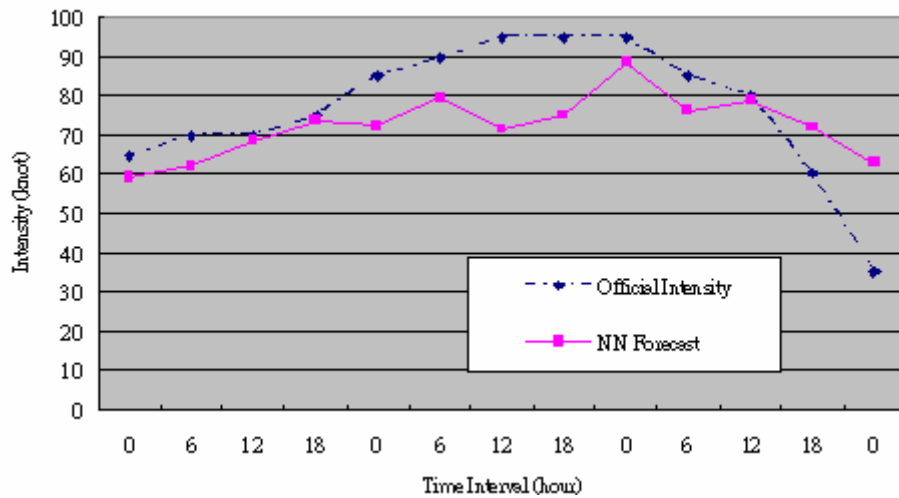


**Figure 4.8:** Forecasting for Dujuan when Rapid Intensity Reductions is Presented (August, 2003)

It can be seen that the outputs from the proposed model failed to follow the official outputs especially in the period of fast intensity reduction. These results show that the model overestimated the tropical cyclone intensity in the fast reduction period. Further analysis is needed to improve the intensity prediction for fast intensity reduction.

A characteristic that is also hard to predict is the re-intensification. This behaviour challenges the model to response as soon as it is detected. Re-intensification means that the tropical cyclone has gained (lost) enough strength to rise (decrease) its intensity. Nari was the tropical cyclone with the most unusual track in 2001 and had a long life span of 15 days, strengthening and weakening repeatedly for four times. It is used to test the proposed model when the re-intensification is presented. The re-intensification is probably the most hazardous of the three conditions before mentioned because it

challenges the model to look out the new tropical cyclone intensity behaviour that could be increasing or decreasing.

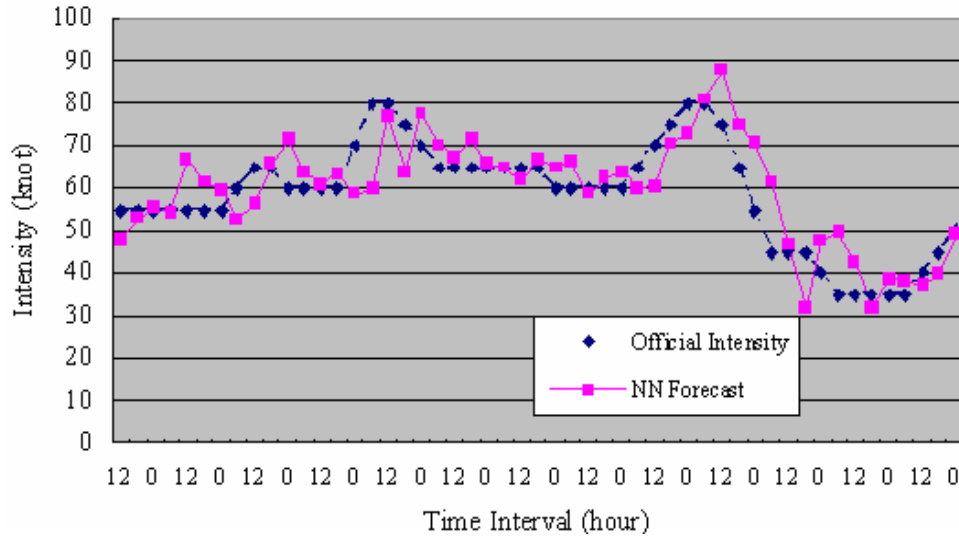


**Figure 4.9:** Re-intensification of Nari (September, 2001)

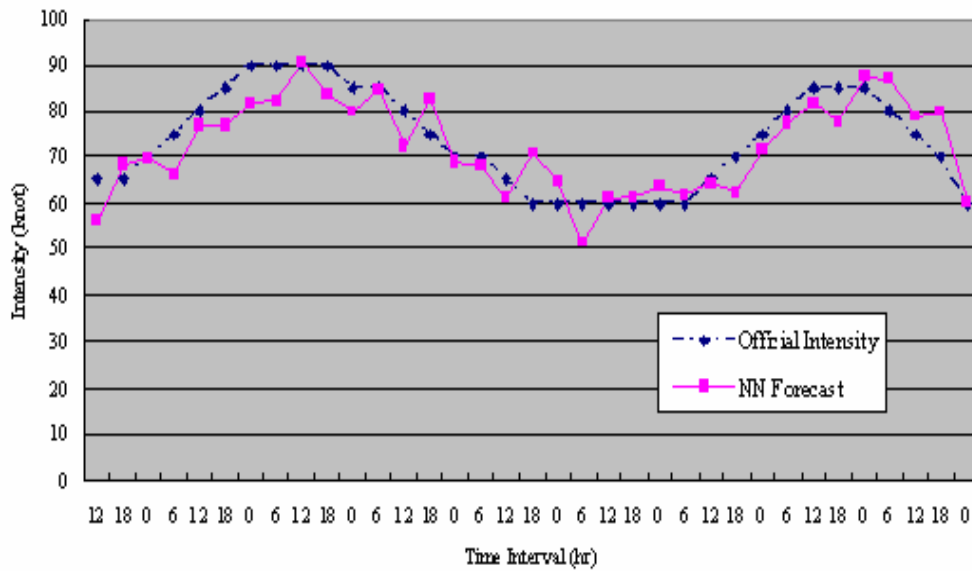


**Figure 4.10:** Re-intensification of Parma (October, 2003)

Figure 4.9 shows the re-intensification process presented in Nari. The average absolute intensity error for Nari is 5.88 knots at 12 hours and 8.63 knots at 24 hours. Figure 4.10 shows another tropical cyclone used for testing the capability of modeling re-intensification. The average absolute intensity error for Parma is 4.71 knots at 12 hours and 8.57 knots at 24 hours.

#### 4.6.4 Experiment with Tropical Cyclone Having Double Eye Walls

Another important aspect for the intensity prediction model is the capability of modelling tropical cyclones with special structure such as double eye walls. The proposed model is tested using storm Dujuan again, which passed to the south of Taiwan and moved towards the Pearl River Estuary in the early September 2003. When Dujuan crossed over the northern part of the South China Sea, it exhibited a double-eye-walled structure. The diameters of the inner and outer eyes are about 20 km and 100 km respectively. The average absolute intensity errors for Dujuan are 7.31 knots and 10.38 knots at 12 and 24 hours interval prediction respectively. The results from the above experiments indicate that the proposed intensity prediction model can provide an effective and efficient way to model storms with double eye walls structure. Figure 4.11 shows the intensity predictions for Dujuan at 12 hours prediction interval.

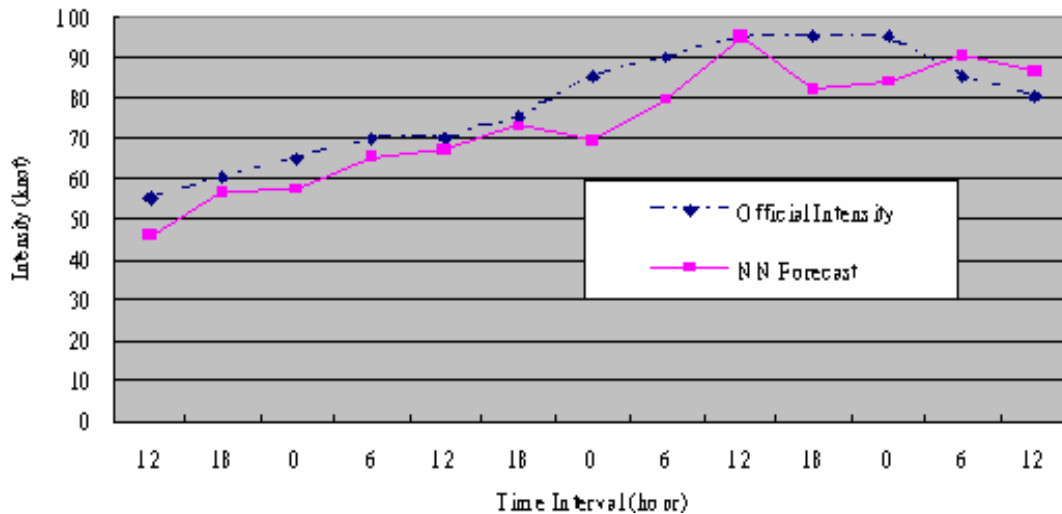


**Figure 4.11:** Intensity predictions for Dujuan at 12 hours (September, 2003)

#### 4.6.5 Comparing With Existing Models

From the experiments, we know that the most important variables in this work are storm pressure, intensity change, sea surface temperature, storm location (latitude and longitude), and vertical wind shear. The detail contributions of variables are shown in Table 4.6 below.

**Table 4.6:** Variable Contribution for the Tropical Cyclone Sample at 6, 12, 18 and 24 hours

No	Variable	Name	Percentage (%)			
			6 hrs	12 hrs	18 hrs	24 hrs
1	LAT	Storm Location Latitude	2.67	5.58	7.50	9.32
2	LON	Storm Location Longitude	7.69	8.71	9.08	8.30
3	TCJDATE	Julian Day	4.36	3.13	4.05	3.86
4	DIR	Direction	1.33	1.42	1.92	3.37
5	SPEED	Translation Speed	6.90	8.08	6.27	6.78
6	MSLP	Minimum Central Pressure	14.35	13.60	12.33	12.36
7	INTCHANGE	Storm Intensity Change	12.05	13.60	11.99	11.25
8	SMV	Northward component of storm motion	1.57	1.14	1.87	2.67
9	SMU	Eastward component of storm motion	4.48	5.35	4.49	3.37
10	SMT	Storm Motion	4.18	0.68	1.09	2.67
11	SST	Sea Surface Temperature	4.48	9.90	10.51	9.53
12	MPI	Maximum Potential Intensity	5.27	3.53	3.16	3.70
13	U850	Eastward component of wind speed at 850 mb	2.48	2.16	2.57	1.23
14	V850	Northward component of wind speed at 850 mb	1.88	1.99	2.81	2.96
15	U200	Eastward component of wind speed at 200 mb	3.21	2.96	2.81	2.09
16	V200	Northward component of wind speed at 200 mb	3.69	1.82	1.97	2.67
17	VWS	Vertical Wind Shear	7.21	6.77	7.05	6.37
18	MOM850	Average Angular Momentum at 850 mb	2.00	1.20	1.83	1.81
19	MOM200	Average Angular Momentum at 200 mb	4.48	3.53	2.71	2.22
20	POT	Potential Intensification	5.69	4.84	4.00	3.49

The storm pressure variable measured in the tropical cyclone’s eye has been the most important predictor in this work. This result is not surprised since the relation between tropical cyclone intensity and storm pressure is directly proportional. These results can be explained using the idea that the smaller the central pressure, the greater winds that surrounded the storm. The intensity change is the second important variable that explains the tropical cyclone intensity for the proposed model. This result comes in agreement with the results found by DeMaria [30] who pointed out that the intensity change provides a pattern of future storm’s behaviour which means that storm that has intensified in the past 6 hours is likely to continue intensifying. The storm latitude and longitude variables have also proved their advantages to explain the tropical cyclone intensity. The sea surface temperature (SST) is another important predictor in the tropical cyclone intensity models. The results of this work agree with the results found by Baik [78]. The last important predictor is vertical wind shear (VWS) which is the difference between 200 mb and 850 mb wind vector. It contributes around 7 % of variable contribution. This shows that the wind components at 850 mb and 200 mb have a close relationship with intensity change of the tropical cyclone.

Results have shown the performance of the proposed model for different types of tropical cyclones. The performance of the model is difficult to compare with existing models because of limitation of published results. However, a comparison with small sample size is conducted. Table 4.7 shows the comparison between the performance of the proposed model and the model used by Joint Typhoon Warning Center [79].

**Table 4.7:** Comparison Between the Proposed Model and JTWC’s Model

Model	Season	12 Hours		24 Hours	
		No Cases	Average Error (kt)	No Cases	Average Error (kt)
NN Model	2001-2003	448	5.90	448	8.86
JTWC Model	2001-2003	625	7.84	602	11.63

Table 4.8 and Table 4.9 show the relative improvement and intensity forecast error by the proposed model over the official JTWC’s model. Note that the proposed model achieved a considerable improvement at 12 and 24 hours interval over the model used by JTWC.

**Table 4.8:** Proposed Model’s Improvement over JTWC’s Model

Model	At 12 Hours (%)	At 24 Hours (%)
JTWC Model	24.74	23.82

**Table 4.9:** JTWC TC Intensity Forecast Error (Sourced by JTWC)

	2004 JTWC 24-h	2003 JTWC 24-h	2002 JTWC 24-h	2001 JTWC 24-h
<b>Average Abs. Intensity Error (kt)</b>	11.0	11.0	10.0	11.0

Figure 4.12 shows the fitness of the NN model (small dotted line) over the multiple linear regression model (continuous line) when both models are tested using the same variables to predict the tropical cyclone intensity. Also, the official forecast is shown (dotted line). This figure shows that the NN model can give a more accurate prediction on intensity (more close to the official forecast line) in the prediction stage than the Regression model that gives the same results obtained by Baik [78].

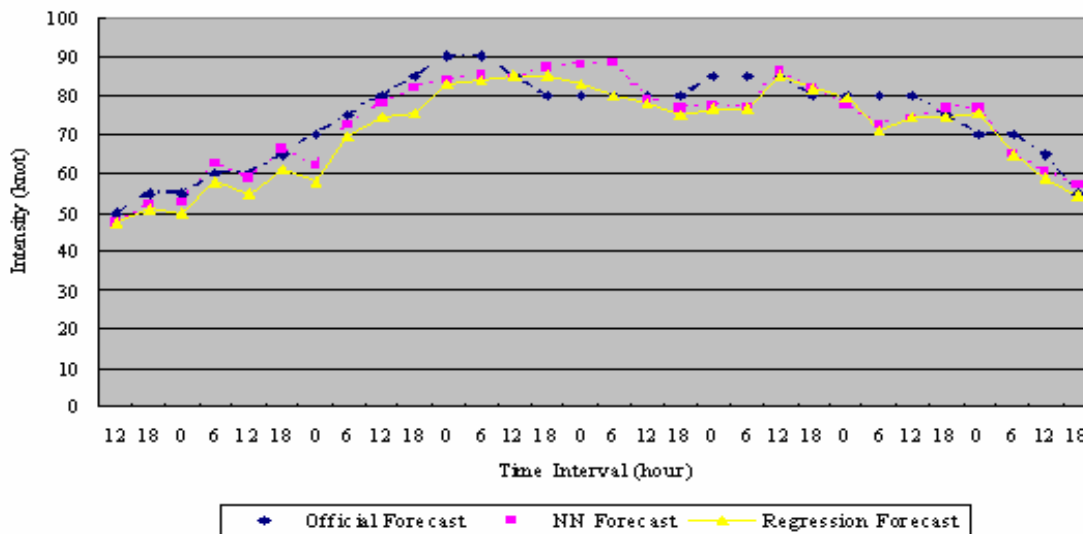


**Figure 4.12:** NN Model Enhancements over Regression Model for Rusa at 12 Hours (August, 2002)

Table 4.10 displays the average absolute errors obtained by the proposed NN model and those obtained by the multiple linear regression models. Furthermore, the percentages of this improvement are shown.

**Table 4.10:** Proposed Model Improvements over Multiple Linear Regression Model

Model	Season	At 12 Hours		At 24 Hours	
		No Cases	Average Error (kt)	No Cases	Average Error (kt)
NN Model	2001-2002	63	5.88	63	8.90
Regression Model	2001-2002	63	6.58	63	10.76
NN improvement over Regression (%)		10.64		17.29	

## 4.7 Summary

In this chapter, artificial neural network and upper air information are used to develop a model for predicting tropical cyclone intensity in the Western North Pacific at 6, 12, 18 and 24 hours. The historical NCEP (National Center for Environment Prediction) analyzing data and the sea surface temperature (SST) values are used along of each storm tracks to develop a set of climatology, persistence and synoptic variables. A competitive neural network (CNN) is adopted to identify analog storms to the current tropical cyclone. Once the analog tropical cyclones are identified, the persistence, climatological and synoptic observations of analog tropical cyclones and the current storm are combined to create a training set and a multiple-regression scheme is used to identify the variables that are best correlated with storm intensity. Experimental results clearly show that the proposed prediction scheme is a potential tool to increase the accuracy in predicting tropical cyclone intensity.

# Chapter 5. A Similarity Retrieval Model for Time-Series Tropical Cyclone Data

The last two decades have seen attempts to solve non-linear forecasting problems using AI technologies such as neural networks, fuzzy logic, genetic algorithms and expert systems. For instance, in [81], the authors allow a user to prescribe a solution based on the context of the current problem and those of selected past samples [82]. In [83], the authors proposed their approaches to allow numerical features to be converted into fuzzy terms and have greater flexibility in the retrieval of candidate cases. However, few of these research works ever tackle the intensity prediction of the tropical cyclone very well, and the critical obstacles to determine the importance of various features also exists. For tropical cyclone prediction, it has its particular characteristics, which are continuous, data-intensive, multidimensional dynamic and chaotic. Besides, tropical cyclones have great relationship with time-series, which increase in complexity but haven't drawn too much attention from researchers.

In this part, we describe a similarity retrieval model to predict tropical cyclone intensity using a feed-forward neural weight generator, which is adopted to generate a set of appropriate weights for various associated features of tropical cyclones. We also propose the time-series similarity adjustment to measure the similarity of samples on consecutive observations of a tropical cyclone. To validate our idea, we have evaluated its performance and results show that our proposed model has achieved a promising output.

The rest of this chapter is organized as follows. In section 5.1, a system overview is given with description for every segment in the retrieval system. Then similarity measure functions for numerical variables such as Position, SMLP and Speed are described in section 5.2. A neural weight generator using a feed forward neural network is designed to determine the importance of each attribute contributing to the similarity of two observations. In this section, a time-series adjustment function is proposed to reflect the

time sensitive to the similarity measure. At last in section 5.3, experiments are carried out to validate this approach by comparing its results with other two existing methods.

## 5.1 System Overview

Figure 5.1 shows a forecasting model to predict the tropical cyclone intensities. This model uses a neural weight generator to estimate the significance of every feature of a tropical cyclone from observation. The time series adjustment is used to improve the similarity calculation among the tropical cyclone samples based on their observation sequence, which will be discussed in latter sections.

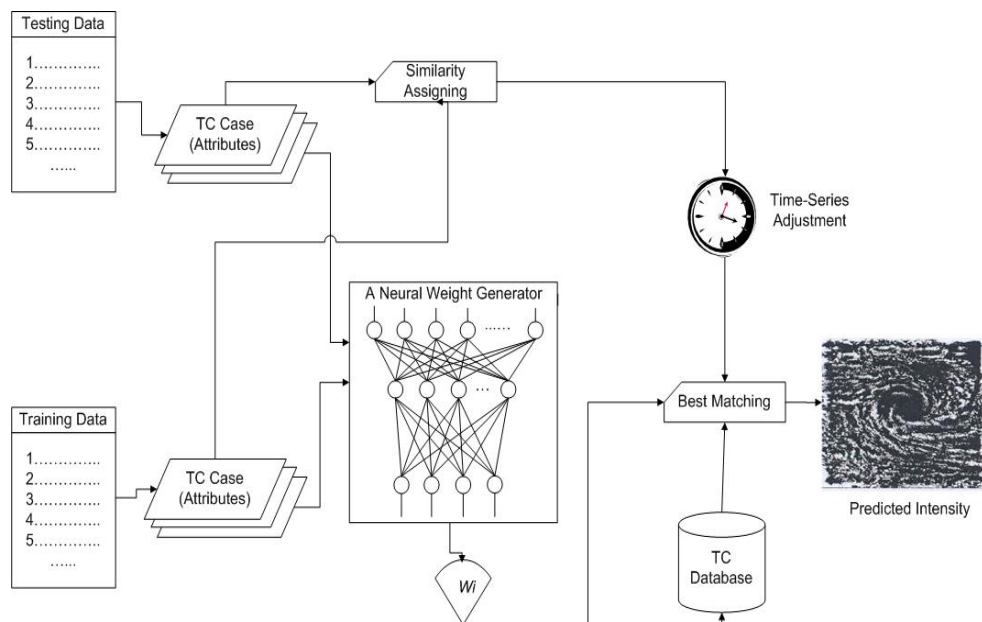


**Figure 5.1:** Overview of the proposed prediction model

In Figure 5.1, for every observation sample, either from the training dataset or the testing dataset, it is fed into a neural weight generator to get a set of most appropriate weights for the attributes. The dataset we used in this study is collected from Hong Kong Observatory including ten years tropical cyclone statistics from 1994 to 2003. Five representative attributes are involved in the dataset, Time, Intensity, Position (Longitude, Latitude), Speed and MSLP (Mean Sea Level Pressure). We divide them into three categories as time-series, positional and numerical attribute. Based on these attributes, we

design different similarity measure functions for them respectively. Integrity of the weights and the similarity measures is used to carry out the prediction.

Each part in Figure 5.1 is described as below:

Training Data: samples (shown in Figure 4.1) used to train the neural weight generator;

Testing Data: samples (shown in Figure 4.1, and are supposed that the intensity of the sample is unknown) used to evaluation the performance of the designed system;

TC Case (Attributes): a database to store tropical cyclone information according to their attributes;

Similarity Assigning: the module in which the similarity measure functions are carried out to do the retrieval. Details will be given in section 5.2;

Neural Weight Generator: a feed-forward neural network to determine the weight of each attribute. Details will be given in section 5.2.2;

Time-series Adjustment: a similarity measure to indicate the time-series sensitive for tropical cyclone retrieval. Integrity of time-series adjustment and other similarity measures will be discussed in section 5.2.3;

Best Matching: a matching module to find the most like sample from the database based on the proposed similarity measure functions.

Predicted Intensity: intensity prediction results from the observation samples of the testing dataset.

## **5.2. Similarity Measure Functions**

### **5.2.1 Positional and Numerical Measure Functions**

From the best track data of tropical cyclones we got from Hong Kong Observatory in Figure 4.1, an observation sample can then be defined as an attribute vector  $C = [TN, TT, I, P, SMLP, Sp]$ , where each symbol represents a corresponding attribute for a tropical cyclone observation:  $TN$  (Tropical cyclone Name),  $TT$  (Tropical cyclone Time),  $I$  (Intensity),  $P$  (Latitude, Longitude),  $SMLP$  (Sea Mean Level Pressure) and  $Sp$  (Speed). In this study, we only consider numerical variables such as  $I, P, S, Sp$  and time-series variable  $TT$  because that these variables can represent basic characteristics of a tropical cyclone other than  $TN$ . Besides, as Intensity ( $I$ ) is used as the predicted output of the forecasting model, we also won't consider it in later discussion. We now discuss their similarity functions separately.

For  $SMLP$  and  $Sp$ , their similarity measures of two observation samples can be determined by their distance measure as shown in equation 5.1:

$$D_{SMLP/Speed} = d_{ij} = \frac{|A_i - A_j|}{\max(A) - \min(A)} \quad (5.1)$$

where  $A_i$  and  $A_j$  are values of the attribute  $A$  ( $SMLP$  or  $Sp$ ) in different observations, and  $\max(A)$  and  $\min(A)$  are the maximum and minimum respectively in all samples of the attribute  $A$  ( $SMLP$  or  $Sp$ ). So  $D_{SMLP}$  and  $D_{Speed}$  are limited into interval  $[0,1]$ .

For variable  $Position$  ( $Latitude, Longitude$ ), as it contains two parameters representing its orientations, the similarity measure can be determined as equation 5.2:

$$D_{position} = d_{ij} = \frac{|P_i - P_j|^2}{(\max X)^2 + (\max Y)^2} \quad (5.2)$$

where  $P_i$  and  $P_j$  are the Position vector [ $latitude, longitude$ ] in observation samples, and  $\max X$  and  $\max Y$  denote the most right-button point in the Latitude-Longitude coordinate system covered in our database. Using  $\max X$  and  $\max Y$ ,  $D_{position}$  can be limited into interval  $[0, 1]$ . The Latitude-Longitude coordinate system is described in Figure 5.2 like below.

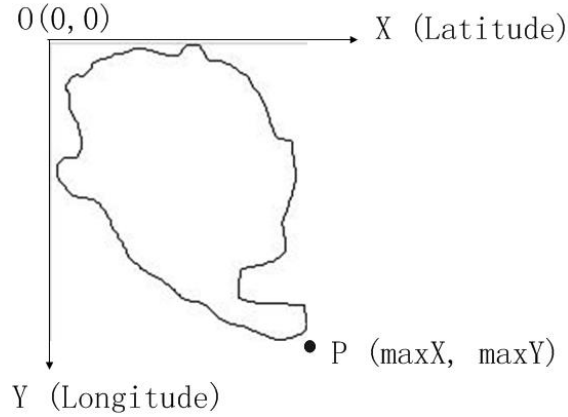


**Figure 5.2:** Latitude-Longitude coordinate system using in similarity functions

Therefore, we get the similarity functions for these three attributes as:

$$Sim(S_i, S_j) = 3 - D_{SMLP} - D_{Speed} - D_{position} \quad (5.3)$$

### 5.2.2 Neural Weight Generator

After we have calculated the similarity measure functions for *SMLP*, *Sp* and *Position*, we calculate the weights of these attributes of each tropical cyclone observation sample. The weight is used to determine the importance of each attribute contributing to the similarity of two observation samples. In this study, a neural weight generator is designed to carry out weight calculation for every attribute, by means of predicting the variable *I* (*Intensity*) for the observation samples in the database using neural network technology. In the neural weight generator, the weight means the positive or negative contribution of that input to the result variable, intensity. Figure 5.3 describes such a neural weight generator.

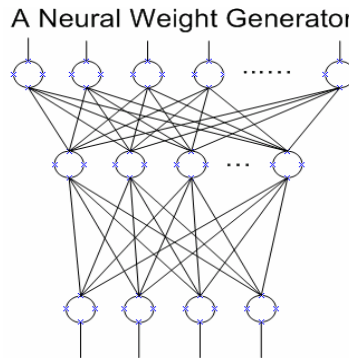


**Figure 5.3:** Structure of the neural weight generator

First of all, the values of these attributes need to be normalized and changed into binary forms, which are the inputs and outputs of the neural weight generator. We use equal width bin approach to normalize each attribute, and the bin width is calculated using equation 5.4.

$$width = \frac{\max(att) - \min(att)}{bin} \quad (5.4)$$

where  $\max(att)$  and  $\min(att)$  are corresponding to the maximum and minimum value of that attribute among all observation samples respectively, and  $bin$  is the number of bins to be divided into. Taking attribute *SMLP* as an example, among all observations in the database, the maximum *SMLP* is 1019 and minimum is 874. We divide interval [874, 1019] into 10 bins. Supposed that we have an observation sample with *SMLP* value 1000, it will be located into the 10<sup>th</sup> bin out of total 10 bins. Binary number 0 or 1 is used to represent whether there is a value located into the bin. So, *SMLP* 1000 can be transformed into 0000000001, where the binary bit 1 represents that there is a value in 10<sup>th</sup> bin and no value in other bins. Based on the best data track from Hong Kong Observatory, tropical cyclones are classified into four types: Tropical Depression, Tropical Storm, Severe Tropical Storm, and Typhoon. We use a four-bit binary number to represent this type such as 0100, denoting a given observation sample is belonging to the second type, Tropical Storm.

After the input pattern has been normalized and well represented, it is fed into a feed forward neural network for training and validation with sigmoid activation function. Assuming that instances of the input observations are  $A_k=(a_k^1, a_k^2, \dots, a_k^n)$  ( $k = 1, 2, \dots, m$ ), where  $k$  is the index for the input observations, and  $n$  is the number of the input unit. The hidden layer unit  $j$  computes its activation values as below:

$$o_j = f\left(\sum_{i=1}^n a_k^i w_{ij} - \beta_j\right) \quad (5.5)$$

where  $\beta_j$  is the bias of the  $j^{th}$  unit of the hidden layer,  $a_k^i$  is the input instance,  $w_{ij}$  is the feed-forward weight connecting hidden unit  $j$  to input unit  $i$ , and  $f$  is the sigmoid function in equation 5.6. Note that  $w_{ij}$  is randomly distributed in [0.0, 1.0].

$$f ( net ) = \frac{1}{1 + e^{-net}} \quad (5.6)$$

Next we apply a winner-take-all style competition in the output layer to determine the classification result for the input pattern. The activation function of the output layer is computing using similar equation 5.5. After the neural network is well-rounded training for a given pattern, the unit of the output layer, which has the largest activation value, will be considered as the category that the input pattern is classified. Or, we can use Equation 5.7 to represent it. For example, if  $c = 0010$ , then the input pattern is classified into the third class, as the third bit is set to 1.

$$C = o_1o_2o_3o_4, \text{ where } \begin{cases} o_i = 1, \text{ if } (o_i = \max(o_1, o_2, o_3, o_4)) \\ o_i = 0, \text{ otherwise} \end{cases} \quad (5.7)$$

When the training progress has completed for a given observation sample, a set of weights  $w_{ij}$  can be achieved for every input node  $i$  connecting to every hidden unit  $j$ . These weights can be regarded as the importance degree of every input node  $i$ , which is the similarity attribute of the observation samples, contributing to determining the network output, intensity classification. After that the similarity of two attribute vectors  $C_i$  and  $C_j$  can be modified as:

$$Sim(C_i, C_j) = \sum_{k=1}^N \left[ \left( \frac{w_{ik} + w_{jk}}{2} \right) * Sim(S_{ik}, S_{jk}) \right] / \sum_{k=1}^N (w_{ik} + w_{jk}) \quad (5.8)$$

where  $S_{ik}$  and  $S_{jk}$  are values of  $k^{th}$  attribute for two observations respectively.

### 5.2.3 Time-series Adjustment Function

A tropical cyclone will be recorded with more than one observation during its life for the analysts' prompt and precise references. The more observation samples for a tropical cyclone are recorded, the more precise prediction results will be achieved, and the earlier we can take action to avoid the disaster for loss of human lives and properties. Besides, empirically the form of the tropical cyclones is sensitive to time in any region all over the world. For example, in Hong Kong, there are more tropical cyclones with stronger intensities from June to August every year. Therefore, the attribute Time will have its particular impact to the similarity measure during the retrieval. The closer the date is to

the current date, the greater the impact is to the current weather. When interval of two Time points exceeds some value, the mutual impact may be ignored.

Based on this idea, the conception of a time-series adjustment function is proposed. The time function  $E(t)$  need to meet the properties:

- Variable  $t$  is the observation time in the cases;  $E(0) = 1$  and  $E(\infty) = 0$ ;
- $E(t)$  is the function of degression, when  $t \in (0, +\infty) \cup (-\infty, 0)$ .

Here the time function is defined as:

$$E(t) = e^{-C|t|} \quad (5.9)$$

where  $C$  is a constant and  $0 < C < 1$ .

The advantages of using  $E(t)$  as the time function exist in two aspects. One is  $\int_0^{+\infty} e^{-|t|} = 1$ , the other is that the current date is supposed to the origin, the  $E(t)$  increases monotonously ( $t \in (-\infty, 0)$ ) and  $E(t)$  decreases monotonously ( $t \in (0, +\infty)$ ). The function  $f(t) = e^{-|t|}$  ( $t \in (0, +\infty) \cup (-\infty, 0)$ ) decreases more heavily. So the constant  $C$  ( $0 < C < 1$ ) is introduced to the function  $E(t)$  in order to prevent  $E(t)$  from decreasing heavily. As a result, we design a time-series adjustment function as below:

$$ST_{ij} = \exp \left[ - \left| \left( \frac{Month_i}{12} + \frac{Day_i}{30} * \alpha \right) - \left( \frac{Month_j}{12} + \frac{Day_j}{30} * \alpha \right) \right| \right] \quad (5.10)$$

where  $Month_i$  ( $Month_j$ ) and  $Day_i$  ( $Day_j$ ) are the recording times for observations  $i$  and  $j$ . To show the dominance of variable Month over variable Date, a parameter  $\alpha$  on Date is adopted to lower its influence to  $ST_{ij}$ , where  $\alpha$  belongs to  $[0.0, 1.0]$ . One of the advantages is that we avoid simply modeling the periodic effect in monotonously increasing or decreasing mode, instead of which a step-wise mode is used. Another advantage is that as  $max(ST) = 1$  and  $min(ST) = 0$ , then the result of  $ST_{ij}$  will not change rapidly even though two recorded times are at a longer time interval of each other, which makes it more feasible to be integrated into the previous similarity functions. Consequently, that the similarity of two attribute vectors  $C_i$  and  $C_j$  can be further modified in equation 5.11.

$$Sim(C_i, C_j) = \sum_{k=1}^N [(\frac{w_{ik} + w_{jk}}{2}) * (ST_{ij} + Sim(S_{ik}, S_{jk}))] / \sum_{k=1}^N (w_{ik} + w_{jk}) \quad (5.11)$$

### 5.3 Experimental Analysis

In order to evaluate the usefulness of our proposed competitive neural network classifier, we carry out a set of experiments to test whether our approach achieves an acceptable prediction precision, and whether there is a superiority comparing to other existing forecast models. We have collected 6,687 observation samples of 324 tropical cyclones passing through Hong Kong in the ten years from 1994 to 2003. These samples are time-series distributed and recorded every 6 hours during their lives. A computer with 2.26 GHz Intel Pentium CPU and 512M RAM memory is used for the simulations. As we cannot afford to take all these samples in our experiments, to ensure the representative, we randomly select 200 observation samples as the training set for the neural weight generator, and select randomly another 30 samples as the testing set. Figure 5.4 gives a detailed similarity retrieval procedure used in our experiments.

#### Procedure Similarity Retrieval

1. We define a TC vector  $C = \{Name, Time, Intensity, Position, SMLP, Sp\}$
2. Suppose  $C_i = \{C_1, C_2, C_3, \dots, C_n\}$  be the set of n historical cases
3. Feed every  $C_i$  to the Neural Weight Generator; calculate the weights  $W_i$  for every attribute of  $C_i$
4. Based on training results, build up a neural network classifier model
5. Given a predicting sample  $C_e$ , feed it into the classifier, get  $W_e$
6. For every sample in  $C_i$ 
  - calculate distance similarity  $Sim(S_{e_i}, S_{e_e})$
  - calculate time adjustment  $ST_{ie}$
  - calculate  $S_i = Sim(C, C_i)$  according to equation 8
- End For
7. If  $S_i = \min(S)$ , then  $Intensity_e = Intensity_i$

#### End Procedure

**Figure 5.4:** Steps to predict the intensity of current tropical cyclone sample

Before we feed the similarity attributes into the neural weight generator, we normalize them into binary representation as mentioned in section 5.2.2. Table 5.1 shows the normalization results and the number of units for every network layer. In total we need 120 bits to represent the input values of three variables; we put 120 neurons in the input layer. Empirically the number of the hidden units needed is equal to one tenth of the number of input units; so 12 nodes are put into the hidden layer. In the last layer,

depending on the predicted intensity category, we use 4 units in this layer to show the classified results from the neural network classifier.

**Table 5.1:** Input attributes normalization and initial number of layer units for neural weight generator

Input Pattern				Initial number of		
				Input units	Hidden units	Output units
<b>Attribute</b>	<b>No.</b>	<b>Example</b>	<b>Representation</b>	120	12	4
<b>Position</b>	<i>Long (10) x Lat (10) = 100</i>	<i>N<sub>ij</sub><sup>th</sup> block, i=20, j=2</i>	<i>100...0 (ninety-nine 0s)</i>			
<b>MSLP</b>	<i>Bin(10) x 1 = 10</i>	<i>109</i>	<i>100...0 (nine 0s)</i>			
<b>Speed</b>	<i>Bin(10) x 1 = 10</i>	<i>136</i>	<i>100...0 (nine 0s)</i>			

In Figure 5.5 we show the predicted results and errors for 30 randomly selected TC observation samples. We can clearly see that the predicted intensities are very close to the original intensities in the database. The largest difference between the predicted intensity and the original one is 8, which is considered acceptable.

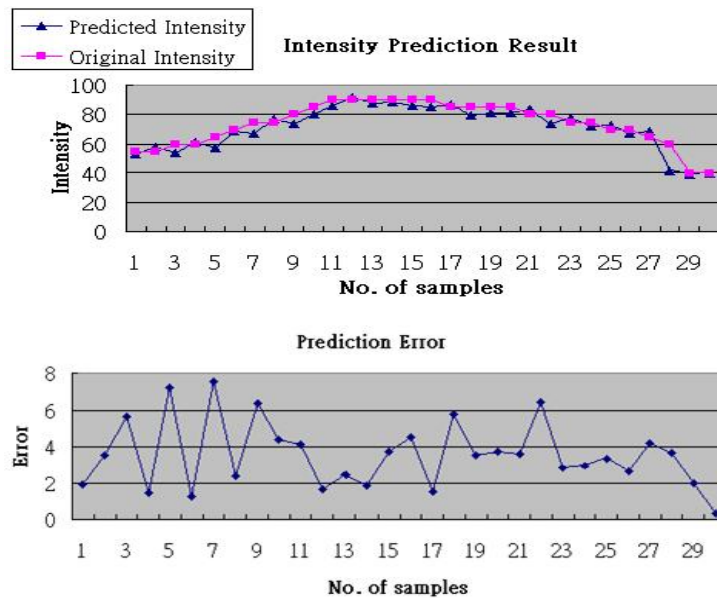


**Figure 5.5:** Intensity prediction results and errors

To justify the performance of our propose model, two existing TC forecasting models developed in our previous works are used for comparison: 1) Satellite Interpretation

(Chapter 3) and 2) Integrated Neural Training (Chapter 4). The totally 20 observation samples selected from the database are used for comparison, which is calculated using following equation:

$$P = \frac{|I_p - I_r|}{I_r} \quad (5.12)$$

where  $I_p$  is the predicted intensity and  $I_r$  is the actual intensity for that observation in the database. As shown in Figure 5.6, the integrated neural training model has the highest prediction precision, followed by the satellite interpretation model and the similarity retrieval model. As the accuracy for more than half of samples is more than 70%, we still consider the similarity retrieval model has its potential in future research if we improve the corresponding algorithms, equations and parameters.

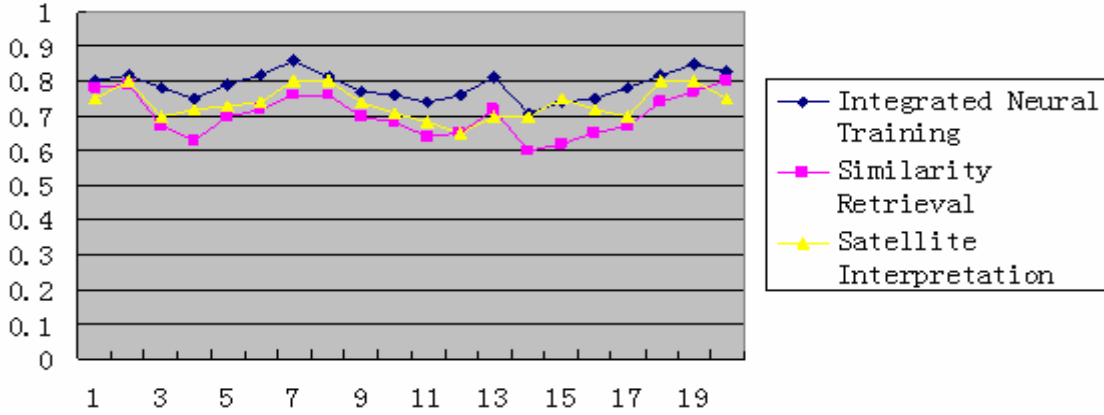


**Figure 5.6:** Predicted precision of three approaches

## 5.4 Summary

In this chapter, we have presented an intensity forecast model for tropical cyclones based on similarity retrieval from non-linear tropical cyclone observations. Neural network is adopted to generate a set of appropriate weights for various feature variables of a tropical cyclone instance. We also have proposed the time-series adjustment function to measure the particular impact of the variable Time. Ten years of data comprising 6,687 observation samples of 324 tropical cyclones passing through Hong Kong is used for the experiments. Results show that our proposed approach has research potential in the future if we put more efforts on algorithms modifications.



# Chapter 6. Future Research and Conclusion

## 6.1 Limitations and Future Works

In this section, we discuss shortages and difficulties of above three forecasting models one by one, and then propose possible efforts needed to be devoted to achieve a more scientific, practical and accurate forecasting model for tropical cyclone intensity.

### 6.1.1 Satellite Interpretation Based Forecasting

Firstly, in this study, the eye of a tropical cyclone is determined based on the positional centroid of the extracted contour points from a satellite image. Actually the eye found using this approach leads to a highly inaccurate forecasting result as it may be far away from the real eye of the tropical cyclone. However, depending on the complexity of the internal structure of a tropical cyclone, it is very difficult to determine the real eye accurately only using information of the satellite images. In later part of this forecasting system, only contour points are used to form angles to match two tropical cyclones. Moreover, we plan to measure the significance of a contour point according to its distance to the cyclone eye, which should be located within the extracted contour. As a result, we decide to use its positional centroid as the tropical cyclone eye for later weight assignment. In the future, with more efforts, an efficient method to locate the real eye of a tropical cyclone needs to be developed to give a better forecasting result.

Secondly, in this thesis, we assume that there is only one tropical cyclone existing in the satellite image, or, we choose the tropical cyclone with the largest area using a fast sequential neighbour checking algorithm. The reason is twofold. Firstly in most situations, there exist many small clouds near the tropical cyclone in the satellite image. When active contour model is carried out on the satellite image, there will be more than one cyclone contours including a big cyclone and many small ones. Those small cyclones are

considered as noises and will be removed. However, the disadvantage of choosing the largest cyclone is that, if there are two big tropical cyclones existing in the satellite image at one time, and we only select the largest one for prediction, we could omit the influence of the other tropical cyclones leading to inaccurate results. In future, the influence of multiple tropical cyclones in the forecasting system should be considered.

Thirdly, future research efforts will be directed towards improving the matching module's efficiency and matching accuracy, with special emphasis on improving the algorithm for finding the optimal time warping path. The weight assignment algorithm is needed to be improved to determine clear significance for each contour points.

### **6.1.2 Neural Training Based Forecasting**

Firstly, in this study, the selection of the analog tropical cyclones for a given storm is an important aspect. We use the competitive neural network as the technique to perform this selection. In the future, a different unsupervised or supervised technique may be used to improve the classification algorithm. Supervised techniques based on a preliminary classification could be an alternative to improve the analog identification procedure. One of the most relevant supervised techniques that can be used in the future is the Learning Vector Quantization (LVQ).

Secondly, the addition of new predictors must be done in the future. It has been proved that some predictors such as k-index, REFC (200-mb relative eddy angular momentum flux convergence), PEFC (200-mb planetary eddy angular momentum flux convergence), etc have close relationships with the tropical cyclone intensity. Also, different non-linear transformations such as logarithm, or quadratic can be applied to the predictors of the existing model to increase the pool of potential predictors and to explore a possible non-linear relationship between the predictors and the storms intensity.

Thirdly, the present study provides tropical cyclone intensity prediction up to 24 hours. The experimental results show that the proposed model can provide reliable storm

intensity prediction at 6, 12, 18, and 24 hr. The results also show that there is no significant increase in the error when the prediction interval increases. The forecast can be extended to 72 hr in the future. Moreover, the present work only uses the historical data to test the proposed model. In future, it is possible to apply the real-time meteorological observations to system and evaluate the accuracy of the model. And the proposed model is optimal for use in Western North Pacific basin since the equations used to derive some predictors are specific to this region only while these equations may not be applicable to other basins. Same performance may not be shown in other basins.

In the future, more measure functions for more feature variables should be considered as add on. A more flexible structure of the neural network is going to be proposed and algorithms to determine the weights for each variable are also going to be elaborated in the future. Enhancement on the measure for the time series is also going to be conducted for the impact among different observation sample that are imprecise in nature. Therefore, investigation on the use of fuzzy theory and case base adaptation to counteract exceptional TC behaviour can be useful in the course of providing an accurate forecast.

### **6.1.3 Similarity Retrieval Forecasting**

In this model, we only consider four numerical features of a tropical cyclone, which are Time, Position, SMLP and Speed, to form different similarity measure functions. It is definitely insufficient and can only achieve rough retrieval results. In the future, more measure functions for more feature variables should be considered as add on. A more flexible structure of the neural network (such as to optimized the inputs of the neural network by reducing the number of Longitude and Latitude inputs neurons from 10x10 to 4x4) is going to be proposed and algorithms to determine the weights for each variable are also going to be elaborated in the future. Enhancement on the measure for the time series adjustment is also going to be conducted for the timing impact among different observation sample that are imprecise in nature. A powerful and well-correlated TC database is going to be built up in the future. Moreover, investigation on the use of fuzzy

theory and case base adaptation to counteract exceptional TC behaviour can be useful to provide accurate forecasts.

## 6.2 Conclusions

In this thesis we have been discovering new approaches in designing reformative forecasting models to predict the intensity of tropical cyclones using methodologies at different levels that are more reliable for the collected data types, more efficient and effective in terms of predicted accuracy and computational costs, and more scalable to future system expansion. In our study, three different approaches, based on different characteristics of tropical cyclones, have been proposed to achieve our research target: A satellite interpretation based tropical cyclone forecasting system, an integrated neural training based tropical cyclone forecasting system, and a similarity retrieval approach for time-series tropical cyclone data. Relative experiments show that our proposed approaches are effective and can achieve promising results.

In satellite interpretation approach, we propose an integrated prototype for tropical cyclone (TC) comparison that is based on typical spiral shapes of TCs using time warping technology. Gradient Vector Flow (GVF) snake model is adopted to extract the contour points of TCs from the satellite image. A series of accessorial algorithms, including a fast sequential neighbor-checking algorithm, a pixel distance algorithm, and a weight calculation algorithm have been proposed for pre-processing input data. Given two sets of contour points, one for the input tropical cyclone image and the other for an image in the database, we use angle features between successive contour points to determine the degree of similarity of two cyclone shapes. To better reflect the spiral shape of tropical cyclones and to produce a fast, accurate comparison, we adopt a time warping approach. The proposed approach was tested against and found to be superior to an approach that uses a modified Hausdorff distance measure.

In the neural training based approach, we use artificial neural network for predicting TC intensity in the Western North Pacific at 6, 12, 18 and 24 hours. The historical NCEP (National Center for Environment Prediction) reanalysis data and the sea surface temperature values are used along with each storm track to develop a set of climatology, persistence and synoptic variables. A competitive neural network is adopted to identify analog storms associated with the current TC. Once the analog TCs are identified, the database observations of analog TCs and the current storm are combined to create a training set. A multiple regression scheme is used to identify the variables that are best correlated with storm intensity. Experimental results show that the proposed prediction scheme is a potential tool to increase the accuracy in predicting TC intensity.

In similarity retrieval approach, an intensity-forecasting model for TCs is developed based on similarity mining from various features of time-series TC observations. A feedforward neural network is adopted to generate a set of appropriate weights for different features of a TC instance. We also have proposed the time-series adjustment function to measure the particular impact of the Time feature. Ten years of data comprising 6,687 observation samples of 324 tropical cyclones passing through Hong Kong are used for the experiments. Results show that our proposed approach can achieve a satisfactory forecasting result and has its potential to be improved in the future on the algorithms, equations and parameters.

# References

- [1]. Demaria M. and Kapla. J.; A statistical hurricane intensity prediction scheme (SHIPS) for the Atlantic basin. *Weather and Forecasting*, vol.9, pp.209-220, 1994
- [2]. Jones W.L., Park J.D, Donnelly W.J., Carswell J.R., McIntosh R.E., Zec J. and Yueh S.; An improved NASA Scatterometer geophysical model function for tropical cyclones, *IEEE International Symposium on Geoscience and Remote Sensing*, vol.4, pp.1994-1997,1998
- [3]. Petrenko B.Z, Nerushev A.F., Milekhin L.I. and Zagorin G.K.; Validation of models and algorithms for microwave radiometric investigations of tropical cyclones, *International Symposium on Geoscience and Remote Sensing*, vol.1, pp.359–361, 1997
- [4]. Yueh S.H., Stiles B.W. and Liu W.T.; QuikSCAT wind retrievals for tropical cyclones, *IEEE Transactions on Geoscience and Remote Sensing*, vol.41, issue.11, pp. 2616–2628, 2003
- [5]. Dvorak V.F.; A technique for the analysis and forecasting of tropical cyclone intensities from satellite pictures, *NOAA Technical Memo, NESS 45*, U.S Department of Commerce, Washington D.C., 1973
- [6]. Dvorak V. F.; Tropical cyclones intensity analysis and forecasting from satellite imagery, *Mon. Wea. Rev.*103, pp.420 – 430, 1973
- [7]. Weiss C. E.; Cloud-location corrections near the horizon of a SMS image, *Satellite Applications Information Note 78/8*, NOAA/NESDIS, U.S. Department of Commerce, Washington, D.C., 1978
- [8]. Weber E. M. and Wilderotter S.; *Satellite Interpretation*, Air Weather Service Technical Note 81/001, Offutt AFB, NE, 1981
- [9]. Velden C. S., Olander W. S. and Raymond M. Z.; Objective Dvorak Technique (ODT), *Weather and Forecasting*, Regional and Mesoscale Meteorology branch, NOAA/NESDIS, U.S. Department of Commerce, Washington, D.C., 1998
- [10]. Velden C. S., Olson W. S. and Roth B. A.; Tropical cyclones centre-fixing using DMSP SSM/I data, *Proc. of 4th Conf. Satellite Meteorology*, San Deigo, USA, pp.36 – 39, 1989

- [11]. Adler R. F.; Determination of thunderstorm heights and intensities from GOES infrared data, Proc. Int. Conf. Weather Forecasting and Analysis, American Meteorological Society, pp.250 – 257, 1982
- [12]. Brandli H. W.; Satellite meteorology, AWS-TR-79-264, Hq. Air Weather Service, Scott AFB IL., 1976
- [13]. Weldon R.; Synoptic scale cloud systems, NESDIS Training Notes, Satellite Applications Laboratory, NOAA, U.S. Department of Commerce, Washington, D.C., 1983
- [14]. Brandli H. W.; Satellite meteorology, AWS-TR-79-264, Hq. Air Weather Service, Scott AFB IL., 1976.
- [15]. Weldon R. and Holmes S.; Characteristics of water vapour imagery, NESDIS Training Notes, Satellite Applications Laboratory, NOAA, U.S. Dept. of Commerce, Washington D.C., 1984
- [16]. Spencer R.W. and Goodman H.M.; Precipitation retrieval over land and ocean with the SSM/I, Journal. Atmos. Oceanic Tech. 6, pp.253-273, 1988
- [17]. McGregor J. L., Walsh K. J., and Katzfey J. J.; Climate simulations for Tasmania, 4<sup>th</sup> Int. Conf. Southern Hemisphere Meteorological and Oceanography, American Meteorological Society, pp.514 – 515, 1993
- [18]. ----, “Evaluation of western north pacific tropical cyclone objective forecast aids”, Weather and Forecasting Aids, no.3, pp.76 – 85, 1988
- [19]. Tsui T. and Miller R. J.; Evaluation of JTWC tropical cyclone objective forecast aids, Naval Environmental Prediction Research Facility, Monterey, CA, Technical Report TR 86-05, 1986
- [20]. Madala R. V.; Efficient time integration scheme for atmosphere and ocean model: Finite-difference techniques for vectorize fluid dynamics, Springer - Verlag, New York, pp.56 – 70, 1978
- [21]. Kuo H. L.; On formation and intensification of tropical cyclones through latent heat release by cumulus convection, Journal. Atmos. Sci., vol.22, pp.40 – 63, 1965
- [22]. Jeng B.F., Chen H.J., Lin S.C., Leou T.M., Peng M.S., Chang S.W., Hsu W.R., and Chang C.P.; The limited-area forecast system at the central weather bureau in Taiwan, Weather and Forecasting, no.6, pp.155-178, 1991

- [23]. Dvorak V. F.; Tropical cyclone intensity analysis using satellite data, NOAA Technical Report, NESDIS 11, Washington D.C., 1984
- [24]. Wang Y.Y, Wang H., Chen H. and Sun W.C.; Tropical cyclone center location with digital image process, International Conferences on Info-tech and Info-net, vol.3, pp.563 – 567, 2001
- [25]. Lee R. S. T. and Liu J. N. K.; Tropical cyclone identification and tracking system using integrated neural oscillatory elastic graph matching and hybrid RBF network tracking mining techniques, IEEE Transaction on Neural Networks, vol.11, no.3, pp.680 – 689, 2000
- [26]. Hope, J. and C. Nuemann; An operational technique for relating the movement of existing tropical cyclones to past tracks, Mon. Wea. Rev., vol.98, pp.925 – 933, 1970
- [27]. Nuemann, C. J.; An alternate to the HURRAN tropical cyclone forecast system, NOAA. Tech. Memo, NWS SR-62, 1972
- [28]. Jarvinen, B.R. and C.J. Neumann; Statistical forecasts of tropical cyclone intensity (SHIFOR), NOAA Tech.Memo.NWS NHC, 10, 22, 1979
- [29]. DeMariz, M., and Kaplan J.; A Updated Statistical Hurricane Intensity Prediction Scheme (SHIPS) for the Atlantic and Eastern North Pacific Basins, Weather Forecasting, 14, pp.326-337,1999
- [30]. Knaff, J., DeMaria, M. and Sampson, C.; An introduction to the statistical typhoon intensity prediction scheme (STIPS), Proc. of 26<sup>th</sup> Conf. on Hurricanes and Tropical Meteorology, pp.145-150, 2004
- [31]. Knaff, J., Demaria, M., Sampson, C. and Gross J; Statistical, 5-Day Tropical Cyclone Intensity Forecasts Derived from Climatology and Persistence, Weather and Forecasting, vol. 18, pp.80-92, 2003
- [32]. Kurihaha, Y., M.A. Bender, R. E. Tuleya, and R.J. Ross; Improvements in the GFDL hurricane prediction system, Mon. Wea. Rev., vol.123, pp.2791 – 2801, 1995
- [33]. Kidder, S. and M. Goldberg; Satellite analysis of tropical cyclones using the Advanced Microwave Sounding Unit (AMSU), Bulletin of the American Meteorological Society, vol.81, pp.1241-1259, 2003
- [34]. Richard L.B and Paul M. T.; An Automated Method to Estimate Tropical Cyclone Intensity Using SSM/I Imagery, Journal of Applied Meteorology, vol.41, pp.461 – 472,

2002

- [35]. Lee R. S. T. and Liu J. N. K.; An automatic satellite interpretation of tropical cyclone patterns using elastic graphic dynamic link model, *Int. Journal of Pattern Recognition and Artificial Intelligence*, vol.13, pp.1251 – 1270, 1999
- [36]. Seo K.H. and Lee J.J.; Object tracking using adaptive colour Snake model, *Int. Conf. on Advanced Intelligent Mechatronics*, vol.2, pp.1406 – 1410, 2003
- [37]. Malsburg V. D. C.; The correlation theory of brain theory, *Internal Report, MPI Biophysical Chemistry*, pp.81 -182, 1981
- [38]. Lewcock A.; Computerised signature verification, *Proc. of 29<sup>th</sup> Int. Carnahan Conf. on Security Technology*, pp.72-78, 1995
- [39]. Borghese N. A., Ferrari S. and Piuri V.; Real-time surface meshing through HRBF networks, *Proc. of Int. Joint Conf. on Neural Networks*, vol. 2, pp.1361 – 1366, 2003
- [40]. Sun J., Shen R.M. and Yang F.; A new adaptive RBF network structure learning algorithm, *Proc. of Int. Conf. on Machine Learning and Cybernetics*, vol.1, pp.35 – 40, 2002
- [41]. LU Y.H. and Morris J. M.; Fast design of Gabor filters, *Proc. of the 16th Annual Int. Conf. of the IEEE Engineering in Medicine and Biology Society*, vol.2, pp.1334 – 1335, 1994
- [42]. Horn D. and Usher M.; Segmentation and binding in an oscillatory neural network, *Proc. of Int. Joint Conf. Neural Networks*, vol.1, pp.243 – 248, 1991
- [43]. Malsburg V.D.C and Buhmann J.; Sensory segmentation with coupled neural oscillators, *Biological Cybernetics*, vol. 67, pp.233 – 242, 1992
- [44]. Lee R. S. T. and Liu J. N. K.; An oscillatory elastic graph matching model for scene analysis, *Proc. of Int. Conf. Imaging Science, Systems and Technology, Las Vegas, NV*, pp. 42 – 45, 1999
- [45]. Hely T.; The role of activity in corpus callosum development in the visual cortex, *Ninth Int. Conf. Artificial Neural Networks*, vol.1, pp.413 – 418, 1999
- [46]. Xu D.M. and Gao L.; Wavelet transform and its application to autonomous underwater vehicle control system fault detection, *Proc. of Int. Symposium on Underwater Technology*, pp.99 – 104, 2000

- [47]. Feng G. C., Yuen P. C. and Dai D. Q.; Human face recognition using PCA on wavelet subband, *Journal of Electronic Imaging*, vol. 09(02), pp.226 – 233, 2000
- [48]. Liu J. N.K., Kwong J., Wang M., Sin D. K.Y. and Jain L.C.; An Integrated Approach for the Prediction of Tropical Cyclone and Weather Forecast, *WSEAS Transactions on Systems*, Issue 3, vol.2, pp.716-723, 2003
- [49]. Mallat S.; Multi-resolution approximations and wavelet orthonormal bases of  $L^2(\mathbb{R})$ , *Trans. Amer. Math. Soc.*, pp.69 – 87, 1989
- [50]. Haupt R. L. and Haupt S. E.; *Practical Genetic Algorithms*, Jone Wiley & Son, Inc. 1998
- [51]. Pedro J. S. and Burstein F.; A framework for case-based fuzzy multicriteria decision support for tropical cyclone forecasting, *Proc. of the 36<sup>th</sup> Annual Hawaii Int. Conf. on System Sciences*, pp.85 – 92, 2003
- [52]. Hurricane Alberto, <http://www.nhc.noaa.gov/2000alberto.html>
- [53]. Sivaramakrishnan M. V. and Selam M.; On the use of the spiral overlay technique for estimating the center positions of tropical cyclones from satellite photographs taken over the Indian region, *Proc. of the 12<sup>th</sup> Int. Conf. on Radar Meteorology*, pp 440 - 460, 1966
- [54]. Tuttle J. and Gall R.; A single-radar technique for estimating the winds in tropical cyclones, *Buttetin of the American Meteorological Society*, vol.80, pp.653 - 668, 1999
- [55]. Hasler A. F., Palaniappan K., Kambhamettu C., Black P., Uhlhorn E. and Chesters D.; High resolution wind fields within the inner-core and eye of a mature tropical cyclone from GOES one-minute images, *Buttetin of american Meteorological Society*, vol.79, pp. 2483 - 2496, 1998
- [56]. Lai E. S. T.; TREC application in tropical cyclone observation, *ESCAP/WMO Typhoon Committee Anual Review*, pp.135 - 139, 1998
- [57]. Wood V. T.; A technique for detecting a tropical cyclone center using a Doppler radar, *Journal of Atmospheric and Oceanic Technology*, vol.11, pp.1207 - 1216, 1994
- [58]. Wong K. Y., Yip C. L., Li P. W. and Tsang W. W.; Automatic template matching method for tropical cyclone eye fix, *Proc. of 17<sup>th</sup> Int. Conf. on Pattern Recognition*, pp. 234-240, 2004

- [59]. Wang Y., Wang H., Cheng H. and Sun W. C.; Tropical cyclone center location with digital image process, Proc. of Int. Conf. on Info-tech and Info-net, vol.3, pp.563 - 567, 2001
- [60]. Yip C. L. and Wong K. Y.; Efficient and effective tropical cyclone eye fix using genetic algorithms, Proc. of 8<sup>th</sup> Int. Conf. on Knowledge-based Intelligent Information and Engineering Systems, pp. 89-93, 2004
- [61]. Hong P.Y. and Huang, T.S.; Automatic temporal pattern extraction and association, Proc. of IEEE Int. Conf. on Acoustics, Speech, and Signal Processing, vol.2, pp.2005 – 2008, 2002
- [62]. Xu, C.Y. and Prince, J.L.; Snakes, Shapes and Gradient Vector Flow, IEEE Transactions on Image Processing, vol.7, pp.359-369, 1998
- [63]. Morii, F.; Distortion analysis on discrete Laplacian operators by introducing random images, Proc. of 3<sup>rd</sup> Int. Conf. on Image and Graphics, pp.80 - 83, 2004
- [64]. Kim, B.Y., Kim, H.J. and Jang, S.J.; Image retrieval based on colour coherence, the IEEE Region 10 Conf., vol.1, pp.178 – 181, 1999
- [65]. Saengow, W., Thipakorn, B. and Cochran, D.; An energy spreading transform approach to efficient image retrieval, 34<sup>th</sup> Asilomar Conf. on Signals, Systems and Computers, vol.2, pp.1861 – 1864, 2000
- [66]. Kiran, V. and Bora, P.K.; Watersnake: integrating the watershed and the active contour algorithms, Int. Conf. on Convergent Technologies for Asia-Pacific Region, vol. 2, pp.868 – 871, 2003
- [67]. Feng B. and Liu, J.N.K.; Semo-Mamo, A 3-phase module to compare tropical cyclone satellite images using a modified Hausdorff distance, Proc. of the Int. Conf. on Machine Learning and Cybernetics, pp.3808-3813, 2003
- [68]. Dubuisson, M.P. and Jain A.K.; A modified Hausdorff distance for object matching, Int. Conf. on Pattern Recognition, pp.566 – 568, 1994
- [69]. Rath, T.M. and Manmatha, R.; Word image matching using dynamic time warping, IEEE Computer Society Conf. on Computer Vision and Pattern Recognition, vol. 3, pp. 521 – 527, 2003
- [70]. Theodoridis S. and Koutroumbas K.; Pattern recognition, San Diego: Academic Press, 1999

- [71]. Automated Tropical Cyclone Forecast System, U.S. Navy official website:  
[http://www.nrlmry.navy.mil/atcf\\_web](http://www.nrlmry.navy.mil/atcf_web)
- [72]. Huttenlocher, D.P., Klanderman, G.A., and Rucklidge, W.J.; Comparing images using the Hausdorff distance, IEEE Transaction on Pattern Analysis and Machine Intelligence, pp.850 – 863, 1993
- [73]. Achermann, B. and Bunke, H.; Classifying range images of human faces with Hausdorff distance, Int. Conf. on Pattern Recognition, vol.2. pp.809 – 813, 2000
- [74]. Pan G., Wu Z.H., and Pan Y.H; Automatic 3D face verification from range data, IEEE Int. Conf. on Acoustics, Speech, and Signal, vol.3, 193-196, 2003
- [75]. Yaniv, R. and Burshtein, D.; An enhanced dynamic time warping model for improved estimation of DTW parameters, IEEE Transactions on Speech and Audio Processing, vol.11, pp.216 – 228, 2003
- [76]. Hagan, M., Demuth H. and Beale M.; Neural Network Design, PWS Publishing Co., Boston, 1996
- [77]. NetCDF Toolbox  
[http://woodshole.er.usgs.gov/staffpages/cdenham/public\\_html/MexCDF/nc4ml5.html](http://woodshole.er.usgs.gov/staffpages/cdenham/public_html/MexCDF/nc4ml5.html)
- [78]. Baik, J.J. and Hwang H.S.; Tropical Cyclone Intensity Prediction Using Regression Method and Neural Network, J. Meteor. Soc. Japan, vol.76, pp.711-717, 1995
- [79]. Joint Typhoon Warning Center (JTWC).  
[http://www.npmoc.navy.mil/jtwc/atcr/atcr\\_archive.html](http://www.npmoc.navy.mil/jtwc/atcr/atcr_archive.html)
- [80]. Hong Kong Observatory (HKO). <http://www.hko.org.hk>
- [81]. Aguirre, J.L., Montano, O., Sanchez-Castellanos; Knowledge flow leveraged through case-based and data mining agents in a just in time information and knowledge system, Proc. of Int. IEEE Conf. on Intelligent Systems, vol.1, pp.200 – 205, 2004
- [82]. Kolodner, J.; Case-Based Reasoning, Morgan Kaufmann, California, USA, 1993
- [83]. Louis, S.J. and McDonnell, J.; Learning with case-injected genetic algorithms, IEEE Transactions on Evolutionary Computation, vol.8, issue.4, pp.316 – 328, 2004